

From complex to simple : hierarchical free-energy landscape renormalized in deep neural networks

Hajime Yoshino^{1,2*}

¹ Cybermedia Center, Osaka University, Toyonaka, Osaka 560-0043, Japan

² Graduate School of Science, Osaka University, Toyonaka, Osaka 560-0043, Japan

* yoshino@cmc.osaka-u.ac.jp

June 6, 2022

Abstract

We develop a statistical mechanical approach based on the replica method to study the design space of deep and wide neural networks constrained to meet a large number of training data. Specifically, we analyze the configuration space of the synaptic weights and neurons in the hidden layers in a simple feed-forward perceptron network for two scenarios: a setting with random inputs/outputs and a teacher-student setting. By increasing the strength of constraints, i.e. increasing the number of training data, successive 2nd order glass transition (random inputs/outputs) or 2nd order crystalline transition (teacher-student setting) take place layer-by-layer starting next to the inputs/outputs boundaries going deeper into the bulk with the thickness of the solid phase growing logarithmically with the data size. This implies the typical storage capacity of the network grows exponentially fast with the depth. In a deep enough network, the central part remains in the liquid phase. We argue that in systems of finite width, the weak bias field remains in the center and plays the role of a symmetry-breaking field that connects the opposite sides of the system. The successive glass transitions bring about a hierarchical free-energy landscape with ultrametricity, which evolves in space: it is most complex close to the boundaries but becomes renormalized into progressively simpler ones in deeper layers. These observations provide clues to understand why deep neural networks operate efficiently. Finally, we present the results of a set of numerical simulations to examine the theoretical predictions.

Contents

1	Introduction	3
2	Model	5
2.1	Multi-layer feed-forward network	5
2.2	Two scenarios for inputs/outputs patterns	8
2.2.1	Random inputs/outputs	8
2.2.2	Teacher-student setting	9
3	Replica theory	9

3.1	Order parameters	9
3.2	Replicated Gardner volume	10
3.3	Random inputs/outputs	11
3.3.1	“Quenched” boundary	12
3.3.2	Liquid phase	12
3.3.3	The 1st glass transition	13
3.3.4	The 2nd glass transition	14
3.3.5	More glass transitions	16
3.4	Fluctuating boundary	19
3.4.1	One RSB type boundary	20
3.4.2	Full RSB type boundary	21
3.5	Teacher-student setting	22
3.5.1	Training	22
3.5.2	Generalization	24
3.6	Summary	25
4	Simulations of learning	27
4.1	Relaxational dynamics of a soft-core model with random inputs/outputs	27
4.2	Learning by a binary perceptron in a teacher-student setting	29
5	Conclusion and outlook	31
5.1	Conclusion	31
5.2	Outlook	32
	References	33
A	Replicated free-energy	44
A.1	Basic strategy	44
A.1.1	Explicit replica symmetry breaking	44
A.1.2	Ergodicity breaking	45
A.1.3	What is the symmetry breaking field?	46
A.1.4	Plefka expansion	46
A.2	Evaluation of the entropic part of the free-energy	47
A.2.1	Entropic part of the ‘bonds’	48
A.2.2	Entropic part of the ‘spins’	48
A.3	Evaluation of interaction part of the free-energy	49
A.3.1	Bulk part	49
A.3.2	Boundaries - quenched vs slightly annealed one	50
A.4	Total free-energy	51
A.5	Parisi’s ansatz	51
A.5.1	Random inputs/outputs	51
A.5.2	Teacher-student setting	52
B	RSB solution for the random inputs/outputs	53
B.1	Entropic part of the free-energy	53
B.1.1	Entropic part of the free-energy due to ‘bonds’	53
B.1.2	Entropic part of the free-energy due to ‘spins’	54
B.2	Interaction part of the free-energy	56

B.3	Saddle point equations	57
B.3.1	Variation of $q_i(l)$'s	57
B.3.2	Variation of $G_i(l)$'s	58
B.3.3	Procedure to solve the saddle point equations	58
C	RSB solution for the teacher-student setting	59
C.1	Entropic part of the free-energy	59
C.1.1	Entropic part of the free-energy due to 'bonds'	59
C.1.2	Entropic part of the free-energy due to 'spins'	60
C.2	Interaction part of the free-energy	61
C.3	Saddle point equations	61
C.3.1	Variation of $q_i(l)$'s	61
C.3.2	Variation of $G_i(l)$'s	62
C.3.3	Variation of r	62
C.3.4	Variation of R	63

1 Introduction

Machine learning by deep neural networks (DNN) is successful in numerous applications [1]. However, it remains challenging to understand why DNNs actually work so well. Given the enormous parameter space, which is typically orders of magnitude larger than that of the data space, and the flexibility of non-linear functions used in DNNs, it is not very surprising that they can express complex data [2]. What is surprising is that such extreme machines can be put under control. On one hand, one would naturally fear that learning such a huge number of parameters would be extremely time-consuming because the fitness landscape is presumably quite complex with many local traps. Moreover, over-fitting or poor generalization ability seems unavoidable in such over-parametrized machines. We would not dare to fit a data set of 10 points by a 100th order polynomial, which does not make sense usually. Quite unexpectedly, these issues seem to be somehow resolved in practice and such extreme machines turned out to be very useful. Thus it is a very interesting scientific problem to uncover what is going on in DNNs [3, 4]. This is also important in practice because we wish to use DNNs not merely as mysterious black boxes but control/design them in rational ways. In the present paper we develop a statistical mechanical approach based on the replica method to obtain some insights into these issues.

In this paper, we investigate a class of simple machines made of feed-forward networks of layered perceptrons whose depth is L and the width is N (see Fig. 1). Such a machine is parametrized by a configuration of synaptic weights in the hidden layers. For a given pair of inputs/outputs patterns imposed on the input and output layers, there can be different realizations of the synaptic weights that match the same constraints. We call each of them as a 'solution'. Following the work of Gardner [5, 6] for the single perceptron, we consider statistical mechanics of the design space of the neural network which is compatible with a large number $M = \alpha N$ patterns of training data, in the large width $N \rightarrow \infty$ limit with fixed α . For the choice of the training data, we consider two simple scenarios: 1) pairs of purely

random inputs/outputs patterns 2) teacher-student setting - pairs of random input and the corresponding output of a teacher machine with random synaptic weights are handed over to a student machine.

From a broader perspective, the setting 1) can be viewed as a random constraint satisfaction problem (CSP) [7, 8], which is deeply related to the physics of glass transitions and jamming [9–11]. In the context of neural networks, it is a standard setting to study the storage capacity [5, 12]. If α is small so that the constraint is weak enough, it is natural to expect that the phase space looks like that of a liquid: there are so many realizations of machines compatible with a given set of constraints that essentially all solutions are continuously connected. Increasing α the system becomes more constrained so that the volume of the solution space shrinks and ultimately vanishes at some critical value α_j . This is an SAT/UNSAT (jamming) transition and α_j defines the storage capacity. Interestingly, before reaching α_j , the solution space can become clustered into mutually disconnected islands. This is a glass transition and it accompanies some type of replica symmetry breaking (RSB) [13, 14]. Recently non-trivial glass transitions accompanying continuous replica symmetry breaking, which imply the emergence of hierarchical free-energy landscape and ultrametricity [14–17], and common jamming critically as that of the hard-spheres [10] were found in a family of CSPs including a single perceptron problem [18, 19] and a family of vectorial spin models [20]. Understanding the nature of such glass transitions and jamming is a fundamental problem in CSPs since it is intimately related to the efficiency of algorithms to solve CSPs. In the context of DNN, it is certainly important to understand the characteristics of the free-energy landscape to understand the efficiency of various learning algorithms for DNNs [21–23].

On the other hand the setting 2), is a statistical inference (SI) problem. While the constraint satisfaction problems are related to the physics of glass transitions and jamming, solving a statistical inference problem can be said to be equivalent to searching of a hidden (planted) crystalline state [8]. In the context of neural networks, it is a standard setting to study *learning* [6, 12]. As α becomes sufficiently large, the synaptic weights of the student machine starts to become closer to those of the teacher machine. If this happens, the student machine starts to generalize: the probability that the student machine yields the same output as the teacher machine for a test data (not used during training), increases with α . Although very simple, this setting will provide useful insights into the generalization ability of DNNs.

The present work is following the standard statistical mechanical approach to machine learning [12]. Extension of it to deeper neural networks has remained challenging. Our key strategy is to regard a DNN, not as a system of long-ranged interaction between the input and output through a highly convoluted non-linear mappings but rather as a system with short-ranged interactions between adjacent layers. This is enabled by the 'internal representation' [24], in which one takes into account not only 'bonds' (synaptic weights) but also 'spins' (neurons) in the hidden layers as dynamical variables which are constrained to satisfy proper inputs/outputs relations at each perceptron embedded in the hidden layers. Representing the states of a neuron associated with M -patterns as M -component vectorial spins, the system can be represented as a network of dynamical variables with a large number of components with intermediately dense connections to each other (intermediate between sparse and global coupling) similar to the one studied in [20].

The system is almost disorder-free in the sense that the 'quenched disorder' is present only on the boundaries so that one would fear that the replica theory for the single perceptron [5] cannot be easily extended for DNNs. However, the replica approach is not merely a trick to take the average over the quenched disorder. The recent progress on the exact replica theory

in disorder-free systems like simple hard-spheres [10, 11, 25–27] in the large dimensional limit and disorder-free glassy spin systems [20] have proved that spontaneous replica symmetry breaking (RSB) exist in such systems which become manifest by considering infinitesimal symmetry breaking field explicitly as pointed out by Parisi and Virasoro [28]. One can even study spontaneous glass transitions of multiple degrees of freedoms such as translational and orientational degrees of freedom in aspherical particulate systems by the same approach [29].

The above observations motivate us to investigate the interior of the DNN through local glass or crystalline order parameters, for both the spins (neurons) and bonds (synaptic weights), which are allowed to vary over the space. We formulate a replica theory to analyze the design space of the deep perceptron network analyzing a free-energy expressed as a functional of the space-dependent, local order parameters.

The main result of the present paper is that the solutions of the glass/crystalline order parameters of over-parametrized DNNs become quite heterogeneous in space. In both settings 1) and 2), the amplitude of the order parameters close to the inputs/outputs boundaries become finite and take higher values as the strength of the constraint α increases while the amplitudes decay down to 0 going deeper into the bulk. Moreover, in the case of setting 1) random inputs/outputs, even the pattern of the replica symmetry breaking (RSB) varies in space: it is most complex close to the boundaries with $k(+\text{continuous})$ -RSB, which becomes $k-1(+\text{continuous})$ -RSB in the next layer, ... down to a replica symmetric (0 RSB) state in the central part. The thickness ξ of the region around the boundaries where the glass/crystalline order parameters become finite roughly scales as $\xi \propto \ln \alpha$. This implies the storage capacity of the network $\alpha_j(L)$ for *typical* instances grows exponentially fast with the depth L , while the worst case scenarios [30] would predict linear growth with L .

Thus if the network is deep enough $L > \xi$, the central part of a typical network remains in the liquid phase: there are so many possibilities left in the central part all of which meet the same constraints imposed at the boundaries. The heterogeneous profile of the order parameters should have important implications on how DNNs work.

The organization of the paper is the following. In sec. 2 we define the deep neural network model studied in the present paper and explain the two scenarios : 1) random inputs/outputs and 2) teacher-student setting. In sec. 3 we formulate a replica theory to perform statistical mechanical analyses of the design space of the deep neural network. In sec. 3.3 and sec. 3.5 we study the cases of 1) random inputs/outputs and 2) teacher-student settings respectively using the replica theory. In sec. 4, we present some results of numerical simulations to examine the theoretical predictions. Finally in sec. 5, we conclude the paper and present some outlook. In the appendices A, B and C we present some details of the theoretical formulation.

2 Model

2.1 Multi-layer feed-forward network

We consider a simple multi-layer neural network (See Fig. 1) which consists of an input layer ($l = 0$), output layer ($l = L$) and hidden layers ($l = 1, 2, \dots, L-1$). Each layer consists of $i = 1, 2, \dots, N$ neurons $\mathbf{S}_{l,i}$, each of which consists of M -component Ising spins $\mathbf{S}_{l,i} = (S_{l,i}^1, S_{l,i}^2, \dots, S_{l,i}^M)$ with $S_{l,i}^\mu = \pm 1$. Here the label $\mu = 1, 2, \dots, M$ is used to distinguish different firing patterns of the neurons (spins). The spins in the inputs/outputs layers represent 'data' provided by external sources. We follow the notation of [20] to represent

a factor node, which is a perceptron here, as \blacksquare . We consider a feed-forward network of $N_{\blacksquare} = NL$ perceptrons. A perceptron \blacksquare receives N inputs from the outputs of perceptrons $\blacksquare(k)$ ($k = 1, 2, \dots, N$) in the previous layer, weighted by $\mathbf{J}_{\blacksquare} = (J_{\blacksquare}^1, J_{\blacksquare}^2, \dots, J_{\blacksquare}^N)$. Its output S_{\blacksquare} is given by,

$$S_{\blacksquare}^{\mu} = \text{sgn} \left(\frac{1}{\sqrt{N}} \sum_{k=1}^N J_{\blacksquare}^k S_{\blacksquare(k)}^{\mu} \right) \quad \mu = 1, 2, \dots, M. \quad (1)$$

We assume that the synaptic weights J_{\blacksquare}^k take real numbers normalized such that,

$$\sum_{k=1}^N (J_{\blacksquare}^k)^2 = N. \quad (2)$$

For simplicity, we call the variable for the neurons $S_{l,i}$'s as 'spins', and the synaptic weights J_{\blacksquare}^k s as 'bonds' in the present paper.

We will consider random input data of size

$$N_{\text{data}} = NM = N^2\alpha \quad (3)$$

while the number of parameters is

$$N_{\text{parameter}} = N_{\blacksquare}N = N^2L. \quad (4)$$

Here we introduced a parameter

$$\alpha \equiv \frac{M}{N}. \quad (5)$$

The task of *learning* is to design the synaptic weights J_{\blacksquare}^k to build a mapping (function) between the imposed random input data and output data, which can be completely different, by a network of width N and depth L .

We will consider the limit $N, M \rightarrow \infty$ with fixed α . This scaling is known for the single perceptron [5] and we will find that it continues to be the key parameter for the bigger network much like the inverse temperature for condensed matters. Apparently the system is over parametrized $N_{\text{parameter}} > N_{\text{input}}$ if it is deep enough $L > \alpha$. (Actually our results imply that typical storage capacity grows exponentially with the depth L as we see later so that the system is essentially over-parametrized if $L > \ln \alpha$. (see sec. 3.3.5))

The trajectories of such highly non-linear mapping as Eq. (1) along the random deep network is known to be highly chaotic [31, 32]: small differences in the input data leads to rapid decorrelation of the resulting trajectories. This feature is considered as responsible for the high expressive power of DNNs [32]. Similarly, small changes made on the weights J_{\blacksquare}^k also leads to chaotic decorrelation of trajectories [33]. But then we immediately face the obvious question: how the high generalization ability observed in DNNs can be explained when the system is so chaotic? In the present paper we construct a statistical mechanics point of view to answer such questions. Out of the set of all possible realizations of random deep networks, which typically give chaotic dynamics, we focus on a substantially smaller sub-manifold of it in which all trajectories (accidentally) meet the externally imposed boundary conditions put at the two opposite ends. This *selection* (learning) may have significant consequences on the properties of the resultant ensemble.

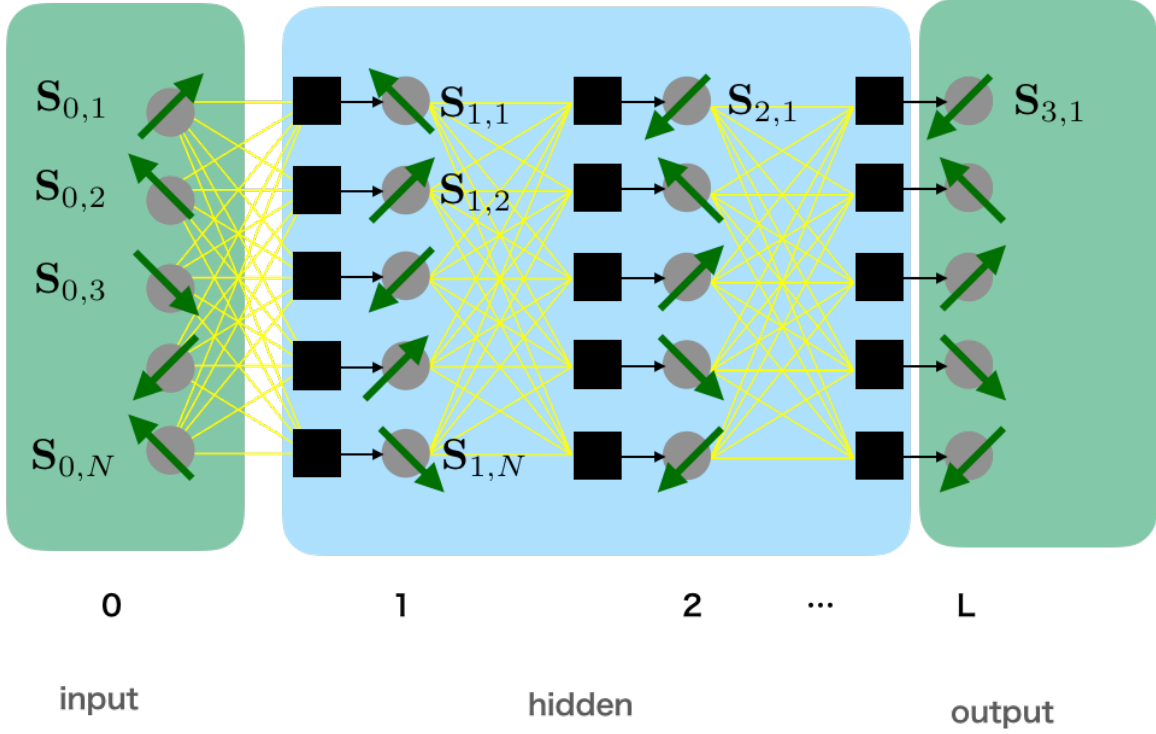


Figure 1: A simple multi-layer perceptron network of depth L and width N . In this example the depth is $L = 3$. Each arrow represent a M -component vector spin $\mathbf{S}_i = (S_i^1, S_i^2, \dots, S_i^M)$ with its component $S_i^\mu = \pm 1$ representing the state of a 'neuron' in the μ -th pattern.

Following the pioneering work by Gardner [5,6] we consider the volume of the design space of the system associated with a given set of inputs/outputs patterns represented by \mathbf{S}_0 and \mathbf{S}_L , which can be expressed as,

$$\begin{aligned}
 V(\mathbf{S}_0, \mathbf{S}_L) &= e^{NMS(\mathbf{S}_0, \mathbf{S}_L)} = \left(\prod_{\mathbf{J}} \text{Tr}_{\mathbf{J}} \right) \left(\prod_{\mathbf{S} \in \text{output}} \text{Tr}_{\mathbf{S}} \right) \prod_{\mu=1}^M \prod_{\mathbf{S}} e^{-\beta V(r_{\mathbf{S}}^\mu)} \\
 &= \int_{-\infty}^{\infty} \prod_{\mathbf{J}} \prod_{j=1}^N \left\{ dJ_{\mathbf{J}}^j \delta \left(\sum_{k=1}^N (J_{\mathbf{J}}^k)^2 - N \right) \right\} \left(\prod_{l=1}^{L-1} \prod_{i=1}^N \sum_{S_{l,i}^\mu = \pm 1} \right) \prod_{\mu=1}^M \prod_{\mathbf{S}} e^{-\beta V(r_{\mathbf{S}}^\mu)} \quad (6)
 \end{aligned}$$

where

$$e^{-\beta V(r)} = \theta(r) \quad (7)$$

and we introduced the 'gap',

$$r_{\mathbf{S}}^\mu \equiv S_{\mathbf{S}}^\mu \sum_{i=1}^N \frac{J_{\mathbf{S}}^i}{\sqrt{N}} S_{\mathbf{S}(i)}^\mu \quad (8)$$

Note that in Eq. (6) summations are taken not only over the bonds (synaptic weights) but also over the spins (neurons) in the hidden layers. This is the internal representation [24]

which allows us to avoid viewing the system as a system with long-ranged interaction between the input and output through a highly convoluted non-linear mappings but rather as a system with short-ranged interactions between adjacent layers. From a physicist's point of view, this is far more convenient. Indeed we can now write the effective Hamiltonian of the system as

$$\mathcal{H}_{\text{eff}} = \sum_{\mu=1}^M \sum_{\blacksquare} V \left(S_{\blacksquare}^{\mu} \sum_{i=1}^N \frac{J_{\blacksquare}^i}{\sqrt{N}} S_{\blacksquare(i)}^{\mu} \right) \quad (9)$$

This trick works because of the simple 'sgn' activation function Eq. (1) we consider in the present paper. Let us emphasize here that both the spins $S_{\blacksquare s}^{\mu}$ and bonds J_{\blacksquare}^i are dynamical variables, except for the spins on the boundaries $l = 0, L$ which are frozen.

Now our task is to analyze the equilibrium statistical mechanics of the system of many variables with the effective Hamiltonian Eq. (9). In this point of view, we can forget about the 'feed-forwardness' of the original dynamical representation Eq. (1). The system is locally asymmetric (at the scale of each layer) but globally homogeneous except at the boundaries. In the $N \rightarrow \infty$ limit, even the latter should become irrelevant.¹

The problem at our hands is similar to the statistical mechanics of an assembly of hard-spheres. Each of the configurations which meet the hard-core constraint Eq. (7) represents a valid trajectory (more precisely a set of M perceptron trajectories all of which meet the corresponding inputs/outputs boundary conditions) of the original feed-forward problem. Like in the statistical mechanics of hard-spheres [11], everything that matters here is the entropy effect. For instance, we can expect that assembly of trajectories which consists of many nearby valid trajectories (which meet the same inputs/outputs boundary conditions) have richer (local) entropy so that they make important contributions to the total entropy. This corresponds to the notion of 'free-volume' of an assembly of hard-spheres. Such an equilibrium statistical mechanics may not be merely academic. Indeed the standard schemes of deep learning involve Stochastic Gradient Descent (SGD) algorithms [1] which explores the solution space of DNNs in a stochastic way. There also trajectories with richer local entropy would appear more often during the sampling. In this paper we will find often that the analogy with the physics of hard-sphere glass [11] is very useful to understand our results in physical terms.

2.2 Two scenarios for inputs/outputs patterns

For the input and output patterns \mathbf{S}_0 and \mathbf{S}_L , we consider the following two scenarios.

2.2.1 Random inputs/outputs

As the simplest setting, we consider the case of completely random inputs/outputs patterns, which is the standard setting to study the storage capacity of the perceptrons [5, 12]. More precisely all components of $\mathbf{S}_{0,i} = (S_{0,i}^1, S_{0,i}^2, \dots, S_{0,i}^M)$ and $\mathbf{S}_{L,i} = (S_{L,i}^1, S_{L,i}^2, \dots, S_{L,i}^M)$ for $i = 1, 2, \dots, N$ are assumed to be iid random variables which take Ising values ± 1 . As we noted in the introduction, this setting can be regarded as a random constraint satisfaction problem (CSP).

¹For instance, think about cutting out a square of size $L \times L$ in an arbitrary way out of a bigger triangular lattice. The boundary of the resultant square is inhomogeneous. But the effect of the inhomogeneity should become irrelevant in $L \rightarrow \infty$ for thermodynamic quantities such as the surface energy per unit length.

2.2.2 Teacher-student setting

As a complementary approach, we consider the teacher-student setting, which is a standard setting to study statistical inference problems [8]. We consider two machines : a teacher machine and student machine and assume that they have exactly the same architecture, i.e. the same width N and the depth L .

We assume that the teacher is a 'quenched-random teacher': the set of the synaptic weights $\{(J_{\blacksquare}^k)_{\text{teacher}}\}$ of the teacher machine are iid random variables which obey the normalization Eq. (2). Such a teacher machine is subjected to a set of random inputs, which are iid random variables, $\mathbf{S}_{0,i} = (S_{0,i}^1, S_{0,i}^2, \dots, S_{0,i}^M)$ for $(i = 1, 2, \dots, N)$ and produces the corresponding set of outputs,

$$(\mathbf{S}_{L,i})_{\text{teacher}} = ((S_{L,i}^1)_{\text{teacher}}, (S_{L,i}^2)_{\text{teacher}}, \dots, (S_{L,i}^M)_{\text{teacher}}) \quad (10)$$

The task of the student machine is to try to infer the synaptic weights $\{(J_{\blacksquare}^k)_{\text{teacher}}\}$ of the teacher machine, by adjusting its own synaptic weights $\{(J_{\blacksquare}^k)_{\text{student}}\}$ such that it successfully reproduces all the outputs of the teacher $(\mathbf{S}_{L,i})_{\text{teacher}}$ starting from the same input data.

Note that the student is given the full information of the input $\mathbf{S}_{0,i}$ and the output of the teacher $(\mathbf{S}_{L,i})_{\text{teacher}}$ plus full information on the architecture of the teacher. In the context of statistical inference, this is an idealized situation called as Bayes optimal case [8] and we limit ourselves to this in the present paper for simplicity.

3 Replica theory

Now let us formulate a replica approach to study the solution space of the deep neural network. To study the case of random inputs/outputs (sec. 2.2.1) we consider n replicas $a = 1, 2, \dots, n$ which are independent machines subjected to the common set of inputs $\mathbf{S}_{0,i}$ and outputs $\mathbf{S}_{L,i}$ for $i = 1, 2, \dots, N$. For the case of the teacher-student setting (sec. 2.2.2) we consider $n = 1 + s$ replicas, with replica $a = 0$ to represent the teacher machine and other replicas $a = 1, 2, \dots, s$ to represent the replicas of the student.

3.1 Order parameters

For the setting with random inputs/outputs, which is a constraint satisfaction problem, we anticipate that the solution space exhibit clustering (glass transition) as we noted in the introduction. Thus it is natural to consider order parameters that detect the glass transitions. Given the dense connections of the network, we naturally introduce 'local' glass order parameters (see [20]),

$$Q_{ab,\blacksquare} = \frac{1}{N} \sum_{i=1}^N (J_{\blacksquare}^i)^a (J_{\blacksquare}^i)^b \quad q_{ab,\blacksquare} = \frac{1}{M} \sum_{\mu=1}^M (S_{\blacksquare}^{\mu})^a (S_{\blacksquare}^{\mu})^b \quad (11)$$

Note that the normalization condition for the bonds Eq. (2) and the spins (which take Ising values ± 1) implies $Q_{aa,\blacksquare} = q_{aa,\blacksquare} = 1$.

For the teacher-student setting, we continue to use the above order parameters for $a = 0, 1, 2, \dots, s$ replicas where 0-th replica is for the teacher machine. Thus $Q_{0a} = Q_{a0}$ and $q_{0a} = q_{a0}$ for $a = 1, 2, \dots, s$ represent the overlap between the teacher machine and student machines.

There are two comments regarding some trivial symmetries left in the system. First, the system is symmetric under permutations of the labels put on the data $\mu = 1, 2, \dots, M$. The labels put on different replicas could be permuted differently. In the 2nd equation of Eq. (11) it is assumed that all replicas follow the same labels breaking this permutation symmetry. Second, the system is symmetric under permutations of perceptrons \blacksquare within the same layer and the permutations could be done differently on different replicas. In Eq. (11), this permutation symmetry is also broken. Note that solutions with other permutations regarding the two symmetries mentioned above give exactly the same free-energy so that one choice is enough.

3.2 Replicated Gardner volume

The Gardner's volume Eq. (6) fluctuates depending on the realizations of the boundaries \mathbf{S}_0 and \mathbf{S}_L . In the present paper we wish to analyze the *typical* behavior for stochastic realizations of the boundaries. To this end we consider the replicated phase space volume (the Gardner volume),

$$\begin{aligned} V^n(\mathbf{S}_0, \mathbf{S}_L) &= e^{NM S_n(\mathbf{S}_0, \mathbf{S}_L)} \\ &= \prod_{a=1}^n \left(\prod_{\blacksquare} \text{Tr} \mathbf{J}_{\blacksquare}^a \right) \left(\prod_{\blacksquare \setminus \text{output}} \text{Tr} \mathbf{S}_{\blacksquare}^a \right) \left\{ \prod_{\mu, \blacksquare, a} \int \frac{d\eta_{\mu, \blacksquare, a}}{\sqrt{2\pi}} e^{-\beta V(r_{\blacksquare, a}^{\mu})} \right\} \end{aligned} \quad (12)$$

with

$$r_{\blacksquare, a}^{\mu} \equiv (S_{\blacksquare}^{\mu})^a \sum_{i=1}^N \frac{(J_{\blacksquare}^i)^a}{\sqrt{N}} (S_{\blacksquare(i)}^{\mu})^a \quad (13)$$

The *typical* behavior can be studied by considering the $n \rightarrow 0$ limit [34], i. e. $\partial_n \overline{V^n(\mathbf{S}_0, \mathbf{S}_L)}^{\mathbf{S}(0), \mathbf{S}(L)} \Big|_{n=0}$ where the overline represents the average over the different realizations of the boundaries (see below for the details.)

As shown in appendix A, following similar steps as in [20], we obtain the replicated free-entropy functional $S_n(\{Q_{\blacksquare}, q_{\blacksquare}\})$ in terms of the order parameters Q_{\blacksquare} and q_{\blacksquare} defined in Eq. (11) in the limit $N, M \rightarrow \infty$ with fixed $\alpha = M/N$. Given the structure of the network, it is natural to assume that order parameters are uniform within each layer $l = 0, 1, 2, \dots, L$,

$$Q_{ab, \blacksquare} = Q_{ab}(l) \quad q_{ab, \blacksquare} = q_{ab}(l), \quad (14)$$

To represent the quenched boundaries, we impose the boundary conditions on the inputs/outputs layers by simply putting $q_{ab}(0) = q_{ab}(L) = 1$ (see below). As explained in A.3.2 this is a slightly annealed boundary condition in the sense that sub-extensive fluctuations on the boundaries are not excluded. While this is not a faithful realization of the quenched boundary condition, it significantly simplifies the theory allowing us to make analytical progress.

The above general formulation can be adapted for the two scenarios introduced in sec. 2.2 as follows,

- Random inputs/outputs

In the case of random inputs/outputs (sec. 2.2.1) we consider the free-energy functional,

$$\frac{-\beta F[\{\hat{Q}(l), \hat{q}(l)\}]}{NM} = \frac{\partial_n \overline{V^n(\mathbf{S}_0, \mathbf{S}_L)}^{\mathbf{S}_0, \mathbf{S}_L} \Big|_{n=0}}{NM} = \partial_n S_n[\{\hat{Q}(l), \hat{q}(l)\}] \Big|_{n=0}. \quad (15)$$

The presence of the imposed random inputs/outputs can be specified by providing values of $q_{ab}(0)$ and $q_{ab}(L)$. Since all replicas are subjected to the same inputs and outputs, we can simply set,

$$q_{ab}(0) = q_{ab}(L) = 1. \quad (16)$$

As we discuss later we will also consider the case of fluctuating boundary conditions.

- Teacher-student setting

In the case of the teacher-student setting (sec. 2.2.2) we consider instead the so called Franz-Parisi potential [35],

$$\begin{aligned} \frac{-\beta F_{\text{teacher-student}}[\{\hat{Q}(l), \hat{q}(l)\}]}{NM} &= \frac{\overline{\partial_s V^{1+s}(\mathbf{S}_0, \mathbf{S}_L(\mathbf{S}_0, \mathcal{J}_{\text{teacher}}))}^{\mathbf{S}_0, \mathcal{J}_{\text{teacher}}}}{NM} \Big|_{s=0} \\ &= \partial_s S_{1+s}[\{\hat{Q}(l), \hat{q}(l)\}] \Big|_{s=0}. \end{aligned} \quad (17)$$

where the over-line denotes the average over the imposed random inputs imposed commonly on both the teacher and student machines. The outputs are just those of the teacher machine $a = 0$, $\mathbf{S}_L(\mathbf{S}_0, \mathcal{J}_{\text{teacher}})$ which are of course functions of the inputs \mathbf{S}_0 and the synaptic weights of the teacher machine $\mathcal{J}_{\text{teacher}} = \{(J_{\blacksquare}^k)_{\text{teacher}}\}$. Since both the teacher and student machines are subjected to the same inputs, we set,

$$q_{ab}(0) = 1 \quad (18)$$

for $a, b = 0, 1, \dots, s$. In addition, since the outputs of the student machine are forced to agree perfectly with that of the teacher machine we set,

$$q_{ab}(L) = 1 \quad (19)$$

for $a, b = 0, 1, \dots, s$.

3.3 Random inputs/outputs

Now we analyze the case of random inputs/outputs introduced in sec. 2.2.1 by the replica theory using the Parisi's ansatz explained in sec. A.5.1. We will consider not only the usual case of 'quenched' random inputs/outputs [5] (sec. 3.3.1) but also the case of 'fluctuating' random inputs/outputs (sec. 3.4).

We assume the Parisi's ansatz with k -step RSB (see sec. A.5) for the order parameters of the bonds $Q_i(l)$ for $l = 1, 2, \dots, L$ and spins $q_i(l)$ for $l = 1, 2, \dots, L - 1$ which characterize the Parisi's matrices (see Fig. 20). We solve the saddle point equations numerically to obtain the glass order parameters as described in sec. B.3.3. For $i = 0, 1, 2, \dots, k$ we have parameter m_i (see Eq. (84)). In the $k \rightarrow \infty$ limit, $Q_i(l)$ s become continuous functions $Q(x, l)$ which can be well approximated by $Q_i(l)$ plotted vs m_i for large enough k (See Fig. 20 d)). The same holds for the order parameter of spins $q_i(l)$ s, i. e. we obtain continuous functions $q(x, l)$ in $k \rightarrow \infty$ limit. From the functions $Q(x, l)$ and $q(x, l)$, we can obtain the overlap distribution functions $P(q, l)$ and $P(Q, l)$ (see Eq. (86)).

3.3.1 “Quenched” boundary

Let us start with the case of the “quenched” boundary : the configurations of the spins on the input and output boundaries are chosen randomly and then fixed (Fig. 2). It amounts to choose ‘replica symmetric’ boundaries, because all replicas are subjected to the same inputs/outputs pattern, we put,

$$q_{ab}(0) = 1 \quad q_{ab}(L) = 1 \quad (20)$$

or

$$q_0(0) = q_0(L) = 1 \quad (21)$$

$$q_i(0) = q_i(L) = 0 \quad (i = 1, 2, \dots, k) \quad (22)$$

We note again that this is not a faithful realization of quenched boundary condition because we are not excluding sub-extensive fluctuations

In the following we present results using $k = 100$ step RSB and the depth of the system $L = 5 - 20$. Because of the choice of the boundary condition, the system becomes symmetric with respect to reflections at the center: we confirmed that the solutions satisfy $q_i(l) = q_i(L-l)$ and $Q_i(l) = Q_i(L-l)$. Maybe one would not easily expect such asymmetry in the feed-forward network. However, let us recall that we can forget about ‘feed-forwardness’ of the original dynamical problem in our statistical mechanics’ problem as we emphasized below Eq. (9). In finite N systems some asymmetry can be present but it should disappear in $N \rightarrow \infty$ limit as we noted in sec. 2.1.



Figure 2: “Quenched” boundary

3.3.2 Liquid phase

For small $\alpha = M/N$ we find the whole system is in the liquid phase where the glass order parameters are all zero: for $i = 1, 2, \dots, k$ $q_i(l) = 0$ ($l = 1, 2, \dots, L-1$) and $Q_i(l) = 0$ ($l = 1, 2, \dots, L$). This means that the parameter space is so large so that there are simply too many solutions compatible with the constraints. Here the replica symmetry is not broken. This means that the solution space looks like a giant continent in which all typical solutions are continuously connected to each other.

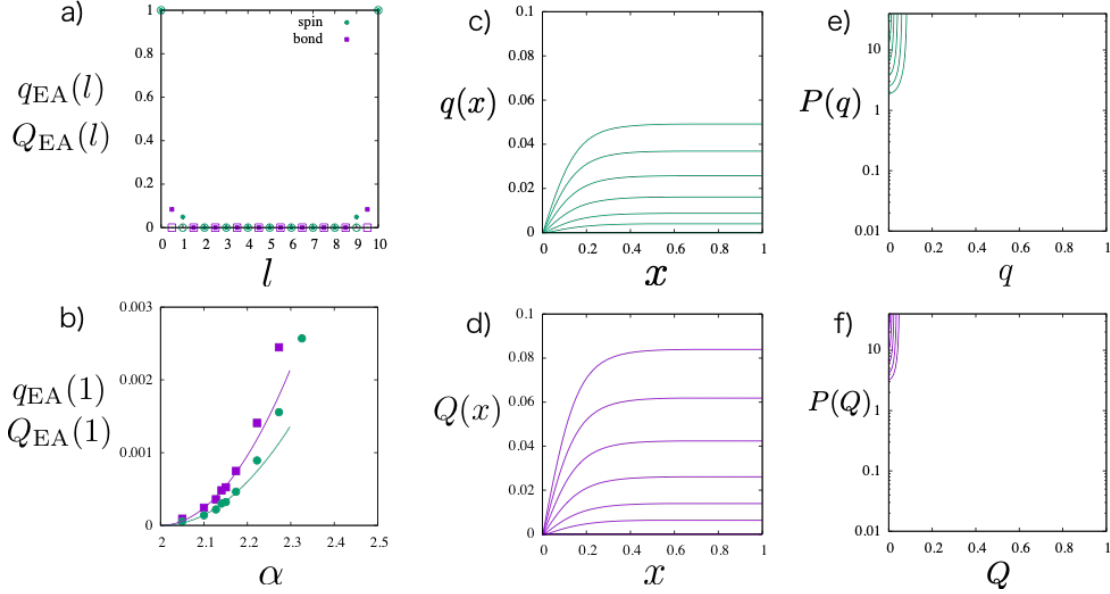


Figure 3: The 1st glass transition: a) spatial profile of the Edwards-Anderson (EA) order parameter for spins $q_{\text{EA}}(l)(=q_{k=100}(l))$ and bonds $Q_{\text{EA}}(l)(=Q_{k=100}(l))$ slightly before $\alpha = 2.0$ (empty symbols)/after $\alpha = 3.125$ (filled symbols) the 1st glass transition. The depth is $L = 10$ in this example. b) Evolution of the EA order parameters $q_{\text{EA}}(1) = q_k(1)$ and $Q_{\text{EA}}(1) = Q_k(1)$ at the 1st layer after passing the critical point of the 1st glass transition $\alpha_g(1) \simeq 2.03$. c),d) Glass order parameter function $q(x, l)$ for spins and $Q(x, l)$ for bonds at the 1st layer $l = 1$ at around the 1st glass transition. Here $\alpha = 3.13, 2.94, 2.78, 2.63, 2.50, 2.38$ from the top to the bottom. e),f) the overlap distribution function of spins $P(q) = dx(q)/dq$ and bonds $P(Q) = dx(Q)/dQ$ (see Eq. (86)).

3.3.3 The 1st glass transition

With increasing α , the system becomes more constrained. We find a continuous (2nd order) glass transition at $\alpha_g(1) \simeq 2.03$ on the 1st layers $l = 1, L - 1$ just beside the “quenched” inputs/outputs boundaries as shown in Fig. 3 a). The emergence of the finite glass order parameters signals that the solution space is shrinking there. The rest of the system ($l = 2, 3, \dots, L - 2$) remains in the liquid phase $q_{\text{EA}}(l) = Q_{\text{EA}}(l) = 0$ at this stage. As shown in Fig. 3 b) the Edwards-Anderson (EA) order parameters of the spins $q_{\text{EA}}(l) = q_k(l)$ and bonds $Q_{\text{EA}}(l) = Q_k(l)$ at the 1st layer $l = 1$ grow continuously across the critical point $\alpha_g(1)$. Exactly the same happens on the other side at $l = L - 1$. The fact that the glass transition takes place in a *continuous* way, is different from the random first-order transition (RFOT) in structural glass models [9–11, 36–39].

Since the transition is a 2nd order transition, the liquid state $(Q, q) = (0, 0)$ becomes unstable and a glass state can emerge smoothly at the transition. Then what would play the role of symmetry breaking field (see sec. A.1.3) to pick up a particular glass state out of many candidates? In the learning dynamics, the random inputs/outputs data imposed at the boundaries ($l = 0$ and $l = L$) and choices of the initial condition for learning will play the role of the symmetry breaking field.

The fact that the glassy regions emerge next to the boundaries is reasonable because the effect of constraints should be strongest there. The situation does not change even in the limit $L \rightarrow \infty$ where the two boundaries are infinitely separated. But this may appear bizarre. Why specification of the just the initial condition or final condition for the dynamics Eq. (1) can constrain the 1st layers ($l = 1, L - 1$) so much? With such a huge liquid-like region left in the bulk, any information starting from the input layer will be completely randomized before reaching the output layer. Here let us remind ourselves that we are considering statistical mechanics of the solution space which is like the statistical mechanics of hard-spheres as we noted below Eq. (9). The reason for the glass transition on the 1st layers is an entirely entropic reason: a certain set of configurations of the bonds in the 1st layers ($l = 1, L - 1$) allow exceedingly larger fluctuation in the hidden layers compared with others so that they dominate the entropy of the solution space. In this sense it is a glass version of entropy-driven ordering like the crystallization of hard-spheres (Alder transition) [40] and order-by-disorder transitions oftenly observed in frustrated magnets [41].

As shown in Fig. 3 c,d), the functions $q(x, l)$ and $Q(x, l)$ at the 1st layers $l = 1, L - 1$ are continuous functions of x with plateaus at q_{EA} and Q_{EA} for some range $x_1(\alpha) < x < 1$ with $x_1(\alpha)$ decreasing with α . Thus the replica symmetry is fully broken much as in the SK model for spin-glasses [13, 14]. Correspondingly the overlap distribution functions Eq. (86) $P(q) = dx(q)/dq$ and $P(Q) = dx(Q)/dQ$ shown in Fig. 3 e,f), exhibit delta peaks at $q = q_{\text{EA}}$, $Q = Q_{\text{EA}}$ plus non-trivial continuous parts extending down to $q = 0$ and $Q = 0$.

The RSB means that the solution space is now clustered, i. e. the giant continent of the solutions is now split into mutually disconnected islands. The EA order parameters q_{EA} and Q_{EA} represent the size of the islands, i. e. larger EA order parameters mean smaller islands. The probability that two solutions sampled in equilibrium belong to the same island is $1 - x_1(\alpha)$. The continuously changing part of the functions $Q(x)$ and $q(x)$ in the range $0 < x < x_1(\alpha)$ means that the islands or clusters are organized into meta-clusters, meta-meta-clusters,... in a hierarchical way: the mutual overlap (distance in the phase space) between the islands is ultrametric [14–17, 42]. In general, the continuous RSB phase is marginally stable [14, 27, 43, 44].

The strong spatial heterogeneity of the glass order parameters is striking. It means that the solution space is clustered in the 1st layers but the islands of solutions merge into a big continent in the rest of the system which remains in the liquid phase. The spatial heterogeneity is very interesting from the algorithmic point of view since this implies the learning dynamics is very fast except next to the boundaries. Moreover, it is tempting to speculate that the first dynamics in the liquid region will assist the equilibration of the glassy regions close to the boundaries.

3.3.4 The 2nd glass transition

Increasing α further we meet another glass transition at $\alpha_g(2) \simeq 15.9$ by which the 2nd layers $l = 2, L - 2$ become included in the glass phase while the rest of the system $l = 3, 4, \dots, L - 3$ still remains in the liquid phase as shown in Fig. 4 a). The glass phase has grown a step further into the interior. The transition is again a continuous one as can be seen in Fig. 4 b) where we display the EA order parameters $q_{\text{EA}}(l) = q_k(l)$ and $Q_{\text{EA}}(l) = Q_k(l)$ at $l = 2$. Exactly the same happens on the other side at $l = L - 2$.

As shown in Fig. 4 c,d), the functions $q(x, l)$ and $Q(x, l)$ at the 2nd layers $l = 2, L - 2$ are continuous functions of x with plateaus at $q_{\text{EA}}(2)$ and $Q_{\text{EA}}(2)$ in some range $x_2(\alpha) < x < 1$

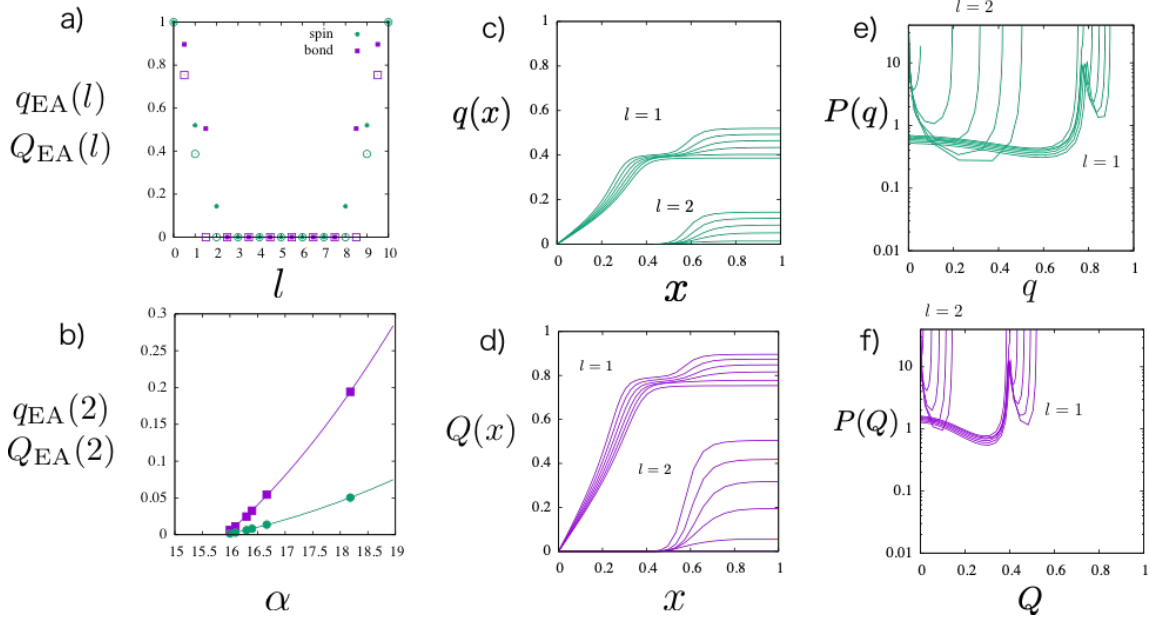


Figure 4: The 2nd glass transition: a) spatial profile of the Edwards-Anderson (EA) order parameter for spins $q_{\text{EA}}(l)$ and bonds $Q_{\text{EA}}(l)$ slightly before $\alpha = 15.38$ (empty symbols)/after $\alpha = 25$ (filled symbols) the 2nd glass transition. The depth is $L = 10$ in this example. b) Evolution of the EA order parameters $q_{\text{EA}}(2)$ and $Q_{\text{EA}}(2)$ at the 2nd layer after passing the critical point of the 2nd glass transition $\alpha_g(2) \simeq 15.9$. c),d) Glass order parameter function $q(x, l)$ for spins and $Q(x, l)$ for bonds at the 1st and 2nd layers at around the 2nd glass transition. Here $\alpha = 25.0, 22.2, 20.0, 18.2, 16.7, 15.4$ from the top to the bottom. e),f) the overlap distribution function of spins $P(q) = dx(q)/dq$ and bonds $P(Q) = dx(Q)/dQ$ Eq. (86).

with $x_2(\alpha)$ decreasing with α . A marked difference to the case of the 1st glass transition which happened at the 1st layers $l = 1, L - 1$ is that the order parameters become finite only in some range $x_2(\alpha) \lesssim x < 1$. As a result, it looks approximately like a step function with the step located at $x_2(\alpha)$. As shown in Fig. 4 e),f), this amounts to induce a delta peak not only at $q_{\text{EA}}(2)$ ($Q_{\text{EA}}(2)$) but also at $q = Q = 0$ in the distribution of the overlaps. In a sense the solution is approximately like one step RSB in the random energy model [45] or models for structural glasses [9–11, 36–39] if we neglect the smoothing part of the step function. This means that, roughly speaking, the solution space in the 2nd layers are basically split into islands that are completely dissimilar from each other. Two solutions sampled in equilibrium, in the 2nd layers, belong to the same island whose size is represented by $Q_{\text{EA}}(2)$ and $q_{\text{EA}}(2)$ with probability $1 - x_2(\alpha)$. Otherwise, they belong to different islands which are very far from each other.

Remarkably, the 2nd glass transition induces another continuous glass transition on the 1st layers $l = 1, L - 1$ which were already glassy. Physically, it is natural because the 1st layers are now more constrained than before having two glassy neighbors while they had just one glassy neighbor before. As can be seen in Fig. 4 c),d), an internal step-like structure emerges

continuously within the region where the glass order parameter was flat $x_1(\alpha) < x < 1$ before the 2nd glass transition. As shown in Fig. 4 e),f), the emergence of the internal step amounts to a continuous splitting of the delta peak at $q_{\text{EA}}(1)$ ($Q_{\text{EA}}(1)$) into two peaks (plus a continuous part in between) meaning that the glass phase has become more complex. This means the smallest bundles or islands of the solutions have been split into multiple sub-bundles. In a sense, this is similar to the Gardner transition found originally in Ising p -spin spin-glass models [46] and in the hard-sphere glass in large-dimensional limit [10, 11, 26, 44].

We could say that the situation in the 2nd layers is roughly like a 2 step RSB: if we neglect the smoothing parts, the functions $Q(x)$ and $q(x)$ look approximately like functions with two steps, one at $x_1(\alpha)$ and the other at $x_2(\alpha)$. This means that two solutions sampled in equilibrium, in the 1st layers, belong to the same island whose size is represented by $1 - Q_{\text{EA}}(2) = 1 - Q(x_2(\alpha), 2)$ and $1 - q_{\text{EA}}(2) = 1 - q(x_2(\alpha), 2)$ with probability $1 - x_2(\alpha)$. Otherwise they belong to different islands. However, with a larger probability $1 - x_1(\alpha)$, they belong at least to the same meta-cluster of islands whose size is represented by $1 - Q(x_1(\alpha), 2)$ and $1 - q(x_1(\alpha), 2)$ which are larger than $1 - Q_{\text{EA}}$ and $1 - q_{\text{EA}}$.

After the 2nd glass transition, the glass order parameters have become more heterogeneous in space. Interestingly the internal step of the glass order parameters on the 1st layers $l = 1, L - 1$ is located around $x_2(\alpha)$ being synchronized with the step on the 2nd layers $l = 2, L - 2$. This means that two solutions sampled in equilibrium belong to the same island in the 1st and 2nd layers with the *same* probability $1 - x_2(\alpha)$. This implies that the same bundle of solutions continue in the 1st and 2nd layers. Since the EA order parameters are bigger in the 1st layers, the bundle becomes more spread out in the 2nd layers than in the 1st layers. The bundles are grouped into meta-bundles in the 1st layer which becomes dissociated in the 2nd layers. Finally, all bundles become dissociated and merge into a gigantic liquid continent after the 3rd layers. The two-step dissociation of the bundles of solutions is quite interesting for learning dynamics.

3.3.5 More glass transitions

Now it is easy to imagine that glass phase will grow further invading the liquid phase by increasing α more. As we show in Fig. 5, this is indeed the case. We observe that the glass transition point $\alpha_g(l)$ of the l -th layer (and $L - l$) grows very rapidly, exponentially fast with l as shown in Fig. 6,

$$\alpha_g(l) \sim 2.7(3)e^{1.03(2)l} \quad (23)$$

In other words, the 'penetration depth' of the glass phase ξ_{glass} grows very slowly as,

$$\xi_{\text{glass}}(\alpha) \sim \ln \alpha \quad (24)$$

The results shown in this section is done on systems with $L = 20$ which is still larger than of $2\xi_{\text{glass}}(\alpha) \sim 18$ of $\alpha = 4000$ which is the largest α used in this section. Note that the system is over-parametrized, in the sense that the size of the data Eq. (3) is smaller than that of the parameters Eq. (4), only for $\alpha < 20$. However once the liquid phase is present at the center, the solution for the glass phase does not change with larger L . So that the results presented in this section are essentially in the situation of over parametrization (for typical instances).

The exponential growth of the glass transition point $\alpha_g(l)$ with the depth l implies that the storage capacity $\alpha_j(L)$, which should be greater than $\alpha_g(L)$, also grow exponentially fast with the depth L ,

$$\alpha_j(L) \propto e^{\text{const}L} \quad (25)$$

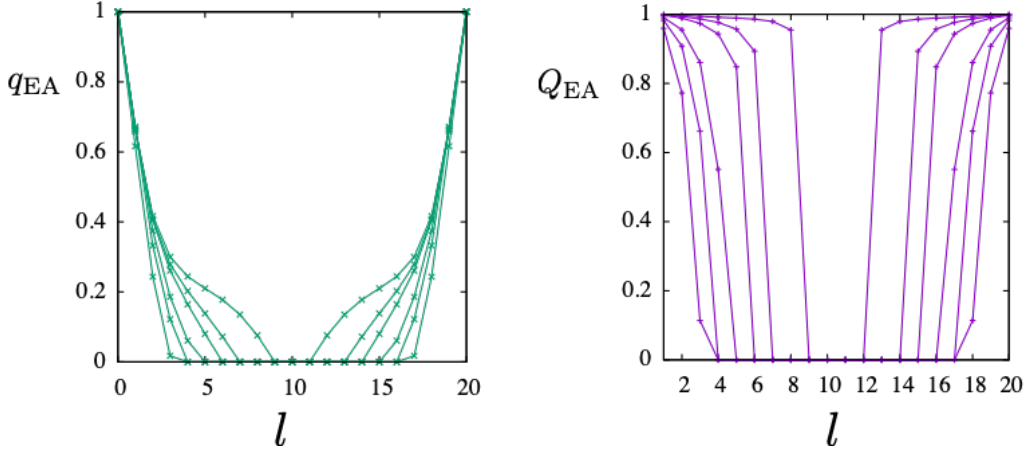


Figure 5: The spatial profile of the EA order parameters $q_{\text{EA}}(l) = q_k(l)$ and $Q_{\text{EA}}(l) = Q_k(l)$ at $\alpha = 50, 100, 200, 1000, 2000, 4000$. Here $L = 20$.

This is surprising because the worst case scenarios [30] would predict linear growth with L . This means the behavior of typical instances are very different from the worst ones in the DNN. Here it is instructive to recall the case of the single perceptron. The storage capacity of typical instances computed by the replica method [5] is $\alpha_j = 2$. The existence of solutions are guaranteed for all instances including the worst ones in the range $0 < \alpha < 1$ while there are exponentially rare $e^{-\text{const}N}$ samples which lacks solutions in the range $1 < \alpha < 2$ [47]. Our result implies the gap between the worst and typical ones become much more enhanced in deeper systems. This may be related to the so-called exponential expressivity [32]. The latter is due to the chaos effect of DNNs with non-linear activation functions like Eq. (1): trajectories starting from slightly different initial condition exponentially decorrelate with the depth l . Perhaps this helps building a mapping (function) between the imposed input and output spin configurations, which are totally different, by a limited depth.

As α increases, the allowed phase space volume becomes suppressed. In Fig. 7 we display $x(Q, l) = \int_0^Q dQ P(Q, l)$ and $x(q, l) = \int_0^q dq P(q, l)$ (see Eq. (86)). The latter is the probability that two replicas (two machines learning independently) subjected to the same inputs/outputs have a mutual overlap of the bonds (spins) at l -th layer smaller than Q (q). As can be seen in the figure, the probability appears to decay as $1/\sqrt{\alpha}$ for all l , Q and q . This implies two independently learning machines become more and more similar to the number of constraints increases.

We note however that the EA order parameter of the spins $q_{\text{EA}}(l)$ shown in Fig. 5 remain significantly smaller than that of the bonds $Q_{\text{EA}}(l)$. Apparently, it implies that even in the jamming limit where $Q_{\text{EA}}(l) \rightarrow 1^-$, $q_{\text{EA}}(l)$ does not reach 1. There are two possible reasons for this. One is that we are using slightly annealed boundary condition which does not exclude sub-extensive fluctuations on the boundaries as we noted before. This may allow some spin fluctuations in the bulk even in the limit $Q_{\text{EA}}(l) \rightarrow 1^-$. As we already mentioned trajectories of random perceptron network with non-linear activation functions show chaotic behavior under infinitesimal changes on the input boundary [31, 32]. We confirmed it is always the case for the present model with the 'sgn' activation function Eq. (1) [33]. The system also

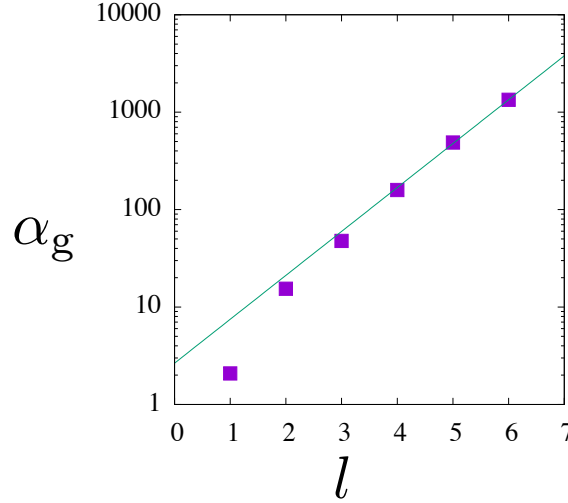


Figure 6: The glass transition point $\alpha_g(l)$ of internal layers. This is obtained by numerical analysis of the saddle point solutions. The solid line is the exponential fit Eq. (23).

shows a chaotic response against infinitesimal changes made on the bonds [33]. Thus even in $Q_{\text{EA}}(l) \rightarrow 1^-$ limit, the spin configuration can fluctuate significantly.

As shown in Fig. 8, the glass order parameter functions become quite complex at large values of α . Closer to the boundaries, the system has experienced larger numbers of successive glass transitions that leave behind river-terrace-like structure with many steps in the glass order parameter functions. This means distribution functions of the overlap with many delta peaks. The steps of the glass order parameter functions at different layers appear to be aligned with each other.

Now let us summarize the essential features of the glass order parameters $q(x, l)$ and $Q(x, l)$ shown in Fig. 3, 4 and 8. The essence of the river-terrace-like glass order parameter functions can be sketched schematically as shown in Fig. 9 a). Here we have simplified the picture representing the functions by staircases neglecting their rounding. Comparing the river-terraces at different layers we notice an interesting feature that the steps at different layers are synchronized: they are all located exactly at the same positions, $\dots, x_{l-1}, x_l, x_{l+1}, \dots$. The river-terraces reflect successive glass transitions in the following way. At the n -th glass transition, a finite glass order parameter emerges continuously in the interval $x_n(\alpha) < x < 1$ at the n -th (and $(L - n)$ -th) layer. The glass order parameter functions at layers between the n -th layer and the boundary, those at $l = 1, 2, \dots, n - 1$ (and the corresponding layers on the other side), which are already in the glass phase, acquire additional steps in the same interval $x_n(\alpha) < x < 1$. At a given α , the layers included in the glass phase are $l = 1, 2, \dots, n$ (and the corresponding ones on the other side) where n is such that $\alpha_g(n) < \alpha < \alpha_g(n + 1)$. Due to the successive glass transitions $1, 2, \dots, n$, the l -th (and $L - l$ th) layer with $1 \leq l \leq n$ have a series of steps at $0 < x_l(\alpha) < x_{l+1}(\alpha) \dots < x_n(\alpha) < 1$. Correspondingly the overlap distribution functions $P(Q, l)$ and $P(q, l)$ exhibit a series of delta peaks at $q(x_l, l) < q(x_{l+1}, l) \dots < q(x_n, l)$ plus another delta peak at $q = 0$ for $2 \leq l \leq n$.

The river-terrace-like glass order parameter function $q(x, l)$ (and $Q(x, l)$) in Fig. 9 a), means spatial evolution of the hierarchical clustering of the solutions as shown schematically

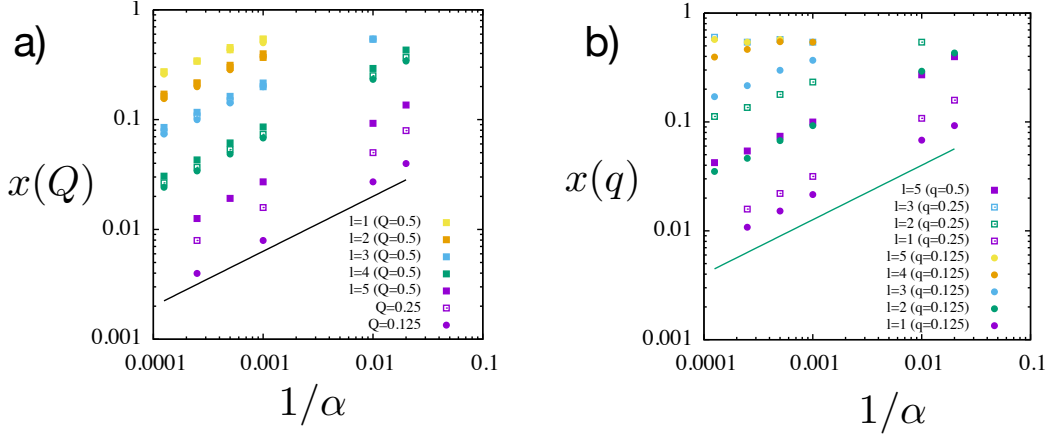


Figure 7: Decay of $x(Q)$ and $x(q)$ with increasing α . Here values of $x(Q, l)$, which is the inverse function of $Q(x, l)$ and $q(x, l)$, are shown at various Q, q and layers l . The slope of the straight line is $1/2$.

in Fig. 9 b). In panel b) clusters (and meta-clusters) of the same color represent those associated with a common value of x . Recalling the probabilistic meaning of x , it is natural to assume such a cluster represents a bundle of solutions that go together through different layers. Sampling two solutions in equilibrium, the two belong to such a common cluster with probability $1 - x$. The size of a cluster represents spreading of the solutions $1 - q(x, l)$, i.e. typical distance between the solutions belonging to the same cluster, which increases with decreasing x and/or going away from the boundary $l = 1, 2, \dots$ (Meta-)clusters with smaller x represent those at a higher level in the hierarchy which includes sub-clusters associated with larger values of x . Going deeper into the bulk starting from the boundary, those clusters with smaller x dissociate earlier.

This, in turn, implies the hierarchical free-energy landscape with basins, meta-basins,... which evolves in space as shown schematically in Fig. 9 c). The free-energy landscape evolves in space in such a way that it progressively becomes less complex and flatter as we go deeper into the interior. For a given α , the penetration depth $\xi_{\text{glass}}(\alpha) \sim \ln \alpha$ is finite. So that in a deep enough network $L/2 > \xi_{\text{glass}}(\alpha)$, the interior remains in the liquid phase. Moreover, the fact that the river-terraces of the glass order parameter functions at different layers are synchronized to each other with common positions of the steps at $x_1 < x_2 \dots$, suggests that the basic backbone structure of the free-energy landscape is preserved (but renormalized) moving away from the boundaries. It is tempting to speculate that these features have important consequences on learning in deep neural networks.

3.4 Fluctuating boundary

To obtain further insights, we next analyze the case of fluctuating boundary: spin configurations on the boundaries are allowed to fluctuate during learning following certain probability distributions. Here we consider cases such that the overlap distribution of the spins on the input layer ($l = 0$) exhibit a hierarchical structure as parametrized in the form of the Parisi's matrix Eq. (81) (Fig. 10). There are two motivations for this analysis:

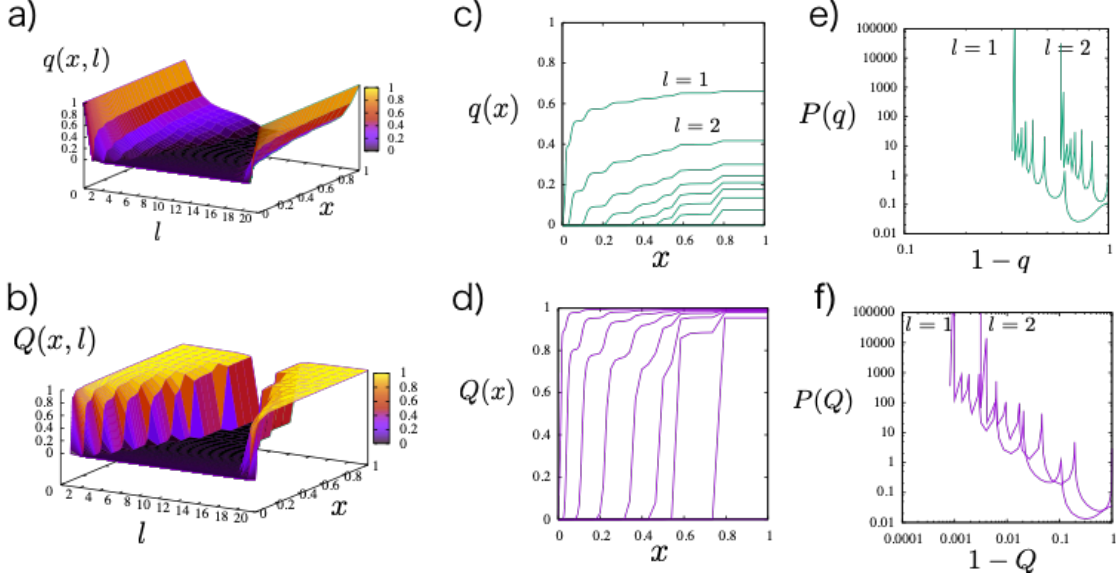


Figure 8: Glass order parameter functions under stronger constraints $\alpha = 4000$. In this example $L = 20$ and the central layers at $l = 8, 9$ still remain in the liquid phase. a), b) 3 dimensional plots of $q(x, l)$ and $Q(x, l)$. c), d) the same in 2 dimensional plots. e), f) the corresponding overlap distribution functions Eq. (86) at $l = 1, 2$ (for clarity others at $l = 3, 4, \dots$ are not shown).

- The perturbation may provide some hints on the stability of the characteristic free-energy landscape of the DNN we found above. Given that random neural networks are typically chaotic with respect to changes made on the inputs [32, 33], it is very interesting to know how training make differences.
- In a typical setting of unsupervised learning, one would be interested with the probability distributions $P(\mathbf{S}_l)$ of hidden variables \mathbf{S}_l ($l = 1, 2, \dots$) when variables on the input boundary \mathbf{S}_0 are forced to obey some probability distribution $P(\mathbf{S}_0)$.

3.4.1 One RSB type boundary

Here we consider the simplest case of '1RSB'.

$$q_i(0) = \begin{cases} r & m_i < x_{\text{input}} \\ 1 & m_i > x_{\text{input}} \end{cases}$$

This means the system subjected to a slightly different input data instead of the original one, which has overlap $0 < r < 1$ with respect the original input data, from time-to-time with some small probability x_{input} .

It can be seen in Fig. 11 that the effect of the perturbation is strong only at $x < x_{\text{input}}$. This means that the trained system is not simply chaotic but the hierarchical organization in the solution space has a certain degree of robustness against perturbations on the inputs (as well as outputs).

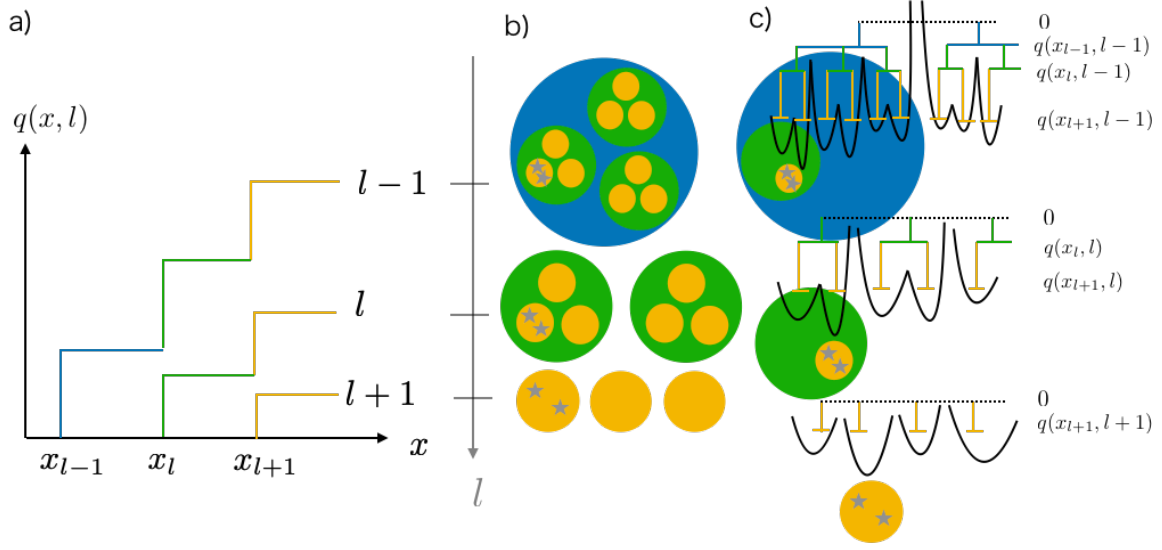


Figure 9: River-terrace like glass order parameter and its implications: a) schematic picture of the river-terrace-like glass order parameter $q(x)$ (or $Q(x)$) b) hierarchical clustering of replicas c) schematic free-energy landscape and trees representing ultra-metric organization of overlaps between meta-stable states.

3.4.2 Full RSB type boundary

Let us next consider the 'full RSB' case. More specifically we consider the simplest full RSB structure in the input layer,

$$q_i(0) = \min(am_i, 1) \quad (26)$$

with a certain constant $a > 0$. Thus $q(x, 0)$ function consists of two parts: 1) 'continuous part' $q(x, 0) = ax$ with slope a in the interval $0 < x < 1/a$ and 2) 'plateau' $q(x, 0) = q_{\text{EA}}(0) = 1$ in the interval $1/a < x < 1$.

We analyze the saddle point solutions numerically as before (see sec. B.3.3). In the following, we present results using $k = 100$ step RSB and the depth of the system $L = 20$. We chose $1/a = 0.8$. As shown in Fig. 12, the glass phase grows increasing α much as in the case of "quenched" (RS) boundary condition discussed in sec. 3.3.1. We limit ourselves to α such that $\xi_{\text{glass}}(\alpha) < L/2$ so that we have a liquid phase left at the center of the system. In this circumstance the boundary condition on the other side $q_{ab}(L)$ is irrelevant.

A remarkable feature of the resulting glass order parameter is that the hierarchical structure put on the input propagates into the interior of the network preserving its basic hierarchical structure. The numerical solution suggests that the $q(x, l)$ function at a given layer l consists of three parts: 0) $q(x, l) = 0$ for some interval $0 < x < x_l$ 1) 'continuous part' $q(x, l) = a(x - x_l)$ in the interval $x_l < x < 1/a$ with the same slope a as in the input 2) 'plateau' $q(x, l) = q_{\text{EA}}(l) = 1 - ax_l$ in the last interval $1/a < x < 1$ as in the input. Correspondingly the overlap distribution function $P(q) = dx(q)/dq$ becomes,

$$P(q, l) = x_l \delta(q) + \frac{1}{a} + \left(1 - \frac{1}{a}\right) \delta(q - (1 - ax_l)) \quad (27)$$

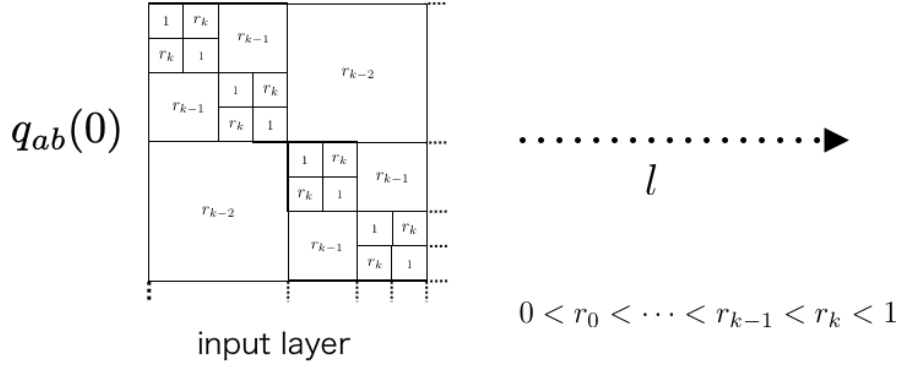


Figure 10: Fluctuating input layer with hierarchical overlap structure

which consists of three parts: 0) delta peak at $q = 0$ 1) constant part with height $1/a$ in the interval $x_l < x < 1/a$ as in the input 2) delta peak at $q = q_{\text{EA}}(l)$.

Going deeper into the interior increasing l , we find x_l grows and $q_{\text{EA}}(l) = 1 - ax_l$ decreases. We can regard this as a kind of 'renormalization' of the input data : the embedded overlap structure at low overlaps in the input data become progressively renormalized into the $q = 0$ sector in the hidden layers, keeping only the important part of the hierarchical structure at higher overlaps. It will be very interesting to study further the implication of this result in the context of data clustering where the idea of ultrametricity is very useful.

3.5 Teacher-student setting

Now let us turn to analyze in detail the teacher-student setting introduced in sec. 2.2.2 by the replica theory using the ansatz explained in sec. A.5.2.

3.5.1 Training

Since we are limiting ourselves to the Bayes optimal case, it is sufficient to consider the replica symmetric ($k = 0$) ansatz so that the Nishimori condition holds [8, 48, 49], which reads in the present system,

$$r(l) = q_0(l) \quad R(l) = Q_0(l). \quad (28)$$

The saddle point equations in sec. C.3 admit such solutions.

In Fig. 13 we show the profile of the solutions obtained at various $\alpha = M/N$. Remarkably the spatial profile of the order parameters are very similar to those of random inputs/outputs (See Fig. 5). This is again due to successive layer-by-layer, 2nd order 'crystalline' phase transitions which start from the boundaries. The overlap of the student machine to the teacher machine grows from the boundary and the penetration depth grows again as

$$\xi_{\text{teacher-student}} \propto \ln \alpha. \quad (29)$$

Remarkably the central part of the student machine remains de-correlated from the teacher machine if the system is deep enough, i. e. $L > \xi$. The solution (for the case $L > \xi$) in the crystalline region does not change even in $L \rightarrow \infty$ limit. The reason for the crystalline

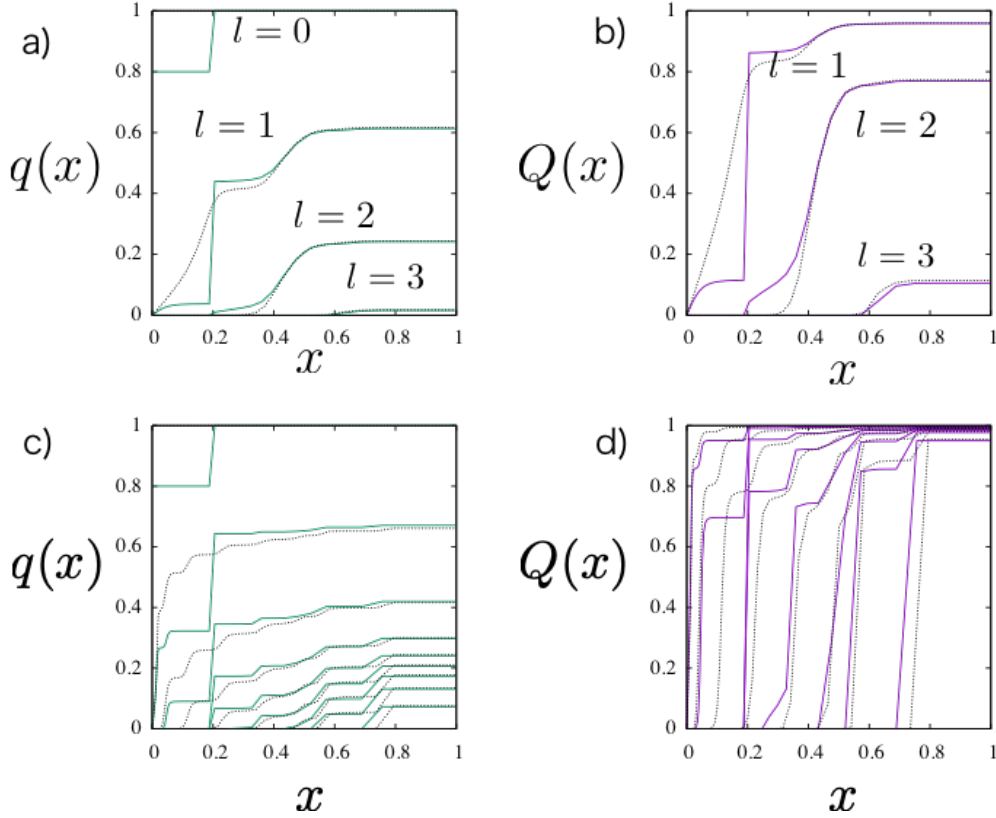


Figure 11: Glass order parameters with 1 RSB input. Here $L = 20$, $x_{\text{input}} = 0.2$ and $r = 0.8$ for the solid lines and $x_{\text{input}} = 0.2$ a), b) $\alpha = 50$ c), d) $\alpha = 4000$. Dotted lines represent the glass order parameters with the frozen boundary.

transition starting from the 1st layers ($l = 0, L - 1$) is again the entropic effect: some set of configurations of the bonds in the 1st layers ($l = 0, L - 1$) allow exceedingly larger fluctuation in the hidden layers compared with others so that they dominate the entropy of the solution space.

Now let us discuss what the above theoretical results mean for practice. The fact that the transitions are 2nd order transitions is a very good news. This is because it implies that inference will not be too difficult [8]: we do not need to worry about the possibility to be trapped in the solution of $R = 0$ (failure of inference) because it becomes unstable at the transition. However, very importantly, we have to ask what plays the role of symmetry breaking field by which the student machine can detect the teacher's configuration during learning. In our theory, we had the convenient 'fictitious' symmetry breaking field (see sec. A.1.1) but it must be realized by some 'real' field (in the computer!). Actually, if the central part remains really random, how can the student machine ever develop some finite overlap to the teacher machine at the opposite ends disconnected by the liquid phase in between? Our analysis for the case of the random inputs/outputs would suggest otherwise: the student machine should not be able to pick up the minima planted by the teacher machine correctly hidden in the ocean of many (wrong) minima, all of which correctly satisfy the constraints

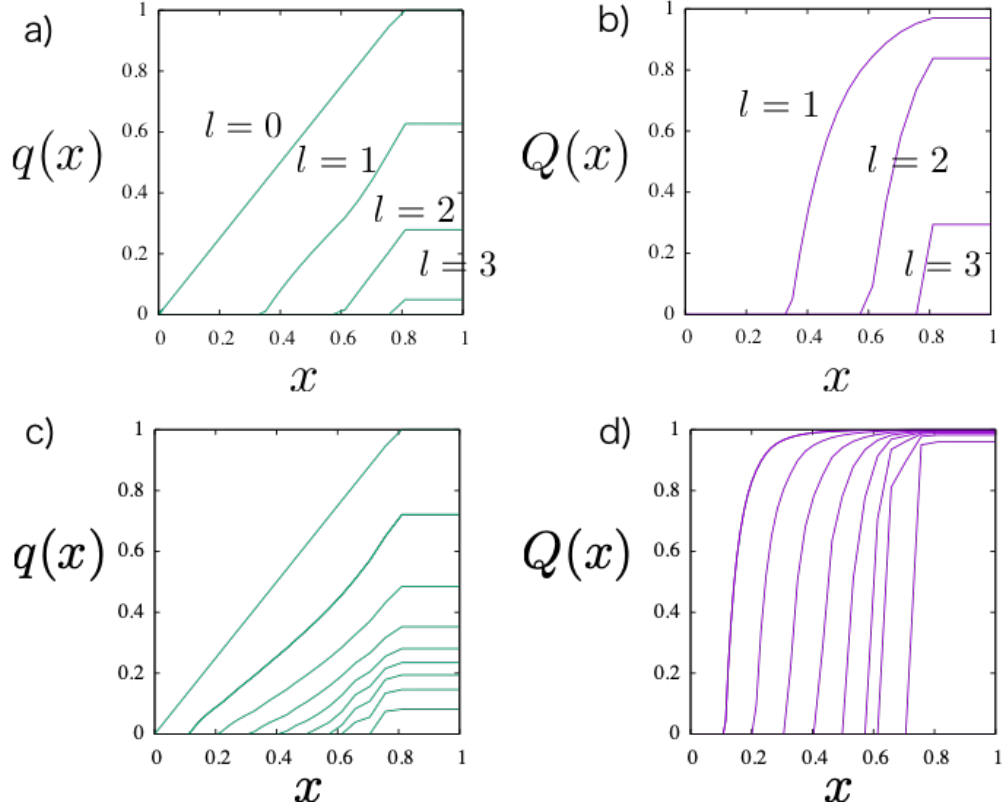


Figure 12: Glass order parameters with full RSB input. Here $L = 20$ and $1/a = 0.8$. a),b) $\alpha = 50$ c),d) $\alpha = 4000$.

on the input and output boundaries. The most likely scenario for the symmetry breaking during learning is that some weak correlation between the teacher and student machines of order, say $O(\log(N)/N)$ which does not contribute the order parameter Eq. (11) in the limits $N, M \rightarrow \infty$ (with fixed $\alpha = M/N$), remains in the central part of the system and plays the role of the symmetry-breaking field: the free-energy of the selected state will be lowered by an amount of order $O(\log(N))$ to other low lying (wrong) states. Such logarithmic correction naturally arises by integrating out the fluctuation of the order parameters around the saddle point. Since replica symmetry holds in the present case, all eigenvalues of the stability matrix (Hessian matrix) around the saddle point are positive so that the saddle point integrations are well defined. We leave the detailed analysis of the correction term for future studies.

3.5.2 Generalization

To test the generalization ability of the student machine, we should compare the output of the teacher and student machines to a set of *test data*, i.e. a new set of input data that is not used for the training. We can consider monitoring the response of the teacher and student machine against M -patterns of test data, during learning the M -patterns of training data. This monitoring should not disturb the learning itself.

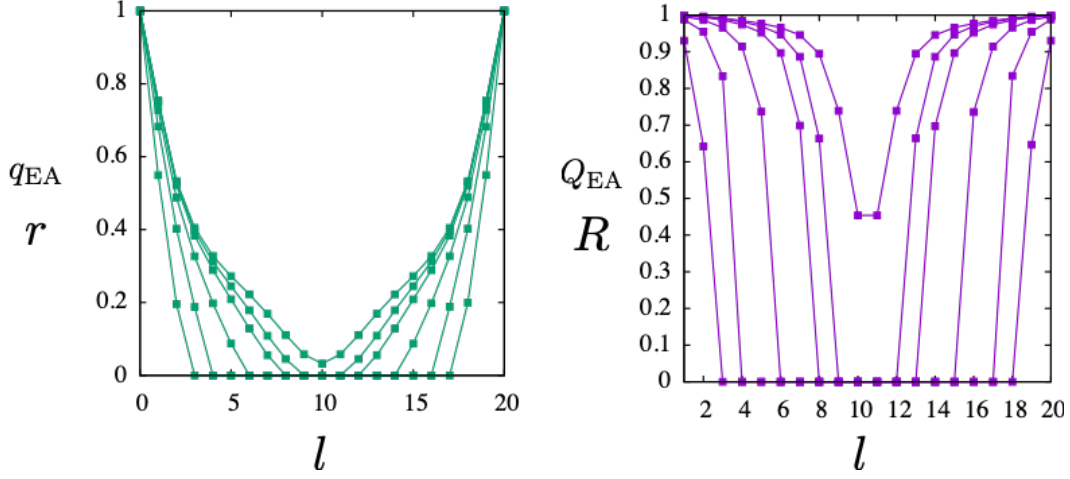


Figure 13: The spatial profile of the EA order parameters $q_{\text{EA}}(l) = q_0(l) = r(l)$, $Q_{\text{EA}}(l) = Q_0(l) = R(l)$ (RS solution $k = 0$) at $\alpha = 25, 100, 250, 500, 625, 714$. Here $L = 20$. For the largest α , $\xi > L$ and the liquid phase disappears, which is a 'finite depth' effect .

To simulate this process within our framework we consider the following: solve again the replica symmetric saddle point equations for the order parameters of the spins $q(l)$ and $r(l) (\leq q(l))$ for $l = 1, 2, \dots, L$ but with the order parameters of the bonds $Q(l) = R(l)$ for $l = 1, 2, \dots, L$ fixed as determined above. At the input boundary $l = 0$ we again set $q(0) = r(0) = 1$ because the teacher and student machines are subjected to a common set of input data of the test data. On the other hand, now the output of the student machine is not constrained. Thus we do not put the other constraint $q(L) = r(L) = 1$ but treat $q(L)$ and $r(L) (\leq q(L))$ also as additional variational parameters.

By solving the equations we recovered the same solutions as before, shown in Fig. 13. The result implies that, within our theory, the performance of the student machine to the test data is essentially the same as that for the training data. Thus the generalization ability becomes poor entering the central liquid region but rapidly improves going through the crystalline region around the output. Again we emphasize that this solution makes sense only in the presence of the symmetry breaking field.

3.6 Summary

The non-linear dynamics Eq. (1) in random perceptron networks is known to be highly chaotic [31, 32]. Among all such random perceptrons, which typically give chaotic dynamics, we considered statistical mechanics on the ensemble of extremely *rare* samples which happen to meet a large number of externally imposed inputs/outputs boundary conditions. Our theory predicts that such a *selection* (learning) on the ensemble of chaotic trajectories give rise to a hierarchical clustering of the trajectories (solutions) which evolves in space as shown in Fig. 14. The presence of the liquid phase in the center is consistent with the chaos. The spatial evolution of RSB smoothly connects the free-liquid like center and strongly constrained boundaries.

Imagine that we are monitoring the behavior of multiple machines that are subjected to

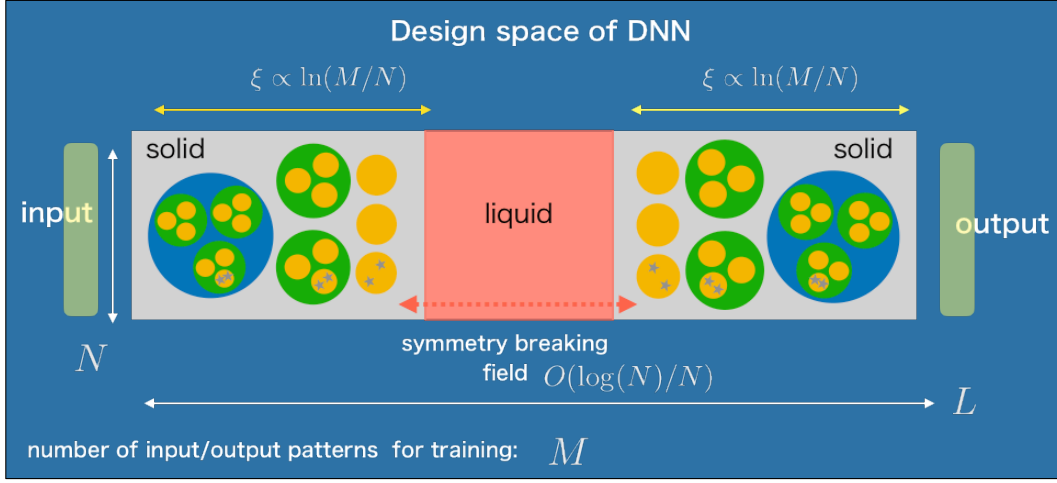


Figure 14: Schematic picture of the design space of deep neural network based on the present theory

the same inputs/outputs boundary condition but evolving (learning) independently from each other. Their configurations are represented by 'stars' in Fig. 14. Starting from the input layer, we notice that they progressively become more separated going deeper into the bulk but they become closer again approaching the output layer. The initial part, where different clusters of solutions (machines) merge into bigger cluster look like forgetting the detailed differences (renormalization) and the latter is the reverse: it amplifies mutual differences to produce the desired output (label). This picture appears to be consistent with some intuitions gained in some studies of machine learning in DNNs [50].

Usually (by definition) chaotic systems are extremely weak against perturbations. It is very interesting to ask what happens if selections (learning) come into play. Our theory implies that, during learning, a machine can diffuse chaotically within the huge continent of solutions (liquid) at the center without violating the imposed boundary conditions. Larger fluctuation means entropic stability. Thus it is not inconceivable that the combination of the strong internal chaos and the selection made at the boundaries can create a machine whose output is strong against perturbations. Our theoretical results suggest this is the case.

One can view Fig. 14 as a picture of the phase space of hard-spheres bounded by two walls made by frozen particles. The frozen boundaries act like pinning field for the particles and successive layer-by-layer glass transitions start from the boundaries as the pressure is increased. This is similar to the layer-by-layer growth by physical adsorption on substrates [51]. As the glass region grows in space, the interior of the glass region experiences further glass transitions (like the Gardner transition [46]) by which their phase space become split further. In the teacher-student setting, one of the glass corresponding to that of the teacher and the student tries to find it.

4 Simulations of learning

Now we turn to discuss some numerical simulations to examine our theoretical predictions regarding the two scenarios: 1) the setting of a random constraint satisfaction problem with random inputs/outputs at boundaries (Sec 2.2.1) and 2) the setting of a statistical inference problem with the teacher and student machines (Sec 2.2.2).

4.1 Relaxational dynamics of a soft-core model with random inputs/outputs

In sec. 3.3 we found theoretically that the free-energy landscape of the perceptron network subjected to random constraints on the boundaries exhibit spatially heterogeneous structure: it is very complicated close to the boundaries but very simple in the central part. This naturally implies that learning dynamics is also heterogeneous in space.

To examine the nature of the learning dynamics we perform Monte Carlo simulations of the multi-layer neural network with depth L , width N and randomly quenched inputs/outputs spins. The effective Hamiltonian of the system Eq. (9) reads as,

$$H = \sum_{\mu} \sum_{\blacksquare} V(r_{\blacksquare}^{\mu}) \quad r_{\blacksquare}^{\mu} \equiv \sum_{i=1}^N \frac{J_{\blacksquare}^i}{\sqrt{N}} S_{\blacksquare(i)}^{\mu} S_{\blacksquare}^{\mu} \quad (30)$$

For convenience for the simulation, we replace the hard-core potential Eq. (7) by a soft-core potential,

$$V(h) = \epsilon h^2 \theta(-h) \quad (31)$$

where ϵ is the unit of energy. Note that the statistical mechanics of a system with the soft-core potential becomes the same as the hardcore potential in the zero-temperature limit $k_B T / \epsilon \rightarrow 0$, where k_B is the Boltzmann's constant and T is the temperature, in the region where all the constraints are satisfied (SAT).

The dynamical variables are the M -component vector spins and bonds,

$$S_{\blacksquare}^{\mu} \quad (\mu = 1, 2, \dots, M) \quad (\blacksquare = 1, 2, \dots, NL) \quad (32)$$

$$J_{\blacksquare}^i \quad (i = 1, 2, \dots, N) \quad (\blacksquare = 1, 2, \dots, NL) \quad (33)$$

Each component of the spins only takes Ising values ± 1 while each of the bonds takes continuous values. In order to satisfy the normalization condition Eq. (2) $\sum_{i=1}^N (J_{\blacksquare}^i)^2 = N$, we assume that J_{\blacksquare} follows a Gaussian distribution with 0 mean and variance 1. We performed simple Metropolis updates of the dynamical variables at very low temperatures T to simulate the relaxational dynamics. In a sense the finite temperature Monte Carlo dynamics mimic the 'stochastic' nature of the standard Stochastic Gradient Descent (SGD) algorithms used for training of DNNs [1]. To propose a new spin configuration for the Metropolis algorithm, first we select a spin component S_{\blacksquare}^{μ} randomly out of the $N \times L \times M$ possibilities and then flip it as $S_{\blacksquare}^{\mu} \rightarrow -S_{\blacksquare}^{\mu}$. To update the bond configuration, first we select a bond J_{\blacksquare}^i randomly out of the $N \times L \times N$ possibilities and then shifted its value as,

$$J_{\blacksquare}^i \rightarrow \frac{J_{\blacksquare}^i + rx}{\sqrt{1 + r^2}} \quad (34)$$

where x is a random number following the Gaussian distribution with zero mean and variance 1. We set $r = 0.1$ in our simulations. Within 1 MCS (Monte Carlo Step), the unit step of

the Monte Carlo simulation, we try updates of the spins $N \times L \times M$ times and updates of the bonds $N \times L \times N$ times.

At first the configurations of the frozen spins on the input $l = 0$ and the output $l = L$ layers are generated randomly. The initial configurations of the mobile spins and bonds are also generated randomly. Then spins and bonds are updated using the Metropolis algorithm at a low temperature T . In our simulations we set $k_B T / \epsilon = 0.015$.

We measure the following time autocorrelation functions,

$$C_{\text{bond}}(t, l) = \frac{1}{N^2} \sum_{\blacksquare \in l} \sum_{i=1}^N \overline{(J_{\blacksquare}^i)(t)(J_{\blacksquare}^i)(0)} \quad C_{\text{spin}}(t, l) = \frac{1}{MN} \sum_{\blacksquare \in l} \sum_{\mu=1}^M \overline{(S_{\blacksquare}^{\mu})(t)(S_{\blacksquare}^{\mu})(0)} \quad (35)$$

where $\blacksquare \in l$ stands for summation over the perceptrons within the l -th layer. As we noted in sec. 3.1 the system is symmetric under permutations of the perceptrons \blacksquare within the same layer. This does not matter here as long as we limit ourselves on the time scales where the correlation functions defined above remain positive. The overline $\overline{\cdots}$ represents the average over different samples: the realization of the inputs/outputs spins are chosen randomly for each sample. In the following, we used 240 samples.

In the present simulations we chose the depth as $L = 5, 10$, the width as $N = 20$ and the number of the patterns of data as $M = 100, 200$, which means $\alpha = M/N = 5, 10$. In Fig. 15 we show data of the time autocorrelation functions of the spins and bonds.

From the two panels on the left-hand side in the row a), it can be seen that the dynamics is actually faster in the center and slower close to the boundaries as we expected. However in the semi-logarithmic plots on the right-hand side it can be seen that the dynamics is actually complicated: the dynamics is slow at shorter time scales at all layers that crossovers to faster dynamics at longer time scales. The difference in the speed of the relaxations at different layers is prominent in the longer times scales. The result suggests that the slow dynamics at the shorter time scales reflect the glassy aspect of the free-landscape and the truncation of the slow dynamics at longer time scales reflect the presence of the liquid phase at the center. It is interesting to note that similar truncation of the slow dynamics has been observed in a study of SGD dynamics in DNNs [21].

From the panels in row b), it can be seen that the dynamics become slower as the strength of the constraints α increases. This is consistent with the theoretical expectation that the system becomes more glassy with larger α .

From the panels in row c), it can be seen that the depth L do not change the slow dynamics at shorter time scales but changes the truncation of the slow dynamics. Relaxation at the longer time scale is apparently faster in the deeper system. Interestingly this happens even in the layer just next to the boundaries. Presumably, this implies that the deeper system is more flexible in the center and the fast dynamics at the center assists the relaxation of the whole system.

In Fig. 16, we display the relaxation of energy $e(t, l) = E(t, l)/N$ at each layer l . Here $E(t, l)$ is the contribution of l th layer to the energy (see Eq. (30)-Eq. (31)) at time t (MCS). It can be seen again that relaxation is slower closer to the boundaries.

Note that the behavior of the system is not symmetric to the exchange of input and output sides. We expect that this is a finite N effect which disappears in $N \rightarrow \infty$ limit.

To summarize the numerical observation of the relaxations is qualitatively consistent with the theoretical prediction which implies spatially heterogeneous dynamics.

4.2 Learning by a binary perceptron in a teacher-student setting

Finally, let us discuss the results of some numerical simulations of the teacher-student setting which we studied theoretically in sec. 3.5. The teacher and student machines have exactly the same structures. For simplicity we use the binary perceptron model [52, 53] in which the synaptic weights in Eq. (1) are restricted to take binary (Ising) values $J_{\blacksquare}^k = \pm 1$.

Some details of the simulations are listed below.

- Teacher-machine

For the teacher machine, we consider networks with $L = 4, 6$ and $N = 4$. For each sample of the teacher machine, $N^2 \times L$ values of the bonds $(J_{\blacksquare}^k)_{\text{teacher}} = \pm 1$ are generated randomly with no bias. Given a set of input data $S_{0,i}^\mu = \pm 1$ ($i = 1, 2, \dots, N$), ($\mu = 1, 2, \dots, M$), it produces a set of corresponding output data $(S_{L,i}^\mu)_{\text{teacher}} = \pm 1$ ($i = 1, 2, \dots, N$), ($\mu = 1, 2, \dots, M$).

Each input data $S_{0,i}^\mu = \pm 1$ is also generated randomly without bias. Two independent sets of inputs/outputs data, both with M patterns, are prepared. One set is used to train the student machine and the other set is used to test the student machine.

- Student-machine

The student machine has the same architecture as the teacher machine. We train the student machine by performing a greedy Monte Carlo simulation which attempts to minimize a loss function,

$$\mathcal{L} = \sum_{\mu=1}^M \sum_{i=1}^N ((S_{L,i}^\mu)_{\text{teacher}} - (S_{L,i}^\mu)_{\text{student}})^2. \quad (36)$$

where $(S_{L,i}^\mu)_{\text{teacher}}$ is the output of the teacher-machine. It goes as the following. 0) Initial values of the bonds $(J_{\blacksquare}^k)_{\text{student}}$ are generated randomly with no bias. 1) At each micro-step of the simulation, one bond $(J_{\blacksquare}^k)_{\text{student}}$ out of all bonds of the student machine is selected. 2) If a flip $(J_{\blacksquare}^k)_{\text{student}} \rightarrow -(J_{\blacksquare}^k)_{\text{student}}$ lowers the loss function, the flip is accepted and otherwise rejected. 3) the micro-step 1)-2) is repeated $N \times L$ times for one MCS. 4) Repeat 3) until $\mathcal{L} = 0$ is reached. If it is not reached within 10^6 MCS, we restart the whole process from 0).

- Training and test

For training, the set of inputs/outputs data prepared for the training is given to the student machine and we train the student machine using the greedy Monte Carlo algorithm as explained above. We examine the quality of the student machine after the training by computing the overlap of the bonds $R(l)$ and spins $r(l)$ at each layer l (see below), between the teacher and student machines.

To test the generalization ability of the student machine, we use the other set of inputs/outputs data. We examine the performance of the student machine (now its bonds are fixed) by computing the overlap of the spins between the teacher and student machines, which we denote as $r_{\text{test}}(l)$.

- Overlap between the teacher and student machines

We define the overlaps between the teacher and student machines as

$$R(l) = \frac{1}{N^2} \sum_{\blacksquare \in l} \sum_{i=1}^N \overline{(J_{\blacksquare}^i)_{\text{teacher}} (J_{\blacksquare}^i)_{\text{student}}} \quad r(l) = \frac{1}{MN} \sum_{\blacksquare \in l} \sum_{\mu=1}^M \overline{(S_{\blacksquare}^{\mu})_{\text{teacher}} (S_{\blacksquare}^{\mu})_{\text{student}}} \quad (37)$$

where $\blacksquare \in l$ stands for summation over the perceptrons within the l -th layer. The overline $\overline{\cdot}$ represents the average over different samples: both the realization of the teacher-machine and the input data are chosen randomly for each sample. In the following, we used $O(10^3)$ samples.

As we noted in sec. 3.1 the system is symmetric under permutations of the perceptrons \blacksquare within the same layer. This matters here because we are performing static sampling where permuted configurations should appear with the same statistical weights. In order to remove this unwanted symmetry, we removed 20% (Fig 17) and 40% (Fig 18) of the bonds randomly in each layer, but exactly in the same way, from both the teacher and student machines from the beginning (before training). The normalization in Eq. (35) is redefined accordingly so that $C_{\text{bond}}(0, l) = C_{\text{spin}}(0, l) = 1$.

In Fig. 17 and Fig. 18 we show the result of the simulations where we used systems with $L = 4, 6$ and $N = 4$ with $M = 4, 8, 12, 16$ so that $\alpha = M/N = 1, 2, 3, 4$. Thus the system is surely over-parametrized. The panels in the rows a) and b) show bond and spin overlaps after the training. As one can see in the two panels on the row a), the bond overlap $R(l)$ is large and increases with α on the two layers just next to the inputs/outputs boundaries while it remains very small in the middle. Correspondingly it can be seen in the two panels on row b) that the spin overlap $r(l)$ also shows similar tendencies.

As shown in the two panels on row c), the spin overlap $r_{\text{test}}(l)$ for the test data is almost the same as that for the training data $r(l)$ shown on row b), except for the value at the very end $r_{\text{test}}(L)$. Note that $r(L) = 1$ by construction of the training while $r_{\text{test}}(L)$ can vary during test. It can be seen that $r_{\text{test}}(L)$ increases with α proving the generalization ability of the student machine in spite of the fact that the system is over-parametrized.

Remarkably these features are qualitatively consistent with the theory discussed in sec. 3.5. which predicts that finite overlaps between the teacher and student machines emerge from the boundaries and the saddle point solutions in the training and test stages are essentially the same.

As we pointed out in sec. 3.5 there must be some symmetry breaking field connecting the opposite sides of the system to enable learning in such over-parametrized machines with 'liquid' in the center. Indeed it can be seen that, although small, finite positive overlap remains also in the central area. In Fig 19 we show width N dependence of the bond and spin overlaps after the training (for the case 20% of the bonds removed). It can be seen clearly that the overlaps decreases with increasing width N for fixed $\alpha = M/N$. This consistent with the expectation that the small positive overlap remaining in the center is a finite width N correction term. In addition, it seems that the system becomes more symmetric with respect to the exchange of input and output sides as N increases, as we expected.

5 Conclusion and outlook

5.1 Conclusion

In the present paper, we constructed a statistical mechanical theory for the solution space of a deep perceptron network of depth L , width N subjected to $M = \alpha N$ patterns of data using the internal representation, based on the replica method in the limit $N, M \rightarrow \infty$ with fixed α . We studied two scenarios :

- 1) Random inputs/outputs, which is a random constraint satisfaction problem
- 2) Teacher-student setting, which is a statistical inference problem.

In addition, we performed two sets of simulations to examine the theoretical predictions on 1) and 2).

The main outcome of the theory is the prediction of the strongly heterogeneous spatial profile of states inside the layered network : 1) 'glass-liquid-glass' in the case of the random inputs/outputs 2) 'crystal-liquid-crystal' in the case of the teacher-student setting. The thickness of the glass/crystal phase grows as $\xi \propto \ln \alpha$. This implies exponential growth of the storage capacity of DNN with the depth $\alpha_j(L) \propto e^{\text{const} L}$ for typical instances. Moreover, in the case of setting 1) random inputs/outputs, even the pattern of the replica symmetry breaking (RSB) varies in space : it is most complex close to the boundaries with $k(+\text{continuous})$ -RSB, which becomes $k-1(+\text{continuous})$ -RSB in the next layer, ... down to a replica symmetric (0 RSB) state in the central part. The hierarchical structures in different layers are synchronized. We argued that in the 2) teacher-student setting, the small positive overlap can remain in the liquid phase as a finite N correction and plays the role of symmetry-breaking field.

There are some weak points in our theory.

- Our theory assumes the wide limit $N \rightarrow \infty$ (with $\alpha = M/N$ fixed) while real networks have finite width N so that 'phase transitions' we found here become at most just crossovers. Nonetheless, we believe our results still provide useful guidelines to understand real DNNs.
- Although we believe our ansatz for the glass phase is reasonable, we do not have proof that our set of order parameters is complete.
- We are considering slightly annealed boundary condition which does not exclude sub-extensive fluctuations on the boundary. At the moment we do not fully understand the differences with case of strictly quenched boundary conditions. Because of the chaotic properties of DNN [32] [33], this is a subtle problem.

For 1), we performed a simulation of the relaxational dynamics. We found spatially heterogeneous dynamics which is fast in the center and slow closer to the boundaries in agreement with the theory. For 2) we simulated learning in a teacher-student setting. We found heterogeneous learning and generalization as expected from the theory. The presence of remnant bias in the center is found, which appears to be compatible with the interpretation as due to a finite width N correction.

To summarize, both the theory and the simulation suggest spatially heterogeneous free-energy landscape in the over parametrized DNNs. (See Fig. 14) We speculate that this is responsible for the efficiency of DNNs in three respects:

- a) The presence of the liquid phase in the center may facilitate the equilibration (learning) of the whole system. This is an interesting point which deserves further studies. In this respect, it is interesting to note that the so-called ultra-stable glasses [54–56] are created by vapor deposition which allows rapid equilibration at layers close to the surface. As we noted in sec. 3.6, the analogy to the hard-spheres is suggestive. One could also think about the analogy with the replica-exchange Monte Carlo method [57] which dramatically accelerates the equilibration of complex systems.
- b) In spite of the over-parametrization the system can generalize well because of the presence of the crystalline phase close to the boundaries. The weak bias which remains in the liquid phase as a finite width N correction plays the crucial role of the symmetry breaking field to select the hidden crystalline state out of many glass states.
- c) Hierarchical free-energy landscapes with ultra-metric structure has been known in glass physics since the discovery of replica symmetry breaking [14, 15, 42]. Our theory suggests that it evolves in space in the DNN, during learning, progressively from the complex to simple ones going deeper into the interior from both the input and output boundaries. Probably the spatial ‘renormalization’ of the hierarchical clustering and the presence of the liquid phase at the center stabilize the system against external perturbations or incompleteness of equilibration and contributes positively to the generalization ability of DNNs.

5.2 Outlook

Here we list some possibilities for further investigations. First of all, it will be very interesting to perform extensive numerical simulations with realistic algorithms and realistic large-scale data to examine our predictions. Second, a more detailed theoretical/numerical analysis of the remnant bias field in the liquid phase is needed. Third, the storage capacity and critical properties at jamming (SAT/UNSAT transition) [18–23] can be studied in detail by analyzing the regime $\xi \gg L$. We speculate that the exponential growth of the storage capacity $\alpha_g(L) \propto e^{\text{const}L}$ for typical instances that we expect may be related to the so-called exponential expressivity [32] due to the chaos effect. Lastly, it will be interesting to extend the present work to other cases regarding the activation function, architecture, and learning methods.

Our system may be viewed as a $1+\infty$ dimensional glass which is an interesting playground to analyze spatial heterogeneity with mean-field theoretical approaches [51, 58–60]. The present work may also have implications on various complex systems with spatial heterogeneity, including ultra-stable glass [54–56] mentioned above, gene regulatory networks [61–63] which are often viewed like perceptrons and allosteric systems [64–66]. The central liquid region may be related to the idea of *neutral space* [61, 62] which is considered as responsible for robustness of biological systems.

Acknowledgments

We thank Giulio Biroli, Silvio Franz, Koji Hashimoto, Sungmin Hwang, Kyogo Kawaguchi, Macoto Kikuchi, Kota Mitsumoto, Tomoyuki Obuchi, Haruki Okazaki, Akinori Tanaka, Pierfrancesco Urbani, Takaki Yamamoto, Lenka Zdeborová and Francesco Zamponi for useful discussions.

Numerical analysis in this work has been done using the supercomputer systems OCTOPUS and SX-ACE at the Cybermedia Center, Osaka University. The author thanks the Simons collaboration on “cracking the glass problem” for opportunities of stimulating discussions. The author thanks the Yukawa Institute for Theoretical Physics at Kyoto University for discussions during the YITP workshop YITP-W-19-18 “Deep Learning and Physics 2019”.

Founding information This work was supported by KAKENHI (No. 19H01812) from MEXT, Japan.

References

- [1] Y. LeCun, Y. Bengio and G. Hinton, Deep learning, *nature* **521**(7553), 436 (2015), doi:[10.1038/nature14539](https://doi.org/10.1038/nature14539).
- [2] G. Cybenko, Approximation by superpositions of a sigmoidal function, *Mathematics of control, signals and systems* **2**(4), 303 (1989), doi:[10.1007/BF0213401](https://doi.org/10.1007/BF0213401).
- [3] C. Zhang, S. Bengio, M. Hardt, B. Recht and O. Vinyals, Understanding deep learning requires rethinking generalization, *arXiv preprint arXiv:1611.03530* (2016), <https://arxiv.org/abs/1611.03530>.
- [4] G. Carleo, I. Cirac, K. Cranmer, L. Daudet, M. Schuld, N. Tishby, L. Vogt-Maranto and L. Zdeborová, Machine learning and the physical sciences, *arXiv preprint arXiv:1903.10563* (2019), [http:https://arxiv.org/abs/1903.10563](https://arxiv.org/abs/1903.10563).
- [5] E. Gardner, The space of interactions in neural network models, *Journal of physics A: Mathematical and general* **21**(1), 257 (1988), doi:[10.1088/0305-4470/21/1/030](https://doi.org/10.1088/0305-4470/21/1/030).
- [6] E. Gardner and B. Derrida, Three unfinished works on the optimal storage capacity of networks, *Journal of Physics A: Mathematical and General* **22**(12), 1983 (1989), doi:[10.1088/0305-4470/22/12/004](https://doi.org/10.1088/0305-4470/22/12/004).
- [7] M. Mezard and A. Montanari, Information, physics, and computation, Oxford University Press (2009).
- [8] L. Zdeborová and F. Krzakala, Statistical physics of inference: Thresholds and algorithms, *Advances in Physics* **65**(5), 453 (2016), doi:[10.1080/00018732.2016.1211393](https://doi.org/10.1080/00018732.2016.1211393).
- [9] L. Berthier and G. Biroli, Theoretical perspective on the glass transition and amorphous materials, *Reviews of Modern Physics* **83**(2), 587 (2011), doi:[10.1103/RevModPhys.83.587](https://doi.org/10.1103/RevModPhys.83.587).
- [10] P. Charbonneau, J. Kurchan, G. Parisi, P. Urbani and F. Zamponi, Fractal free energy landscapes in structural glasses, *Nature communications* **5**, 3725 (2014), doi:[10.1038/ncomms4725](https://doi.org/10.1038/ncomms4725).
- [11] G. Parisi, P. Urbani and F. Zamponi, Theory of Simple Glasses: Exact Solutions in Infinite Dimensions, Cambridge University Press (2020).
- [12] A. Engel and C. Van den Broeck, Statistical mechanics of learning, Cambridge University Press (2001).

- [13] G. Parisi, Infinite number of order parameters for spin-glasses, Physical Review Letters **43**(23), 1754 (1979), doi:[10.1103/PhysRevLett.43.1754](https://doi.org/10.1103/PhysRevLett.43.1754).
- [14] M. Mézard, G. Parisi and M. A. Virasoro, Spin glass theory and beyond, World Scientific, Singapore (1987).
- [15] M. Mézard, G. Parisi, N. Sourlas, G. Toulouse and M. Virasoro, Nature of the spin-glass phase, Physical review letters **52**(13), 1156 (1984), doi:[10.1103/PhysRevLett.52.1156](https://doi.org/10.1103/PhysRevLett.52.1156).
- [16] K. Nemoto, A numerical study of the pure states of the sherrington-kirkpatrick spin glass model-a comparison with parisi's replica-symmetry-breaking solution, Journal of Physics C: Solid State Physics **20**(9), 1325 (1987), doi:[10.1088/0022-3719/20/9/022](https://doi.org/10.1088/0022-3719/20/9/022).
- [17] K. Nemoto, Metastable states of the sk spin glass model, Journal of Physics A: Mathematical and General **21**(5), L287 (1988), doi:[10.1088/0305-4470/21/5/004](https://doi.org/10.1088/0305-4470/21/5/004).
- [18] S. Franz and G. Parisi, The simplest model of jamming, Journal of Physics A: Mathematical and Theoretical **49**(14), 145001 (2016), doi:[10.1088/1751-8113/49/14/145001](https://doi.org/10.1088/1751-8113/49/14/145001).
- [19] S. Franz, G. Parisi, M. Sevelev, P. Urbani and F. Zamponi, Universality of the sat-unsat (jamming) threshold in non-convex continuous constraint satisfaction problems, SciPost Physics **2**(3), 019 (2017), doi:[10.21468/SciPostPhys.2.3.019](https://doi.org/10.21468/SciPostPhys.2.3.019).
- [20] H. Yoshino, Disorder-free spin glass transitions and jamming in exactly solvable mean-field models, SciPost Phys. **4**, 40 (2018), doi:[10.21468/SciPostPhys.4.6.040](https://doi.org/10.21468/SciPostPhys.4.6.040).
- [21] M. Baity-Jesi, L. Sagun, M. Geiger, S. Spigler, G. B. Arous, C. Cammarota, Y. LeCun, M. Wyart and G. Biroli, Comparing dynamics: Deep neural networks versus glassy systems, Journal of Statistical Mechanics: Theory and Experiment **2019**(12), 124013 (2019), doi:[10.1088/1742-5468/ab3281](https://doi.org/10.1088/1742-5468/ab3281).
- [22] S. Franz, S. Hwang and P. Urbani, Jamming in multilayer supervised learning models, Physical review letters **123**(16), 160602 (2019), doi:[10.1103/PhysRevLett.123.160602](https://doi.org/10.1103/PhysRevLett.123.160602).
- [23] M. Geiger, S. Spigler, S. d'Ascoli, L. Sagun, M. Baity-Jesi, G. Biroli and M. Wyart, Jamming transition as a paradigm to understand the loss landscape of deep neural networks, Physical Review E **100**(1), 012115 (2019), doi:[10.1103/PhysRevE.100.012115](https://doi.org/10.1103/PhysRevE.100.012115).
- [24] R. Monasson and R. Zecchina, Weight space structure and internal representations: a direct approach to learning and generalization in multilayer neural networks, Physical review letters **75**(12), 2432 (1995), doi:[10.1103/PhysRevLett.75.2432](https://doi.org/10.1103/PhysRevLett.75.2432).
- [25] J. Kurchan, G. Parisi and F. Zamponi, Exact theory of dense amorphous hard spheres in high dimension i. the free energy, Journal of Statistical Mechanics: Theory and Experiment **2012**(10), P10012 (2012), doi:[10.1088/1742-5468/2012/10/P10012](https://doi.org/10.1088/1742-5468/2012/10/P10012).
- [26] J. Kurchan, G. Parisi, P. Urbani and F. Zampoi, Exact theory of dense amorphous hard spheres in high dimension. ii. the high density regime and the gardner transition, The Journal of Physical Chemistry B **117**(42), 12979 (2013), doi:[10.1021/jp402235d](https://doi.org/10.1021/jp402235d).

- [27] P. Charbonneau, J. Kurchan, G. Parisi, P. Urbani and F. Zamponi, Exact theory of dense amorphous hard spheres in high dimension. iii. the full replica symmetry breaking solution, Journal of Statistical Mechanics: Theory and Experiment **2014**(10), P10009 (2014), doi:[10.1088/1742-5468/2014/10/P10009](https://doi.org/10.1088/1742-5468/2014/10/P10009).
- [28] G. Parisi and M. A. Virasoro, On a mechanism for explicit replica symmetry breaking, Journal de Physique **50**(22), 3317 (1989), doi:[10.1051/jphys:0198900500220331700](https://doi.org/10.1051/jphys:0198900500220331700).
- [29] H. Yoshino, Translational and orientational glass transitions in the large-dimensional limit: a generalized replicated liquid theory and an application to patchy colloids, arXiv preprint arXiv:1807.04095 (2018), <https://arxiv.org/abs/1807.04095>.
- [30] V. N. Vapnik and A. Y. Chervonenkis, On the uniform convergence of relative frequencies of events to their probabilities, In Measures of complexity, pp. 11–30. Springer, doi:[10.1007/978-3-319-21852-6_3](https://doi.org/10.1007/978-3-319-21852-6_3) (2015).
- [31] H. Sompolinsky, A. Crisanti and H.-J. Sommers, Chaos in random neural networks, Physical review letters **61**(3), 259 (1988), doi:[10.1103/PhysRevLett.61.259](https://doi.org/10.1103/PhysRevLett.61.259).
- [32] B. Poole, S. Lahiri, M. Raghu, J. Sohl-Dickstein and S. Ganguli, Exponential expressivity in deep neural networks through transient chaos, In D. D. Lee, M. Sugiyama, U. V. Luxburg, I. Guyon and R. Garnett, eds., Advances in Neural Information Processing Systems **29**, pp. 3360–3368. Curran Associates, Inc., <http://papers.nips.cc/paper/6322-exponential-expressivity-in-deep-neural-networks-through-transient-chaos> (2016).
- [33] Y. Okazaki and H. Yoshino, in preparation.
- [34] G. Parisi and T. Rizzo, Large deviations in the free energy of mean-field spin glasses, Physical review letters **101**(11), 117205 (2008), doi:[10.1103/PhysRevLett.101.117205](https://doi.org/10.1103/PhysRevLett.101.117205).
- [35] S. Franz and G. Parisi, Recipes for metastable states in spin glasses, Journal de Physique I **5**(11), 1401 (1995), doi:[10.1051/jpl:1995201](https://doi.org/10.1051/jpl:1995201).
- [36] T. R. Kirkpatrick and D. Thirumalai, Dynamics of the structural glass transition and the p -spin-interaction spin-glass model, Phys. Rev. Lett. **58**(20), 2091 (1987), doi:[10.1103/PhysRevLett.58.2091](https://doi.org/10.1103/PhysRevLett.58.2091).
- [37] T. R. Kirkpatrick and P. G. Wolynes, Stable and metastable states in mean-field Potts and structural glasses, Phys. Rev. B **36**(16), 8552 (1987), doi:[10.1103/PhysRevB.36.8552](https://doi.org/10.1103/PhysRevB.36.8552).
- [38] T. R. Kirkpatrick, D. Thirumalai and P. G. Wolynes, Scaling concepts for the dynamics of viscous liquids near an ideal glassy state, Phys. Rev. A **40**(2), 1045 (1989), doi:[10.1103/PhysRevA.40.1045](https://doi.org/10.1103/PhysRevA.40.1045).
- [39] G. Biroli and J. Bouchaud, The random first-order transition theory of glasses: a critical assessment, In P.G.Wolynes and V.Lubchenko, eds., Structural Glasses and Supercooled Liquids: Theory, Experiment and Applications. Wiley & Sons (2012), [arXiv:0912.2542](https://arxiv.org/abs/0912.2542).
- [40] B. Alder and T. Wainwright, Phase transition for a hard sphere system, The Journal of chemical physics **27**(5), 1208 (1957), doi:[10.1063/1.1743957](https://doi.org/10.1063/1.1743957).

- [41] J. Villain, R. Bidaux, J.-P. Carton and R. Conte, Order as an effect of disorder, Journal de Physique **41**(11), 1263 (1980), doi:[10.1051/jphys:0198000410110126300](https://doi.org/10.1051/jphys:0198000410110126300).
- [42] R. Rammal, G. Toulouse and M. A. Virasoro, Ultrametricity for physicists, Reviews of Modern Physics **58**(3), 765 (1986), doi:[10.1103/RevModPhys.58.765](https://doi.org/10.1103/RevModPhys.58.765).
- [43] K. Nemoto and H. Takayama, Tap free energy structure of sk spin glasses, Journal of Physics C: Solid State Physics **18**(18), L529 (1985), doi:[10.1088/0022-3719/18/18/005](https://doi.org/10.1088/0022-3719/18/18/005).
- [44] L. Berthier, G. Biroli, P. Charbonneau, E. I. Corwin, S. Franz and F. Zamponi, Gardner physics in amorphous solids and beyond, The Journal of chemical physics **151**(1), 010901 (2019), doi:[10.1063/1.5097175](https://doi.org/10.1063/1.5097175).
- [45] B. Derrida, Random-energy model: Limit of a family of disordered models, Physical Review Letters **45**(2), 79 (1980), doi:[10.1103/PhysRevLett.45.79](https://doi.org/10.1103/PhysRevLett.45.79).
- [46] E. Gardner, Spin glasses with p -spin interactions, Nuclear Physics B **257**, 747 (1985), doi:[10.1016/0550-3213\(85\)90374-8](https://doi.org/10.1016/0550-3213(85)90374-8).
- [47] T. M. Cover, Geometrical and statistical properties of systems of linear inequalities with applications in pattern recognition, IEEE transactions on electronic computers (3), 326 (1965), doi:[10.1109/PGEC.1965.264137](https://doi.org/10.1109/PGEC.1965.264137).
- [48] Y. Iba, The nishimori line and bayesian statistics, Journal of Physics A: Mathematical and General **32**(21), 3875 (1999), doi:[10.1088/0305-4470/32/21/302](https://doi.org/10.1088/0305-4470/32/21/302).
- [49] H. Nishimori, Statistical physics of spin glasses and information processing: an introduction, 111. Clarendon Press (2001).
- [50] R. Shwartz-Ziv and N. Tishby, Opening the black box of deep neural networks via information, arXiv preprint arXiv:1703.00810 (2017).
- [51] M. De Oliveira and R. B. Griffiths, Lattice-gas model of multiple layer adsorption, Surface Science **71**(3), 687 (1978), doi:[10.1016/0039-6028\(78\)90455-7](https://doi.org/10.1016/0039-6028(78)90455-7).
- [52] E. Gardner and B. Derrida, Optimal storage properties of neural network models, Journal of Physics A: Mathematical and general **21**(1), 271 (1988), doi:[10.1088/0305-4470/21/1/031](https://doi.org/10.1088/0305-4470/21/1/031).
- [53] W. Krauth and M. Mézard, Storage capacity of memory networks with binary couplings, Journal de Physique **50**(20), 3057 (1989), doi:[10.1051/jphys:0198900500200305700](https://doi.org/10.1051/jphys:0198900500200305700).
- [54] S. F. Swallen, K. L. Kearns, M. K. Mapes, Y. S. Kim, R. J. McMahon, M. D. Ediger, T. Wu, L. Yu and S. Satija, Organic glasses with exceptional thermodynamic and kinetic stability, Science **315**(5810), 353 (2007), doi:[10.1126/science.1135795](https://doi.org/10.1126/science.1135795).
- [55] S. Léonard and P. Harrowell, Macroscopic facilitation of glassy relaxation kinetics: Ultrastable glass films with frontlike thermal response, The Journal of chemical physics **133**(24), 244502 (2010), doi:[10.1063/1.3511721](https://doi.org/10.1063/1.3511721).

- [56] T. Pérez-Castañeda, C. Rodríguez-Tinoco, J. Rodríguez-Viejo and M. A. Ramos, Suppression of tunneling two-level systems in ultrastable glasses of indomethacin, *Proceedings of the National Academy of Sciences* **111**(31), 11275 (2014), doi:[10.1073/pnas.1405545111](https://doi.org/10.1073/pnas.1405545111).
- [57] K. Hukushima and K. Nemoto, Exchange monte carlo method and application to spin glass simulations, *Journal of the Physical Society of Japan* **65**(6), 1604 (1996), doi:[10.1143/JPSJ.65.1604](https://doi.org/10.1143/JPSJ.65.1604).
- [58] S. Franz, G. Parisi and M. A. Virasoro, Interfaces and louver critical dimension in a spin glass model, *Journal de Physique I* **4**(11), 1657 (1994), doi:[10.1051/jp1:1994213](https://doi.org/10.1051/jp1:1994213).
- [59] S. Franz and A. Montanari, Analytic determination of dynamical and mosaic length scales in a kac glass model, *Journal of Physics A: Mathematical and Theoretical* **40**(11), F251 (2007), doi:[10.1088/1751-8113/40/11/F01](https://doi.org/10.1088/1751-8113/40/11/F01).
- [60] H. Ikeda and A. Ikeda, One-dimensional kac model of dense amorphous hard spheres, *EPL (Europhysics Letters)* **111**(4), 40007 (2015), doi:[10.1209/0295-5075/111/40007](https://doi.org/10.1209/0295-5075/111/40007).
- [61] A. Wagner, Evolution of gene networks by gene duplications: a mathematical model and its implications on genome organization, *Proceedings of the National Academy of Sciences* **91**(10), 4387 (1994), doi:[10.1073/pnas.91.10.4387](https://doi.org/10.1073/pnas.91.10.4387).
- [62] A. Wagner, Does evolutionary plasticity evolve?, *Evolution* **50**(3), 1008 (1996), doi:[0.1111/j.1558-5646.1996.tb02342.x](https://doi.org/0.1111/j.1558-5646.1996.tb02342.x).
- [63] S. Nagata and M. Kikuchi, Emergence of cooperative bistability and robustness of gene regulatory networks, *arXiv preprint arXiv:1907.12030* (2019).
- [64] J. Monod, J. Wyman and J.-P. Changeux, On the nature of allosteric transitions: a plausible model, *J Mol Biol* **12**(1), 88 (1965), doi:[10.1016/S0022-2836\(65\)80285-6](https://doi.org/10.1016/S0022-2836(65)80285-6).
- [65] J. W. Rocks, N. Pashine, I. Bischofberger, C. P. Goodrich, A. J. Liu and S. R. Nagel, Designing allostery-inspired response in mechanical networks, *Proceedings of the National Academy of Sciences* **114**(10), 2520 (2017), doi:[10.1073/pnas.1612139114](https://doi.org/10.1073/pnas.1612139114).
- [66] L. Yan, R. Ravasio, C. Brito and M. Wyart, Architecture and coevolution of allosteric materials, *Proceedings of the National Academy of Sciences* **114**(10), 2526 (2017), doi:[10.1073/pnas.1615536114](https://doi.org/10.1073/pnas.1615536114).
- [67] R. Monasson, Structural glass transition and the entropy of the metastable states, *Phys. Rev. Lett.* **75**(15), 2847 (1995), doi:[10.1103/PhysRevLett.75.2847](https://doi.org/10.1103/PhysRevLett.75.2847).
- [68] M. Mézard and G. Parisi, A first-principle computation of the thermodynamics of glasses, *The Journal of Chemical Physics* **111**(3), 1076 (1999), doi:[10.1063/1.479193](https://doi.org/10.1063/1.479193).
- [69] S. F. Edwards and P. W. Anderson, Theory of spin glasses, *Journal of Physics F: Metal Physics* **5**(5), 965 (1975), doi:[10.1088/0305-4608/5/5/017](https://doi.org/10.1088/0305-4608/5/5/017).
- [70] S. Franz, M. Mézard, F. Ricci-Tersenghi, M. Weigt and R. Zecchina, A ferromagnet with a glass transition, *EPL (Europhysics Letters)* **55**(4), 465 (2001), doi:[10.1209/epl/i2001-00438-4](https://doi.org/10.1209/epl/i2001-00438-4).

- [71] H. Sompolinsky and A. Zippelius, Relaxational dynamics of the edwards-anderson model and the mean-field theory of spin-glasses, Physical Review B **25**(11), 6860 (1982), doi:[10.1103/PhysRevB.25.6860](https://doi.org/10.1103/PhysRevB.25.6860).
- [72] L. F. Cugliandolo and J. Kurchan, Analytical solution of the off-equilibrium dynamics of a long-range spin-glass model, Physical Review Letters **71**(1), 173 (1993), doi:[10.1103/PhysRevLett.71.173](https://doi.org/10.1103/PhysRevLett.71.173).
- [73] S. Franz and M. Mézard, Off-equilibrium glassy dynamics: a simple case, EPL (Europhysics Letters) **26**(3), 209 (1994), doi:[10.1209/0295-5075/26/3/009](https://doi.org/10.1209/0295-5075/26/3/009).
- [74] L. F. Cugliandolo and J. Kurchan, On the out-of-equilibrium relaxation of the sherrington-kirkpatrick model, Journal of Physics A: Mathematical and General **27**(17), 5749 (1994), doi:[10.1088/0305-4470/27/17/011](https://doi.org/10.1088/0305-4470/27/17/011).
- [75] S. Franz, M. Mézard, G. Parisi and L. Peliti, Measuring equilibrium properties in aging systems, Physical Review Letters **81**(9), 1758 (1998), doi:[10.1103/PhysRevLett.75.2847](https://doi.org/10.1103/PhysRevLett.75.2847).
- [76] R. Monasson, Structural glass transition and the entropy of the metastable states, Physical review letters **75**(15), 2847 (1995), doi:[Structural glass transition and the entropy of the metastable states](https://doi.org/10.1103/PhysRevLett.75.2847).
- [77] T. Plefka, Convergence condition of the tap equation for the infinite-ranged ising spin glass model, Journal of Physics A: Mathematical and general **15**(6), 1971 (1982), doi:[10.1088/0305-4470/15/6/035](https://doi.org/10.1088/0305-4470/15/6/035).
- [78] C. De Dominicis and P. Mottishaw, Replica symmetric solutions in the ising spin glass: the tree approximation, EPL (Europhysics Letters) **3**(1), 87 (1987), doi:[10.1209/0295-5075/3/1/014](https://doi.org/10.1209/0295-5075/3/1/014).
- [79] M. Mézard and G. Parisi, Replica field theory for random manifolds, Journal de Physique I **1**(6), 809 (1991), doi:[10.1051/jp1:1991171](https://doi.org/10.1051/jp1:1991171).
- [80] B. Duplantier, Comment on parisi's equation for the sk model for spin glasses, Journal of Physics A: Mathematical and General **14**(1), 283 (1981), doi:[10.1088/0305-4470/14/1/027](https://doi.org/10.1088/0305-4470/14/1/027).

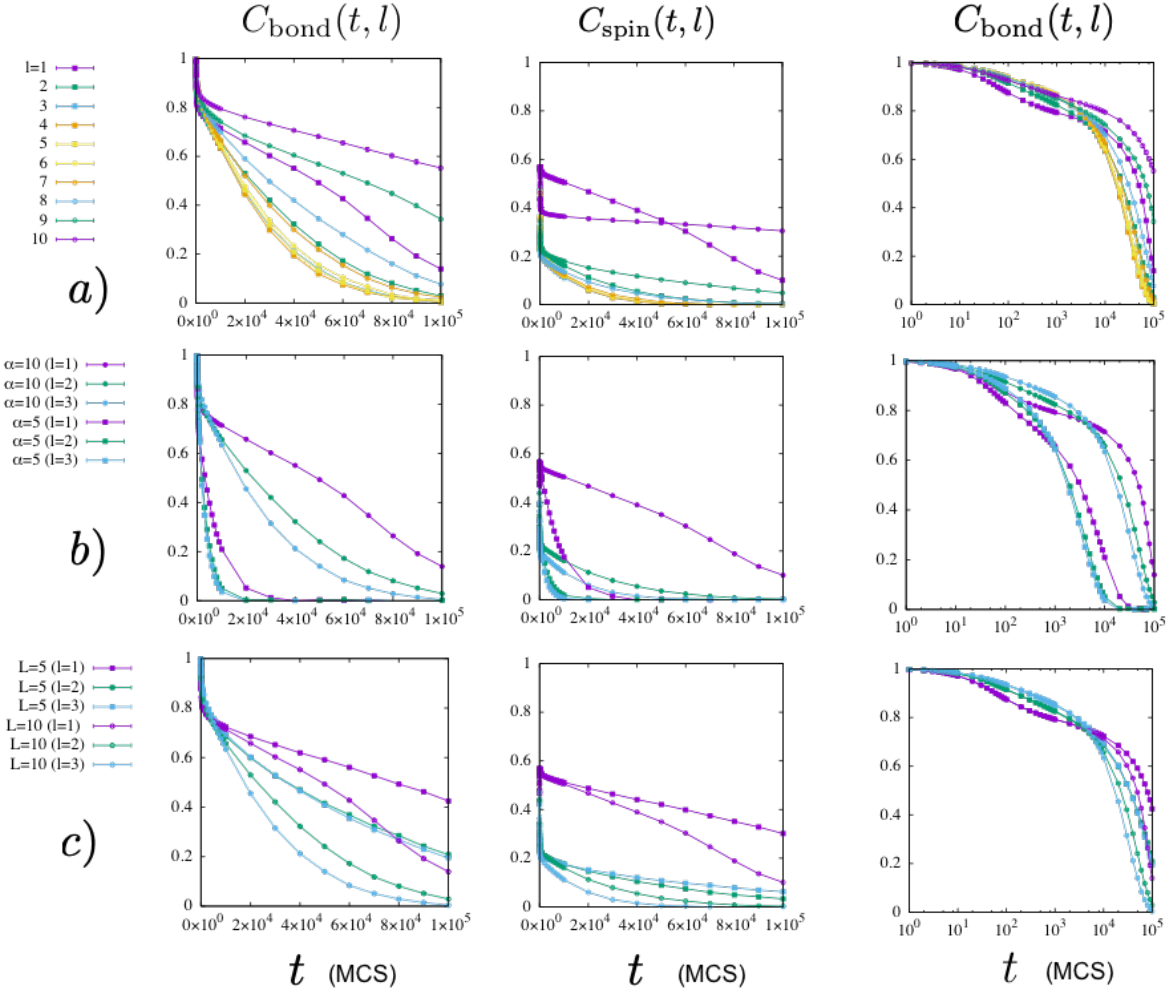


Figure 15: Relaxation of auto-correlation functions of the bonds $C_{\text{bond}}(t, l)$ and spins $C_{\text{spin}}(t, l)$. The two columns on the left-hand side display correlation functions of the bonds and spins plotted against time t . The column on the right-hand side displays the same data of $C_{\text{bond}}(t, l)$ against logarithmic time scale. In the 1st row a) data at different layers $l = 1, 2, \dots, 10$ ($L = 10, \alpha = 10$) are shown. In the 2nd row b) data for $\alpha = 5$ and 10 ($L = 10$) are shown. In the 3rd row c) data obtained with different depth $L = 5$ and 10 ($\alpha = 10$) are shown. Error bars are smaller than the size of the symbols.

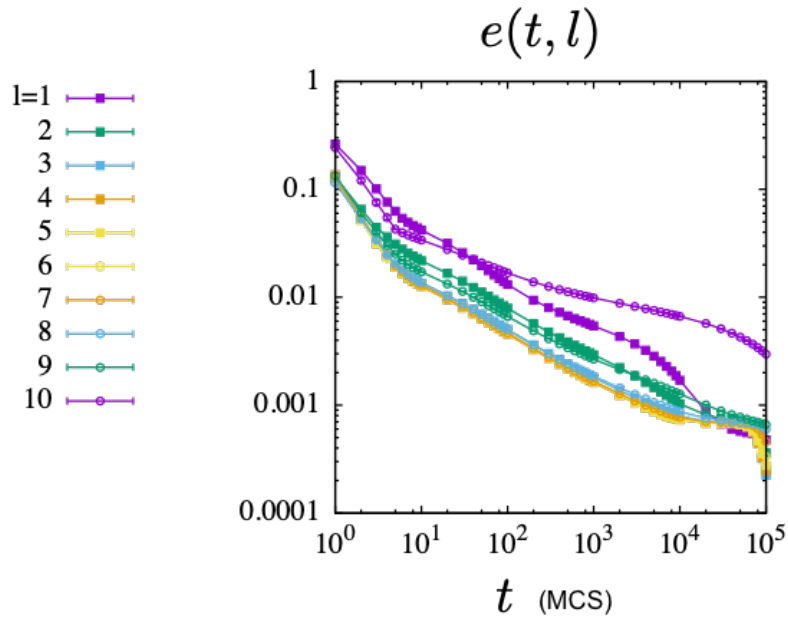


Figure 16: Relaxation of energy $e(t, l)$. Data at different layers $l = 1, 2, \dots, 10$ ($L = 10, \alpha = 10$) are shown. Error bars are smaller than the size of the symbols.

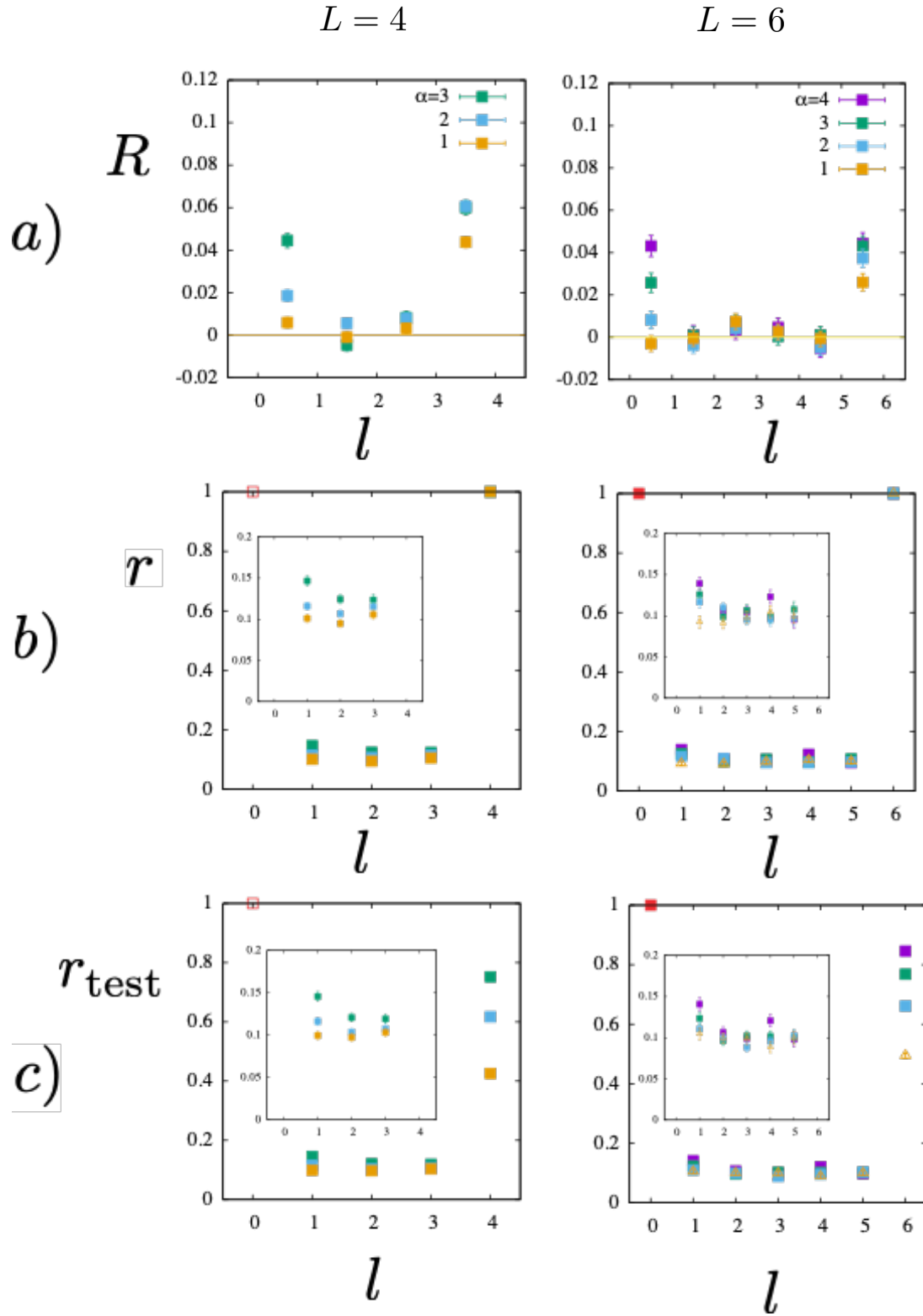


Figure 17: The overlap between the teacher and student machines. a) overlap of the bonds for training data, b) the same as a) but for the spins and c) overlap of the spins for the test data. The left column is for $L = 4, N = 4$ and $\alpha = M/N = 1, 2, 3$. The points in a) are put centered at half-integer values (for instance $1/2$ for the bond between the 0-th and 1st layer). The right column is for $L = 6, N = 4$ and $\alpha = M/N = 1, 2, 3, 4$. Note that

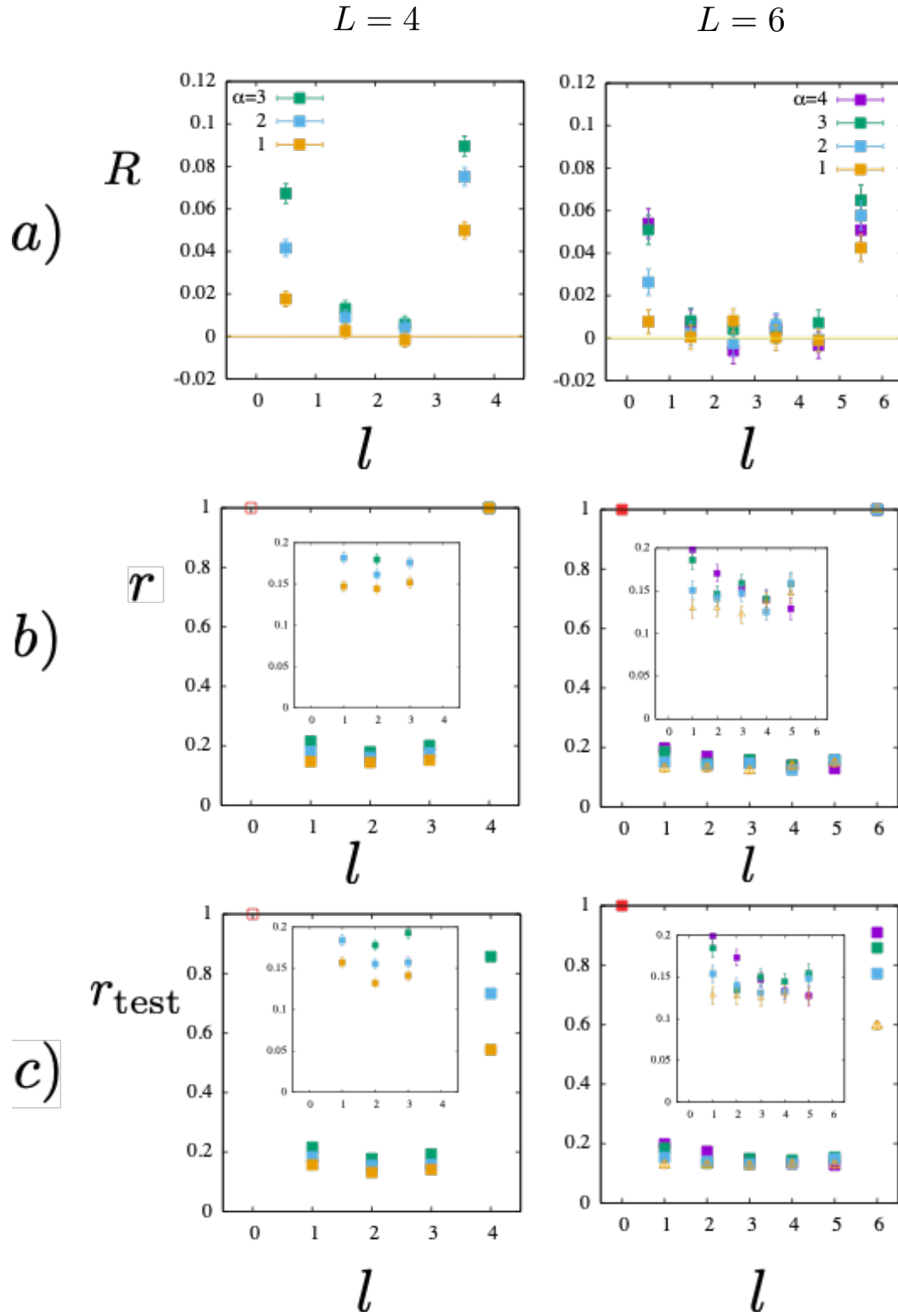


Figure 18: Same as Fig. 17 but 40% of bonds removed.

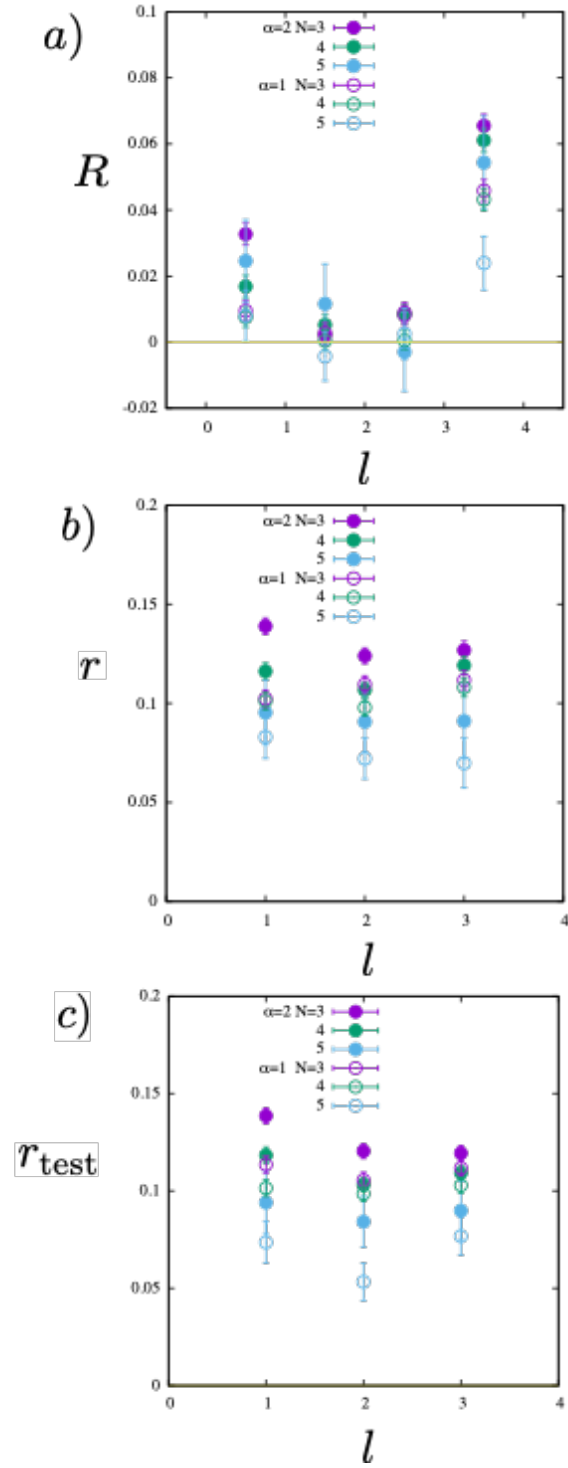


Figure 19: Width N dependence of the a) bond and b) spin overlap for the training data, and c) spin overlap for the test data with $\alpha = M/N = 1, 2$ for $N = 3, 4, 5$. Here $L = 4$. 20% of bonds removed.

A Replicated free-energy

The replicated phase space volume (the Gardner volume) can be written as,

$$\begin{aligned}
V^n(\mathbf{S}_0, \mathbf{S}_L) &= e^{NM\mathcal{S}_n(\mathbf{S}_0, \mathbf{S}_L)} \\
&= \prod_{a=1}^n \left(\prod_{\blacksquare} \text{Tr}_{\mathbf{J}_{\blacksquare}^a} \right) \left(\prod_{\blacksquare \setminus \text{output}} \text{Tr}_{\mathbf{S}_{\blacksquare}^a} \right) \left\{ \prod_{\mu, \blacksquare, a} \int \frac{d\eta_{\mu, \blacksquare, a}}{\sqrt{2\pi}} W_{\eta_{\mu, \blacksquare, a}} e^{i\eta_{\mu, \blacksquare, a} (r_{\blacksquare}^{\mu})^a} \right\} \\
&= \left(\prod_{\mu, \blacksquare, a} \int \frac{d\eta_{\mu, \blacksquare, a}}{\sqrt{2\pi}} W_{\eta_{\mu, \blacksquare, a}} \right) \left(\prod_{\blacksquare} \text{Tr}_{\mathbf{J}_{\blacksquare}^a} \right) \left(\prod_{\blacksquare \setminus \text{output}} \text{Tr}_{\mathbf{S}_{\blacksquare}^a} \right) \\
&\quad \prod_{\mu, \blacksquare, a} e^{i\eta_{\mu, \blacksquare, a} \sum_{\nu=1}^M \frac{\xi_{\mu\nu}}{\sqrt{M}} (S_{\blacksquare}^{\nu})^a \sum_{i=1}^N \frac{(J_{\blacksquare}^i)^a}{\sqrt{N}} (S_{\blacksquare(i)}^{\nu})^a}
\end{aligned} \tag{38}$$

where we introduced a Fourier representation,

$$e^{-\beta V(r)} = \int \frac{d\eta}{\sqrt{2\pi}} W_{\eta} e^{-i\eta r} \tag{39}$$

In the following we derive the free-energy functional of the replicated system starting from Eq. (38), following similar steps as in [20].

A.1 Basic strategy

Before going to the details of the computations, let us sketch the basic strategy to extract properties of glassy phases using the replica approach in the present work as well as [20]. Very importantly, this applies to systems without the quenched disorder. Actually, this strategy lies behind the replica approach to structural glasses [11, 29, 35, 67, 68]. This is an important point for our present problem which is essentially disorder-free except for the boundaries.

A.1.1 Explicit replica symmetry breaking

For simplicity, suppose that we have a generic system which consists of N degrees of freedom $\{x\} = (x_1, x_2, \dots, x_N)$ whose Hamiltonian is $H[\{x\}]$, which can be with/without the quenched disorder. Let us introduce n replicas $a = 1, 2, \dots, n$ and a replicated Hamiltonian,

$$H_n[\hat{\epsilon}] = \sum_{a=1}^n H[\{x_i^a\}] - \sum_{a < b} \epsilon_{ab} \sum_{i=1}^N x_i^a x_i^b. \tag{40}$$

Here we introduced the 2nd term on the r.h.s. which represents an artificial attractive coupling $\epsilon_{ab} > 0$ between replicas. The field ϵ_{ab} explicitly breaks the replica symmetry, i.e. the permutation symmetry of replica index. The free-energy of the replicated system can be defined as,

$$-\beta G[\hat{\epsilon}] = \ln \prod_{a=1}^n \prod_{i=1}^N \text{Tr}_{x_i^a} e^{-\beta H_n[\hat{\epsilon}]}. \tag{41}$$

This allows us to evaluate the overlap between the replicas,

$$q_{ab} = \frac{1}{N} \sum_{i=1}^N \langle x_i^a x_i^b \rangle_{\epsilon} = -\frac{1}{N} \frac{\partial G_{\epsilon}}{\partial \epsilon_{ab}} \tag{42}$$

We are interested with,

$$\lim_{\hat{\epsilon} \rightarrow 0} \lim_{N \rightarrow \infty} q_{ab} \quad (43)$$

and consider that this is the glass order parameter of the system. This is the idea of explicit replica symmetry breaking (RSB) by Parisi and Virasoro [28]. Similarly to the magnetic field h for magnetization in ferromagnetic systems, the field ϵ_{ab} is conjugated to the glass order parameter q_{ab} and plays the role of symmetry breaking field.

Let us then consider the Legendre transform of the free-energy,

$$-\beta F[\hat{q}] = -\beta G[\hat{\epsilon}^*] - N \sum_{a < b} \epsilon_{ab}^* q_{ab} \quad (44)$$

where $\hat{\epsilon}^* = \hat{\epsilon}^*[\hat{q}]$ is defined such that,

$$\frac{1}{N} \frac{\partial}{\partial \epsilon_{ab}} (-\beta G[\hat{\epsilon}]) \Big|_{\hat{\epsilon} = \hat{\epsilon}^*[\hat{q}]} = q_{ab}. \quad (45)$$

The inverse of the Legendre transform is,

$$-\beta G[\hat{\epsilon}] = -\beta F[\hat{q}^*] + N \sum_{a < b} \epsilon_{ab} q_{ab}^* \quad (46)$$

where $\hat{q}^* = \hat{q}^*[\hat{\epsilon}]$ is defined such that,

$$\frac{1}{N} \frac{\partial}{\partial q_{ab}} (-\beta F[\hat{q}]) \Big|_{\hat{q} = \hat{q}^*[\hat{\epsilon}]} = \epsilon_{ab}. \quad (47)$$

The last expression tells us that the order parameter of our interest, which detects the spontaneous RSB Eq. (43), can be obtained by minimizing the free-energy $F[\hat{q}]$ which yields $\epsilon_{ab} = 0$.

A.1.2 Ergodicity breaking

If the field does not depend on the replica indexes $\epsilon_{ab} = \epsilon$, we are not breaking the replica symmetry. But the replica symmetric (RS) field can be used at least to detect the *ergodicity breaking* where the Edwards-Anderson (EA) order parameter [69],

$$q_{\text{EA}} = \frac{1}{N} \sum_{i=1}^N \langle x_i \rangle^2 \quad (48)$$

becomes non-zero. Here $\langle \dots \rangle$ represents an appropriate thermal average. For example, in a model with 3-body interaction $H = -J/N^2 \sum_{i,j,k=1}^N x_i x_j x_k$, the liquid phase where $q_{\text{EA}} = 0$ is realized at high enough temperatures while crystalline or glassy phases where $q_{\text{EA}} > 0$ emerge at lower temperatures [20, 70].

In the context of relaxational dynamics, the EA order parameter can be considered as the long-time limit of the time autocorrelation function [69],

$$q_{\text{EA}} = \lim_{t \rightarrow \infty} C(t) \quad C(t) \equiv \frac{1}{N} \sum_{i=1}^N \langle x_i(0) x_i(t) \rangle. \quad (49)$$

In the liquid phase the auto-correlation function decays down to 0 after finite relaxation time. The latter diverges at the transition leading to $q_{\text{EA}} > 0$. Thus the EA order parameter detects

the Ergodicity breaking (either due to crystalline or glass transitions). Note that the RSB discussed previously in sec. A.1.1 automatically also means an ergodicity breaking, but of a more complicated version involving the hierarchical organization of relaxations [71–75].

In some cases, like a model with 2-body interaction $H = -J/N \sum_{i,j,k=1}^N x_i x_j$, the system is symmetric under global 'spin flip' $x_i \rightarrow -x_i$ for $\forall i$, the perturbation Eq. (40) with the RS field $\epsilon_{ab} = \epsilon$ then breaks this symmetry. In our present problem Eq. (9), the 'spins' have this symmetry. One observes that the system is no longer invariant under global flip in one replica, say a , $x_i^a \rightarrow -x_i^a$ for $\forall i$. Thus the role played by the RS field $\epsilon_{ab} = \epsilon$, in this case, is like the magnetic field conjugated to the magnetization which is the order parameter for usual ferromagnets.

A.1.3 What is the symmetry breaking field?

In the theoretical formulation, we introduced conveniently the symmetry-breaking fields ϵ_{ab} as Eq. (40). But we have to ask ourselves what plays the role of the somewhat fictitious field in reality. The perturbations like Eq. (40) can be introduced by considering 'random pinning fields' [28, 76]. Some sorts of weak random pinning fields may exist in nature. But what about computers? In the context of machine learning, the role of symmetry breaking field may be played by 1) choices of boundary conditions (inputs/outputs data) 2) choices of initial condition for learning.

A.1.4 Plefka expansion

Now our task is to compute the free-energy $F[\hat{q}]$ defined in Eq. (44). To this end, we will follow the idea of Plefka expansion [77]. The computations presented in the following sections follow this strategy.

Suppose that the effect of the interactions between the dynamical variables x_i ($i = 1, 2, \dots, N$) can be treated perturbatively which enable the following decompositions,

$$F = F_0 + \lambda F_1 + \dots \quad G = G_0 + \lambda G_1 + \dots \quad \epsilon_{ab} = (\epsilon_0)_{ab} + \lambda(\epsilon_1)_{ab} + \dots \quad (50)$$

Here the quantities with suffix 0 represent those which are present in the absence of interactions (like the ideal gas free-energy) and those with suffix 1 represent those due to interactions. Here we omitted the higher-order terms. The parameter λ , which is introduced to organize a perturbation theory, is put back to $\lambda = 1$ in the end.

The Legendre transform Eq. (44) becomes, at $O(\lambda^0)$,

$$-\beta F_0[\hat{q}] = -\beta G_0[\hat{\epsilon}_0^*] - N \sum_{a < b} (\epsilon_0^*)_{ab} q_{ab} \quad (51)$$

where $(\epsilon_0^*)_{ab}$ is defined such that,

$$\frac{1}{N} \frac{\partial}{\partial \epsilon_{ab}} (-\beta G_0[\hat{\epsilon}]) \Big|_{\hat{\epsilon} = \hat{\epsilon}_0^*[\hat{q}]} = q_{ab}. \quad (52)$$

Then at $O(\lambda)$ we find,

$$\begin{aligned} -\beta F_1[\hat{q}] &= -\beta G_1[\hat{\epsilon}_0^*[\hat{q}]] + \sum_{a < b} \frac{\partial}{\partial \epsilon_{ab}} (-\beta G_0[\hat{\epsilon}]) \Big|_{\hat{\epsilon} = \hat{\epsilon}_0^*[\hat{q}]} (\epsilon_1^*)_{ab} - N \sum_{a < b} (\epsilon_1^*)_{ab} q_{ab} \\ &= -\beta G_1[\hat{\epsilon}_0^*[\hat{q}]] \end{aligned} \quad (53)$$

In the 2nd equation we used Eq. (52). Minimization of the free-energy $F[\hat{q}]$ (see Eq. (47)) implies $(\epsilon_0^*)_{ab} = -\lambda(\epsilon_1^*)_{ab}$ up to this order.

A.2 Evaluation of the entropic part of the free-energy

We introduce 'local' order parameters [20],

$$Q_{ab,\blacksquare} = \frac{1}{N} \sum_{i=1}^N (J_{\blacksquare}^i)^a (J_{\blacksquare}^i)^b \quad q_{ab,\blacksquare} = \frac{1}{M} \sum_{\mu=1}^M (S_{\blacksquare}^{\mu})^a (S_{\blacksquare}^{\mu})^b \quad (54)$$

through the identities,

$$\begin{aligned} 1 &= \int \prod_{a<b} \left(\frac{N}{2\pi} \right) dQ_{ab,\blacksquare} d\epsilon_{ab,\blacksquare} e^{iN \sum_{a<b} (\epsilon_{ab,\blacksquare} Q_{ab,\blacksquare} - N^{-1} \sum_{i=1}^N (J_{\blacksquare}^i)^a (J_{\blacksquare}^i)^b)} \\ 1 &= \int \prod_{a<b} \left(\frac{M}{2\pi} \right) dq_{ab,\blacksquare} d\varepsilon_{ab,\blacksquare} e^{iM \sum_{a<b} (\varepsilon_{ab,\blacksquare} q_{ab,\blacksquare} - M^{-1} \sum_{\mu=1}^M (S_{\blacksquare}^{\mu})^a (S_{\blacksquare}^{\mu})^b)} \end{aligned} \quad (55)$$

by which we can write

$$\prod_a \text{Tr}_{\mathbf{J}_{\blacksquare}^a} \dots = \left(\prod_{a<b} \int_{-\infty}^{\infty} d(Q_{ab,\blacksquare}) \right) e^{N s_{\text{ent},\text{bond}}[\hat{Q}_{\blacksquare}]} \prod_{i=1}^N \langle \dots \rangle_{J^i} \quad (56)$$

$$\prod_a \text{Tr}_{\mathbf{S}_{\blacksquare}^a} \dots = \left(\prod_{a<b} \int_{-\infty}^{\infty} d(q_{ab,\blacksquare}) \right) e^{M s_{\text{ent},\text{spin}}[\hat{q}_{\blacksquare}]} \prod_{\mu=1}^M \langle \dots \rangle_{S^{\mu}} \quad (57)$$

where we have performed integrations over ϵ_{ab} and ε_{ab} by the saddle point method assuming $c \gg 1$ and $M \gg 1$. We also dropped irrelevant prefactors. We find,

$$s_{\text{ent},\text{bond}}[\hat{Q}] = \sum_{a<b} \varepsilon_{ab}^* Q_{ab} + \ln \prod_{c=1}^n \text{Tr}_{J^c} e^{-\sum_{a<b} \varepsilon_{ab}^* J^a J^b} \quad (58)$$

$$\langle \dots \rangle_{J^i} = \frac{\prod_{c=1}^n \text{Tr}_{J^c} e^{-\sum_{a<b} \varepsilon_{ab}^* (J^a)^{\mu} (J^b)^{\mu}} \dots}{\prod_{c=1}^n \text{Tr}_{J^c} e^{-\sum_{a<b} \varepsilon_{ab}^* (J^a)^{\mu} (J^b)^{\mu}}} \quad (59)$$

and

$$s_{\text{ent},\text{spin}}[\hat{q}] = \sum_{a<b} \epsilon_{ab}^* q_{ab} + \ln \prod_{c=1}^n \text{Tr}_{S^c} e^{-\sum_{a<b} \epsilon_{ab}^* S^a S^b} \quad (60)$$

$$\langle \dots \rangle_{S^{\mu}} = \frac{\prod_{c=1}^n \text{Tr}_{S^c} e^{-\sum_{a<b} \epsilon_{ab}^* (S^a)^{\mu} (S^b)^{\mu}} \dots}{\prod_{c=1}^n \text{Tr}_{S^c} e^{-\sum_{a<b} \epsilon_{ab}^* (S^a)^{\mu} (S^b)^{\mu}}} \quad (61)$$

where $\epsilon_{ab}^* = \epsilon_{ab}^*(\hat{Q})$ and $\varepsilon_{ab}^* = \varepsilon_{ab}^*(\hat{q})$ are determined by

$$Q_{ab} = \frac{\prod_c \text{Tr}_{J^c} e^{-\sum_{a<b} \varepsilon_{ab} J^a J^b}}{\prod_c \text{Tr}_{J^c} e^{-\sum_{a<b} \varepsilon_{ab} J^a J^b}} \Bigg|_{\varepsilon_{ab}=\varepsilon_{ab}^*(\hat{q})} \quad q_{ab} = \frac{\prod_c \text{Tr}_{S^c} e^{-\sum_{a<b} \epsilon_{ab} S^a S^b}}{\prod_c \text{Tr}_{S^c} e^{-\sum_{a<b} \epsilon_{ab} S^a S^b}} \Bigg|_{\epsilon_{ab}=\epsilon_{ab}^*(\hat{Q})} \quad (62)$$

The above equations imply in particular,

$$\langle (J_{\blacksquare}^i)^a \rangle_{J^i} = 0 \quad \langle (J_{\blacksquare}^i)^a (J_{\blacksquare'}^j)^b \rangle_{J^i} = Q_{ab} \delta_{ij} \delta_{\blacksquare, \blacksquare'} \quad (63)$$

$$\langle (S_{\blacksquare}^\mu)^a \rangle_{S^\mu} = 0 \quad \langle (S_{\blacksquare}^\mu)^a (S_{\blacksquare'}^\nu)^b \rangle_{S^\mu} = q_{ab} \delta_{\mu\nu} \delta_{\blacksquare, \blacksquare'} \quad (64)$$

Let us note finally that Eq. (62) correspond to Eq. (52) in the program outlined in sec. A.1.4.

A.2.1 Entropic part of the 'bonds'

The bonds are continuous variables normalized as,

$$\sum_{i=1}^N (J_{\blacksquare(i)}^i)^2 = c \quad (65)$$

which implies,

$$Q_{aa} = 1 \quad (66)$$

and

$$S_{\text{ent, bond}}[\hat{Q}] = \frac{1}{2} \ln \det \hat{Q} \quad (67)$$

A.2.2 Entropic part of the 'spins'

The spins are 'Ising spins'. The entropic part of the free-energy of the spins are [20],

$$\begin{aligned} s_{\text{ent, spin}}[\hat{q}] &= \sum_{a < b} \varepsilon_{ab}^* q_{ab} + \ln e^{-\sum_{a < b} \varepsilon_{ab}^* \frac{\partial^2}{\partial h_a \partial h_b}} \prod_a 2 \cosh(h_a) \Big|_{\{h_a=0\}} \\ &= \frac{1}{2} \sum_{a,b} \varepsilon_{ab}^* q_{ab} + \ln e^{-\frac{1}{2} \sum_{a,b} \varepsilon_{ab}^* \frac{\partial^2}{\partial h_a \partial h_b}} \prod_a 2 \cosh(h_a) \Big|_{\{h_a=0\}} \end{aligned} \quad (68)$$

with $q_{aa} = 1$. Here we performed the spin trace formally as

$$\begin{aligned} \text{Tr}_{\mathbf{S}_c} e^{-\sum_{a < b} \varepsilon_{ab} S^a S^b} &= e^{\frac{1}{2} \sum_a \varepsilon_{aa}} \text{Tr}_{\mathbf{S}_c} e^{-\frac{1}{2} \sum_{a,b} \varepsilon_{ab} S^a S^b} = e^{\frac{1}{2} \sum_a \varepsilon_{aa}} \text{Tr}_{\mathbf{S}_c} e^{-\frac{1}{2} \sum_{a,b} \varepsilon_{ab} \frac{\partial^2}{\partial h_a \partial h_b}} e^{\sum_a h_a S^a} \Big|_{\{h_a=0\}} \\ &= e^{\frac{1}{2} \sum_a \varepsilon_{aa}} e^{-\frac{1}{2} \sum_{a,b} \varepsilon_{ab} \frac{\partial^2}{\partial h_a \partial h_b}} \prod_a 2 \cosh(h_a) \Big|_{\{h_a=0\}} \end{aligned}$$

For the integration over ε_{ab} , the saddle point $\varepsilon_{ab}^* = \varepsilon_{ab}^*[\hat{q}]$ is obtained formally as,

$$q_{ab} = - \frac{\delta}{\delta \varepsilon_{ab}} \ln e^{-\frac{1}{2} \sum_{a,b} \varepsilon_{ab} \frac{\partial^2}{\partial h_a \partial h_b}} \prod_a 2 \cosh(h_a) \Big|_{\{h_a=0\}} \Big|_{\varepsilon_{ab} = \varepsilon_{ab}^*[\hat{q}]} \quad (69)$$

A.3 Evaluation of interaction part of the free-energy

Now we wish to evaluate the partition function Eq. (12) using the tools developed above. What we are doing below is the evaluation of the interaction part of the free-energy Eq. (53) in the program outlined in sec. A.1.4.

In Eq. (57) we notice that different spin components μ are decoupled in the average $\prod_{\mu} \langle \dots \rangle_{S^{\mu}}$. Then we obtain the following cumulant expansion which will become very useful. For any observable $A = A(S^{\mu})$ and writing $\langle \dots \rangle_{S^{\mu}} = \langle \dots \rangle$ for simplicity we find,

$$\begin{aligned} \ln \langle e^{\frac{1}{\sqrt{M}} \sum_{\mu=1}^M A_{\mu}} \rangle &= \sqrt{M} \langle A_{\mu} \rangle + \frac{1}{2!} (\langle A_{\mu}^2 \rangle - \langle A_{\mu} \rangle^2) \\ &+ \frac{1}{3! \sqrt{M}} (\langle A_{\mu}^3 \rangle - 3 \langle A_{\mu}^2 \rangle \langle A_{\mu} \rangle + 2 \langle A_{\mu} \rangle^3) + \dots \end{aligned} \quad (70)$$

Here we just used the fact that $\langle A^{\mu} A^{\nu} \rangle = \langle A^{\mu} \rangle \langle A^{\nu} \rangle$ holds for $\mu \neq \nu$. Thus in the $M \rightarrow \infty$, the lowest non-vanishing cumulant dominates the r.h.s.. For instance if $\langle A_{\mu} \rangle = 0$ and $\langle A_{\mu}^2 \rangle \neq 0$, then $\lim_{M \rightarrow \infty} \ln \langle e^{\frac{1}{\sqrt{M}} \sum_{\mu=1}^M A_{\mu}} \rangle = \frac{1}{2!} \langle A_{\mu}^2 \rangle$. Note that the same property also holds for the averaging in the 'bond space' $\langle \dots \rangle_{J^i}$ in Eq. (56).

A.3.1 Bulk part

Now we are ready to evaluate Gardner's volume Eq. (12). In the bulk part we find,

$$\begin{aligned} & \ln \left\langle \prod_{\mu, \blacksquare, a} \exp \left[i \eta_{\mu, \blacksquare, a} \sum_{i=1}^N \frac{(J_{\blacksquare}^i)^a}{\sqrt{N}} (S_{\blacksquare}^{\mu})^a (S_{\blacksquare(i)}^{\mu})^a \right] \right\rangle_{J^i, S^{\mu}} \\ &= \ln \left\langle 1 + \sum_a \sum_{\blacksquare} \frac{1}{\sqrt{N}} \sum_{i, \mu} i \eta_{\mu, \blacksquare, a} (J_{\blacksquare}^i)^a (S_{\blacksquare}^{\mu})^a (S_{\blacksquare(i)}^{\mu})^a \right. \\ & \quad \left. + \frac{1}{2!} \sum_{a, b} \sum_{\blacksquare, \blacksquare'} \frac{1}{N} \sum_{i, j, \mu, \nu} i \eta_{\mu, \blacksquare, a} i \eta_{\nu, \blacksquare', b} (J_{\blacksquare}^i)^a (J_{\blacksquare'}^j)^b (S_{\blacksquare}^{\mu})^a (S_{\blacksquare'}^{\nu})^b (S_{\blacksquare(i)}^{\mu})^a (S_{\blacksquare'(j)}^{\nu})^b + \dots \right\rangle_{J^i, S^{\mu}} \\ &= \frac{1}{2!} \sum_{a, b} \sum_{\blacksquare, \blacksquare'} \frac{1}{N} \sum_{i, j, \mu, \nu} i \eta_{\mu, \blacksquare, a} i \eta_{\nu, \blacksquare', b} \delta_{\blacksquare, \blacksquare'} \delta_{ij} \delta_{\mu, \nu} Q_{ab, \blacksquare} q_{ab, \blacksquare} q_{ab, \blacksquare(i)} \\ & \quad + \frac{1}{4!} \sum_{a, b, c, d} \sum_{\blacksquare_1, \blacksquare_2, \blacksquare_3, \blacksquare_4} \frac{1}{N^2} \sum_{i, j, k, l, \mu_1, \mu_2, \mu_3, \mu_4} i \eta_{\mu_1, \blacksquare_1, a} i \eta_{\mu_2, \blacksquare_2, b} i \eta_{\mu_4, \blacksquare_3, c} i \eta_{\mu_4, \blacksquare_4, d} \\ & \quad \times \delta_{\blacksquare_1, \blacksquare_2} \delta_{\blacksquare_1, \blacksquare_3} \delta_{\blacksquare_1, \blacksquare_4} \delta_{ij} \delta_{ik} \delta_{il} \delta_{\mu_1, \mu_2} \delta_{\mu_1, \mu_3} \delta_{\mu_1, \mu_4} \times \\ & \quad \left[\langle (J_{\blacksquare}^i)^a (J_{\blacksquare}^j)^b (J_{\blacksquare}^k)^c (J_{\blacksquare}^l)^d \rangle_{J^i} \langle (S_{\blacksquare}^{\mu})^a (S_{\blacksquare}^{\mu})^b (S_{\blacksquare}^{\mu})^c (S_{\blacksquare}^{\mu})^d \rangle_{S^{\mu}} \langle (S_{\blacksquare(i)}^{\mu})^a (S_{\blacksquare(i)}^{\mu})^b (S_{\blacksquare(i)}^{\mu})^c (S_{\blacksquare(i)}^{\mu})^d \rangle_{S^{\mu}} \right. \\ & \quad - Q_{ab, \blacksquare} Q_{cd, \blacksquare} q_{ab, \blacksquare} q_{cd, \blacksquare} q_{ab, \blacksquare(i)} q_{cd, \blacksquare(i)} - Q_{ac, \blacksquare} Q_{bd, \blacksquare} q_{ac, \blacksquare} q_{bd, \blacksquare} q_{ac, \blacksquare(i)} q_{bd, \blacksquare(i)} \\ & \quad \left. - Q_{ad, \blacksquare} Q_{bc, \blacksquare} q_{ad, \blacksquare} q_{bc, \blacksquare} q_{ad, \blacksquare(i)} q_{bc, \blacksquare(i)} \right] + \dots \\ &= \frac{1}{2} \sum_{a, b} \sum_{\blacksquare} \sum_{\mu} i \eta_{\mu, \blacksquare, a} i \eta_{\mu, \blacksquare, b} q_{ab, \blacksquare} Q_{ab, \blacksquare} \frac{1}{N} \sum_{i=1}^N q_{ab, \blacksquare(i)} \end{aligned} \quad (71)$$

In the last equation we assumed $N \gg 1$ by which only the 2nd order term in the cumulant survives. For instance the 4th order term is smaller than the 2nd order term by a factor $O(1/N)$.

A.3.2 Boundaries - quenched vs slightly annealed one

At the output boundary, we have a quenched random spin configuration. For the output boundary we find,

$$\begin{aligned}
& \ln \left\langle \overline{\prod_{\mu, \blacksquare} \exp \left[\sum_a i\eta_{\mu, \blacksquare, a} \sum_{i=1}^N \frac{(J_{\blacksquare}^i)^a}{\sqrt{N}} S_{\blacksquare}^{\mu} (S_{\blacksquare(i)}^{\mu})^a \right]} \right\rangle_{J^i, S^{\mu}}^{S_{\blacksquare}} \\
&= \ln \prod_{\mu, \blacksquare} \left\langle \left\langle \cosh \left[\sum_a i\eta_{\mu, \blacksquare, a} \sum_{i=1}^N \frac{(J_{\blacksquare}^i)^a}{\sqrt{N}} (S_{\blacksquare(i)}^{\mu})^a \right] \right\rangle_{J^i} \right\rangle_{S^{\mu}} \\
&= \ln \prod_{\mu, \blacksquare} \left\langle \exp \left[\frac{1}{2} \sum_{a,b} (i\eta_{\mu, \blacksquare, a})(i\eta_{\mu, \blacksquare, b}) Q_{ab, \blacksquare} \frac{1}{N} \sum_{i=1}^N (S_{\blacksquare(i)}^{\mu})^a (S_{\blacksquare(i)}^{\mu})^b \right] \right\rangle_{S^{\mu}} \\
&= \frac{1}{2} \sum_{a,b} \sum_{\blacksquare} \sum_{\mu} i\eta_{\mu, \blacksquare, a} i\eta_{\mu, \blacksquare, b} Q_{ab, \blacksquare} \frac{1}{N} \sum_{i=1}^N q_{ab, \blacksquare(i)} + \dots
\end{aligned} \tag{72}$$

Here the higher order cumulants cannot be neglected because there is no small factor left in the exponent in the last stage. The situation is similar on the input boundary.

To implement the quenched boundary condition strictly, more complicated order parameters like q_{abcd}, \dots become needed [78]. To avoid such complications we consider slightly annealed boundary condition such that we simply impose,

$$q_{ab}(0) = q_{ab}(L) = 1 \tag{73}$$

on the boundaries. Note that with this we are allowing sub-extensive fluctuations on the boundaries $O(N^a)$ with $0 \leq a \leq 1$.

We note that similar difficulty arises when we 'quench' the bonds. If we wish to consider the bonds J_{\blacksquare}^i s as quenched random variables, we have to take the average over the quenched disorder of the interaction part of the free-energy. By doing so one finds that the result cannot be solely parametrized by the order parameter q_{ab} because higher-order cumulants cannot be neglected.

A.4 Total free-energy

Now we can write

$$\begin{aligned}
V^n(\mathbf{S}_0, \mathbf{S}_L) &= \int \prod_{a < b} \left(\prod_{\blacksquare} dQ_{ab, \blacksquare} e^{N S_{\text{ent}, \text{bond}}[\hat{Q}_{\blacksquare}]} \prod_{\blacksquare \setminus \text{output}} dq_{ab, \blacksquare} e^{M S_{\text{ent}, \text{spin}}[\hat{q}_{\blacksquare}]} \right) \\
&\quad \prod_{\blacksquare} \left\{ \left(\prod_a \int \frac{d\eta_a}{\sqrt{2\pi}} W_{\eta_a} \right) e^{-\frac{1}{2} \sum_{a,b} \eta_a \eta_b Q_{ab, \blacksquare} q_{ab, \blacksquare} \frac{\sum_{i=1}^N q_{ab, \blacksquare}(i)}{N}} \right\}^M \\
&= \int \prod_{a < b} \left(\prod_{\blacksquare} dQ_{ab, \blacksquare} e^{N S_{\text{ent}, \text{bond}}[\hat{Q}_{\blacksquare}]} \prod_{\blacksquare \setminus \text{output}} dq_{ab, \blacksquare} e^{M S_{\text{ent}, \text{spin}}[\hat{q}_{\blacksquare}]} \right) \\
&\quad \prod_{\blacksquare} \left\{ e^{-\frac{1}{2} \sum_{a,b} \frac{\partial^2}{\partial h_{\blacksquare, a} \partial h_{\blacksquare, b}} Q_{ab, \blacksquare} q_{ab, \blacksquare} \frac{\sum_{i=1}^N q_{ab, \blacksquare}(i)}{N}} \prod_a e^{-\beta V(h_{\blacksquare, a})} \Big|_{h_{\blacksquare, a}=0} \right\}^M \quad (74)
\end{aligned}$$

Given the structure of the network, it is natural to assume that the saddle point values only depend on the layer $l = 0, 1, 2, \dots, L$, as Eq. (14),

$$Q_{ab, \blacksquare}^* = Q_{ab}(l) \quad q_{ab, \blacksquare}^* = q_{ab}(l) \quad (75)$$

Then we find,

$$S_n[\{\hat{Q}(l), \hat{q}(l)\}] = \frac{1}{\alpha} \sum_{l=1}^L S_{\text{ent}, \text{bond}}[\hat{Q}(l)] + \sum_{l=1}^{L-1} S_{\text{ent}, \text{spin}}[\hat{q}(l)] - \sum_{l=1}^L \mathcal{F}_{\text{int}}[\hat{q}(l-1), \hat{Q}(l), \hat{q}(l)] \quad (76)$$

with

$$-\mathcal{F}_{\text{int}}[\hat{q}(l-1), \hat{Q}(l), \hat{q}(l)] = \ln e^{\frac{1}{2} \sum_{ab} q_{ab}(l-1) Q_{ab}(l) q_{ab}(l) \partial_{h_{l,a}} \partial_{h_{l,b}}} \prod_{a=1}^n e^{-\beta V(h_{l,a})} \Big|_{h_{l,a}=0} \quad (77)$$

The order parameters must verify saddle point equations,

$$\frac{\partial}{\partial Q_{ab}(l)} \partial_n S_n[\{\hat{Q}(l), \hat{q}(l)\}] \Big|_{n=0} = 0 \quad l = 1, 2, \dots, L \quad (78)$$

$$\frac{\partial}{\partial q_{ab}(l)} \partial_n S_n[\{\hat{Q}(l), \hat{q}(l)\}] \Big|_{n=0} = 0 \quad l = 1, 2, \dots, L-1 \quad (79)$$

A.5 Parisi's ansatz

A.5.1 Random inputs/outputs

In the case of random inputs/outputs (sec. 2.2.1) we have n replicas $a = 1, 2, \dots, n$. Then it is natural to consider the standard Parisi's ansatz with k -step RSB (including RS as $k = 0$

and continuous RSB as $k = \infty$) [13, 14] (See Fig. 20),

$$Q_{ab}(l) = \sum_{i=0}^{k+1} Q_i(l)(I_{ab}^{m_i} - I_{ab}^{m_{i+1}}) \quad l = 1, 2, \dots, L \quad (80)$$

$$q_{ab}(l) = \sum_{i=0}^{k+1} q_i(l)(I_{ab}^{m_i} - I_{ab}^{m_{i+1}}) \quad l = 1, 2, \dots, L-1 \quad (81)$$

$$\varepsilon_{ab}(l) = \sum_{i=0}^k \varepsilon_i(l)(I_{ab}^{m_i} - I_{ab}^{m_{i+1}}) \quad l = 1, 2, \dots, L-1 \quad (82)$$

where I_{ab}^m is a generalized ('fat') Identity matrix of size $n \times n$ composed of blocks of size $m \times m$. Here we assumed $q_{k+1}(l) = Q_{k+1}(l) = 1$ and $I_{ab}^{m_{k+2}} = 0$. In the Parisi's ansatz one considers

$$1 = m_{k+1} < m_k < \dots < m_1 < m_0 = n \quad (83)$$

which becomes

$$0 = m_0 < m_1 < \dots < m_k < m_{k+1} = 1 \quad (84)$$

in the $n \rightarrow 0$ limit. In the $k \rightarrow \infty$ limit, the matrix elements can be parametrized by functions $q(x, l)$, $Q(x, l)$ and $\varepsilon(x, l)$ defined in the range $0 \leq x \leq 1$ (See Fig. 20 d)).

The order parameter functions encode characteristics of the complex free-energy landscape [14]. For example the distribution functions of the overlaps between two replicas (two independent machines) can be related to the order parameter functions as,

$$P(q, l) = \frac{dx(q, l)}{dq} \quad x(q, l) = \int_0^q dq' P(q', l) \quad (85)$$

$$P(Q, l) = \frac{dx(Q, l)}{dQ} \quad x(Q, l) = \int_0^Q dQ' P(Q', l) \quad (86)$$

Thus $x(q, l)$ ($x(Q, l)$) is the probability that the mutual overlap of the spin (bond) patterns at l -th layer between two machine are smaller than q (Q). Equivalently $1 - x(q, l)$ ($1 - x(Q, l)$) is the probability that the mutual overlap of the spin (bond) patterns at l -th layer between two machine are *larger* than q (Q).

The functions $q(x, l)$ and $Q(x, l)$ are expected to have a 'plateau' close to $x = 1$, which gives rise to a delta function in the overlap distribution functions $P(q, l)$ and $P(Q, l)$. As usual we regard the plateau values as the self-overlaps of the meta-stable states or the Edwards-Anderson order parameters $q_{\text{EA}}(l)$ and $Q_{\text{EA}}(l)$. In practice we will use the values of q_k and Q_k in the k -RSB ansatz as the Edwards-Anderson order parameters.

Analysis of the free-energy functional $-\beta F[\{\hat{Q}(l), \hat{q}(l)\}]/MN$ Eq. (15) can be done using these matrices in Eq. (76). In appendix B, we present details of the RSB solution.

A.5.2 Teacher-student setting

For the teacher-student setting (sec. 2.2.2) we have to modify the matrices \hat{Q}, \hat{q} and $\hat{\varepsilon}$ slightly to include $a = 0$ for the teacher machine in addition to $a = 1, 2, \dots, s$ for the student as shown in Fig. 21. We denote the modified matrices as $\hat{Q}^{1+s}, \hat{q}^{1+s}$ and $\hat{\varepsilon}^{1+s}$. The sub-matrices \hat{q}^s , \hat{Q}^s and $\hat{\varepsilon}^s$ are for the student for which we assume the same hierarchical structure as before Eq. (80)-Eq. (82).

Analysis of the Franz-Parisi potential $-\beta F_{\text{teacher-student}}[\{\hat{Q}(l), \hat{q}(l)\}]/MN$ Eq. (17) can be done using these matrices in Eq. (76). In appendix C, we present details of the RSB solution.

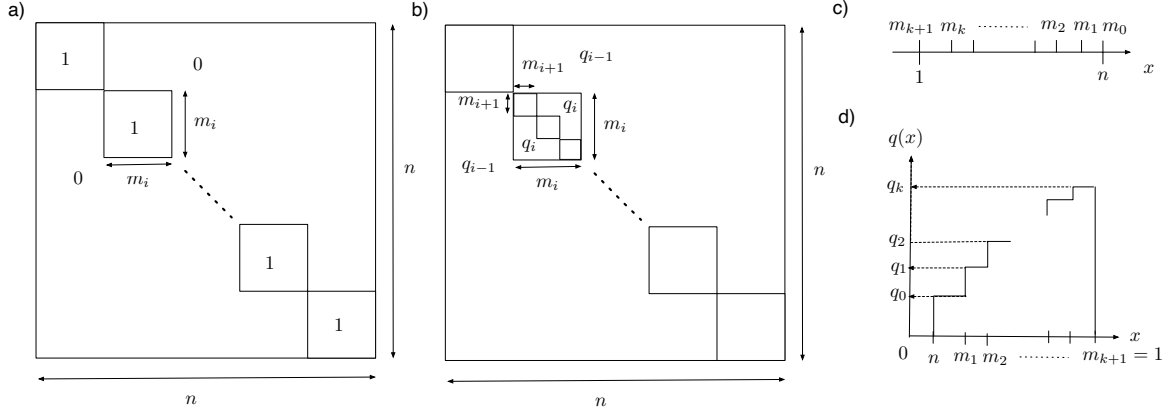


Figure 20: Parametrization of the Parisi's matrix a) the 'fat' identity matrix $I_{ab}^{m_i}$ b) Parisi's matrix given by Eq. (81) (Eq. (80) and Eq. (82) have the same structure with q_i 's replaced by Q_i 's and ϵ_i 's.) c) the hierarchy of the sizes m_i of the sub-matrices d) the $q(x)$ function with $0 < n < 1$ ($Q(x), \epsilon(x)$ functions have the same structure).

B RSB solution for the random inputs/outputs

Here we derive the RSB solution using the Parisi's ansatz explained in sec. A.5.1.

B.1 Entropic part of the free-energy

B.1.1 Entropic part of the free-energy due to 'bonds'

In the k -RSB ansatz, the entropic part of the free-energy Eq. (67) due to the 'bonds' can be evaluated as follows. We find [20, 79],

$$\ln \det \hat{Q} = \ln \left(1 + \sum_{j=0}^k (m_j - m_{j+1}) Q_j \right) \quad (87)$$

$$+ n \sum_{i=0}^k \left(\frac{1}{m_{i+1}} - \frac{1}{m_i} \right) \ln \left(1 + \sum_{j=i}^k (m_j - m_{j+1}) Q_j - m_i Q_i \right) \quad (88)$$

Remembering that $m_0 = n$ we find,

$$\begin{aligned} \partial_n S_{\text{ent, bond}}[\hat{Q}] \Big|_{n=0} &= \frac{1}{2} \partial_n \ln \det \hat{Q} \Big|_{n=0} = \frac{1}{2} \frac{Q_0}{G_0} + \frac{1}{2} \frac{1}{m_1} \ln G_0 \\ &+ \frac{1}{2} \sum_{i=1}^k \left(\frac{1}{m_{i+1}} - \frac{1}{m_i} \right) \ln G_i \end{aligned} \quad (89)$$

with

$$G_i = 1 + \sum_{j=i}^k (m_j - m_{j+1}) Q_j - m_i Q_i \quad i = 0, 1, \dots, k \quad (90)$$

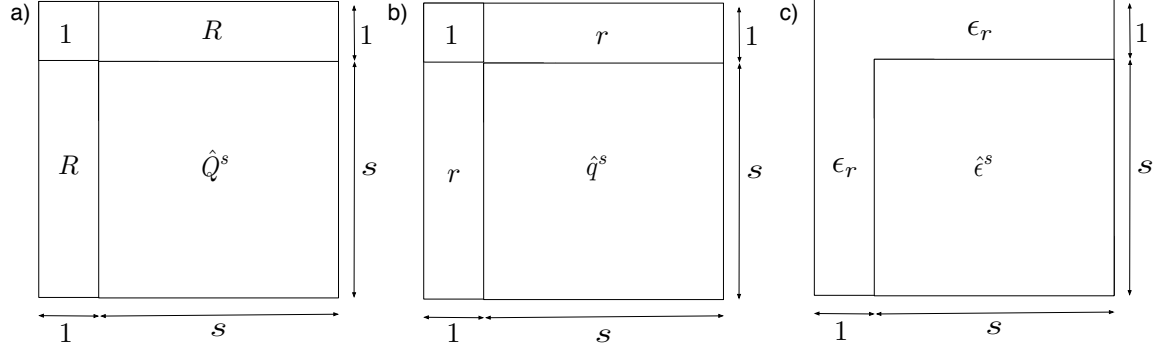


Figure 21: Parametrization of the Parisi's matrices for the teacher-student setting : a) \hat{Q}^{1+s} b) \hat{q}^{1+s} and c) $\hat{\epsilon}^{1+s}$. For the sub-matrices \hat{q}^s , \hat{Q}^s and $\hat{\epsilon}^s$ of size $s \times s$ we assume the same hierarchical structure as those in Eq. (80)-Eq. (82) (see Fig. 20) but with n replaced by s .

which implies

$$Q_i = 1 - G_k + \sum_{j=i+1}^k \frac{1}{m_j} (G_j - G_{j-1}) \quad i = 0, 1, \dots, k \quad (91)$$

B.1.2 Entropic part of the free-energy due to 'spins'

In the k -RSB ansatz, the entropic part of the free-energy Eq. (68) due to the 'spins' can be evaluated as follows

$$\begin{aligned} S_{\text{ent,spin}}[\hat{\epsilon}, \hat{q}] &= \frac{n}{2} \sum_{i=0}^k \epsilon_i q_i (m_i - m_{i+1}) + \frac{n}{2} \epsilon_k \\ &+ \ln \prod_{i=0}^k \exp \left[\frac{\Lambda_i^{\text{Ising}}}{2} \sum_{a,b=1}^n I_{ab}^{m_i} \frac{\partial^2}{\partial h_a \partial h_b} \right] \prod_{a=1}^n (2 \cosh(h_a)) \Bigg|_{\{h_a=0\}} \end{aligned} \quad (92)$$

which implies

$$\begin{aligned} \partial_n S_{\text{ent,spin}}[\hat{\epsilon}, \hat{q}]|_{n=0} &= \frac{1}{2} \sum_{i=0}^k \epsilon_i q_i (m_i - m_{i+1}) + \frac{\epsilon_k}{2} - f_{\text{Ising}}(m_0 = 0, 0) \\ &= \frac{1}{2} \sum_{i=0}^k \epsilon_i q_i (m_i - m_{i+1}) + \frac{\epsilon_k}{2} - \int Dz_0 f_{\text{Ising}}(m_1, \sqrt{\Lambda_0^{\text{Ising}}} z_0) \end{aligned} \quad (93)$$

where ϵ_i 's must be fixed through saddle point equations with respect to variations of them (see below).

In the last two-equation of Eq. (93) we used a family of functions which can be obtained recursively as follows [80]. Using

$$\Lambda_i^{\text{Ising}} = \begin{cases} -\epsilon_0 & (i = 0) \\ -\epsilon_i + \epsilon_{i-1} & (i = 1, 2, \dots, k) \end{cases} \quad (94)$$

we introduce a family of functions defined recursively for $i = 0, 1, 2, \dots, k$,

$$\begin{aligned} e^{-m_i f_{\text{Ising}}(m_i, h)} &= e^{\frac{\Lambda_i^{\text{Ising}}}{2} \frac{\partial^2}{\partial h^2}} e^{-m_i f_{\text{Ising}}(m_{i+1}, h)} \\ &= \gamma_{\Lambda_i^{\text{Ising}}} \otimes e^{-m_i f(m_{i+1}, h)} \\ &= \int Dz_i e^{-m_i f_{\text{Ising}}(m_{i+1}, h - \sqrt{\Lambda_i^{\text{Ising}}} z_i)} \end{aligned} \quad (95)$$

with the initial condition

$$f_{\text{Ising}}(m_{k+1}, h) = -\ln 2 \cosh(h). \quad (96)$$

Here we used an identity

$$\exp\left(\frac{a}{2} \frac{\partial^2}{\partial h^2}\right) A(h) = \gamma_a \otimes A(h) \quad (97)$$

and the following short hand notations: $\gamma_a(x)$ is a Gaussian

$$\gamma_a(x) = \frac{1}{\sqrt{2\pi a}} e^{-\frac{x^2}{2a}}, \quad (98)$$

by which we write a convolution of a function $A(x)$ with the Gaussian as,

$$\gamma_a \otimes A(x) \equiv \int dy \frac{e^{-\frac{y^2}{2a}}}{\sqrt{2\pi a}} A(x - y) = \int \mathcal{D}z A(x - \sqrt{a}z) \quad (99)$$

where

$$\int \mathcal{D}z \dots \equiv \int dz \frac{e^{-\frac{z^2}{2}}}{\sqrt{2\pi}} \dots \quad (100)$$

The saddle point equation with respect to variations of $\hat{\epsilon}$ Eq. (69) becomes in the k -RSB ansatz, for $i = 0, 1, 2, \dots, k$,

$$\begin{aligned} q_i &= \frac{2}{m_i - m_{i+1}} \left[\left(-\frac{\partial}{\partial \epsilon_i} \right) (-f_{\text{Ising}}(m_0 = 0, 0)) - \frac{1}{2} \delta_{ik} \right] \\ &= \int dh P_{\text{Ising}}(m_i, h) (-f'_{\text{Ising}}(m_{i+1}, h))^2 \end{aligned} \quad (101)$$

where $f'_{\text{Ising}}(m, h) = \partial_h f_{\text{Ising}}(m, h)$ and we used (see [20] appendix C)

$$\left(-\frac{\partial}{\partial \epsilon_i} \right) (-f_{\text{Ising}}(m_0 = 0, 0)) = \frac{1}{2} (m_i - m_{i+1}) \int dh P_{\text{Ising}}(m_i, h) (-f'_{\text{Ising}}(m_{i+1}, h))^2 + \frac{1}{2} \delta_{i,k} \quad (102)$$

with

$$P_{\text{Ising}}(m_i, h) \equiv \frac{\delta f_{\text{Ising}}(m_0, 0)}{\delta f_{\text{Ising}}(m_{i+1}, h)} \quad (103)$$

which follows a recursion formula (see [20] sec. 8.3.1),

$$P_{\text{Ising}}(m_j, h) = e^{-m_j f_{\text{Ising}}(m_{j+1}, h)} \gamma_{\Lambda_j^{\text{Ising}}} \otimes h \frac{P_{\text{Ising}}(m_{j-1}, h)}{e^{-m_j f_{\text{Ising}}(m_j, h)}} \quad j = 1, 2, \dots, k \quad (104)$$

with the 'boundary condition'

$$P_{\text{Ising}}(m_0, h) = \frac{1}{\sqrt{2\pi\Lambda_0^{\text{Ising}}}} e^{-\frac{h^2}{2\Lambda_0}} \quad (105)$$

In Eq. (104) \otimes_h stands for a convolution with respect to the variable h .

The derivatives $f'_{\text{Ising}}(m, h) = \partial_h f_{\text{Ising}}(m, h)$ can also be obtained recursively. From Eq. (95) and Eq. (96) we find,

$$f'_{\text{Ising}}(m_i, h) = e^{m_i f_{\text{Ising}}(m_i, h)} \gamma_{\Lambda_i^{\text{Ising}}} \otimes f'_{\text{Ising}}(m_{i+1}, h) e^{-m_i f_{\text{Ising}}(m_{i+1}, h)} \quad (106)$$

for $i = 1, 2, \dots, k$ with the 'boundary condition',

$$f'_{\text{Ising}}(m_{k+1}, h) = -\tanh(h) \quad (107)$$

B.2 Interaction part of the free-energy

The interaction part of the free-energy Eq. (77) becomes in the k -RSB ansatz,

$$\begin{aligned} -\partial_n \mathcal{F}_{\text{int}}[\hat{q}(l-1), \hat{Q}(l), \hat{q}(l)] \Big|_{n=0} &= \partial_n \ln \prod_{i=0}^{k+1} \exp \left[\frac{\Lambda_i(l)}{2} \sum_{a,b=1}^n I_{ab}^{m_i} \frac{\partial^2}{\partial h_a \partial h_b} \right] \prod_{a=1}^n e^{-\beta V(r(h_a))} \Big|_{\{h_a=0\}} \Big|_{n=0} \\ &= f(m_0 = 0, 0, l) \\ &= \int Dz_0 f(m_1, h - \sqrt{\Lambda_0}, l) \Big|_{h=0} \end{aligned} \quad (108)$$

with, for $l = 1, 2, \dots, L$,

$$\Lambda(l) = \begin{cases} \lambda_0(l) & (i = 0) \\ \lambda_i(l) - \lambda_{i-1}(l) & (i = 1, 2, \dots, k+1) \end{cases} \quad (109)$$

and

$$\lambda_i(l) = q_i(l-1) Q_i(l) q_i(l) \quad (110)$$

We introduced a family of functions defined recursively for $i = 0, 1, 2, \dots, k$ and $l = 1, 2, \dots, L$,

$$\begin{aligned} e^{-m_i f(m_i, h, l)} &= e^{\frac{\Lambda_i(l)}{2} \frac{\partial^2}{\partial h^2}} e^{-m_i f(m_{i+1}, h, l)} \\ &= \int Dz_i e^{-m_i f(m_{i+1}, h - \sqrt{\Lambda_i(l)} z_i, l)} \end{aligned} \quad (111)$$

with the initial condition

$$f(m_{k+1}, l) = -\ln \gamma_{\Lambda_{k+1}(l)} \otimes e^{-\beta V(h)} = -\ln \int Dz_{k+1} e^{-\beta V(h - \sqrt{\Lambda_{k+1}(l)} z_{k+1})} \quad (112)$$

For the hard-core potential Eq. (7) we find,

$$f(m_{k+1}, h, l) = -\ln \Theta \left(\frac{h}{\sqrt{2\Lambda_{k+1}(l)}} \right) \quad (113)$$

where

$$\Theta(x) = \int_{-\infty}^x \frac{dy}{\sqrt{\pi}} e^{-y^2} \quad (114)$$

B.3 Saddle point equations

B.3.1 Variation of $q_i(l)$'s

The saddle point equations Eq. (79) becomes, for $i = 0, 1, 2, \dots, k$ and $l = 1, 2, \dots, L - 1$,

$$\begin{aligned}
 0 &= \frac{\partial}{\partial q_i(l)} \partial_n S_n^{\text{ent, spin}}[\hat{q}, \hat{Q}] \Big|_{n=0} \\
 &= \frac{1}{2} \epsilon_i(l) (m_i - m_{i+1}) - \frac{\partial}{\partial q_i(l)} \sum_{l'=1}^L \mathcal{F}_{\text{int}}[\hat{q}(l' - 1), \hat{Q}(l'), \hat{q}(l')] \\
 &= \frac{1}{2} \epsilon_i(l) (m_i - m_{i+1}) + \sum_{l'=1}^L \frac{\partial \lambda_i(l')}{\partial q_i(l)} \left(-\frac{\partial f(m_0 = 0, 0, l')}{\partial \lambda_i(l')} \right)
 \end{aligned} \tag{115}$$

from which we find,

$$\begin{aligned}
 \epsilon_i(l) &= - \sum_{l'=1}^L \frac{\partial \lambda_i(l')}{\partial q_i(l)} \kappa_i(l') \\
 &= -q_i(l-1) Q_i(l) \kappa_i(l) - Q_i(l+1) q_i(l+1) \kappa_i(l+1)
 \end{aligned} \tag{116}$$

where we introduced, for $i = 0, 1, 2, \dots, k$ and $l = 1, 2, \dots, L$,

$$\kappa_i(l) \equiv \int dh P(m_i, h, l) (-f'(m_{i+1}, h, l))^2 \tag{117}$$

with

$$P(m_i, h, l) \equiv \frac{\delta f(m_0, 0, l)}{\delta f(m_{i+1}, h, l)} \tag{118}$$

which follows a recursion formula (see [20] sec. 8.3.1),

$$P(m_j, h, l) = e^{-m_j f(m_{j+1}, h, l)} \gamma_{\Lambda_j} \otimes_h \frac{P(m_{j-1}, h, l)}{e^{-m_j f(m_j, h, l)}} \quad j = 1, 2, \dots, k+1 \tag{119}$$

with the 'boundary condition'

$$P(m_0, h, l) = \frac{1}{\sqrt{2\pi\Lambda_0(l)}} e^{-\frac{h^2}{2\Lambda_0(l)}} \tag{120}$$

The last equation of Eq. (115) is obtained using the following (see [20] appendix C)

$$\frac{\partial}{\partial \lambda_i(l)} (-f(m_0 = 0, 0, l)) = \frac{1}{2} (m_i - m_{i+1}) \int dh P(m_i, h, l) (-f'(m_{i+1}, h, l))^2 \tag{121}$$

The derivatives $f'(m, h, l) = \partial_h f(m, h, l)$ can also be obtained recursively. From Eq. (111) and Eq. (112) we find,

$$f'(m_i, h, l) = e^{m_i f(m_i, h, l)} \gamma_{\Lambda_i(l)} \otimes f'(m_{i+1}, h, l) e^{-m_i f(m_{i+1}, h, l)} \tag{122}$$

for $i = 1, 2, \dots, k$ with the 'boundary condition',

$$f'(m_{k+1}, h, l) = - \frac{\int Dz_{k+1} (e^{-\beta V(h - \sqrt{\Lambda_{k+1}(l)})})'}{\int Dz_{k+1} e^{-\beta V(h - \sqrt{\Lambda_{k+1}(l)})}} \tag{123}$$

which becomes for the hardcore potential (using Eq. (113) and Eq. (114)),

$$f'(m_{k+1}, h, l) = -\frac{1}{\Theta\left(\frac{h}{\sqrt{2\Lambda_{k+1}(l)}}\right)} \frac{1}{\sqrt{2\pi\Lambda_{k+1}(l)}} \exp\left(-\frac{h^2}{2\Lambda_{k+1}(l)}\right) \quad (124)$$

B.3.2 Variation of $G_i(l)$'s

For the saddle point equations Eq. (78) it is convenient to consider instead, for $i = 0, 1, 2, \dots, k$ and $l = 1, 2, \dots, L$,

$$0 = \frac{\partial}{\partial G_i(l)} \partial_n S[\hat{q}, \hat{Q}] \Big|_{n=0} \quad (125)$$

where $G_i(l)$'s are defined in Eq. (90). We obtain (see [20] sec. 8.4),

$$\begin{aligned} \frac{Q_0(l)}{G_0^2(l)} &= \alpha q_0(l) q_0(l-1) \kappa_0(l) \\ \frac{1}{G_i(l)} - \frac{1}{G_0(l)} &= \alpha \left(\sum_{j=0}^{i-1} (m_j - m_{j+1}) q_j(l) q_j(l-1) \kappa_j(l) + m_i q_i(l) q_i(l-1) \kappa_i(l) \right) \end{aligned} \quad (126)$$

for $i = 1, 2, \dots, k$.

B.3.3 Procedure to solve the saddle point equations

The saddle point equations for a generic finite k -RSB ansatz with some fixed values of $0 < m_1 < m_2 < \dots < m_k < 1$ can be solved numerically as follows.

0. Choose a boundary condition by fixing $q_i(0)$ and $q_i(L)$ for $i = 0, 1, 2, \dots, k$.
1. Make some guess for the initial values of $q_i(l)$ ($l = 1, 2, \dots, L-1$) and $Q_i(l)$ ($l = 1, 2, \dots, L$) for $i = 0, 1, 2, \dots, k$. Then compute $G_i(l)$ for $i = 0, 1, \dots, k$ and $l = 1, 2, \dots, L-1$ using Eq. (90).
2. Do the following (1)-(8) for $l = 1, 2, \dots, L$. (1) Compute $\lambda_i(l)$ for $i = 0, 1, 2, \dots, k$ and using Eq. (110). (2) Compute $\Lambda_i(l)$ for $i = 0, 1, 2, \dots, k+1$ using Eq. (109). (3) Compute functions $f(m_i, h, l)$ recursively for $i = k, k-1, \dots, 0$ using Eq. (111) with the boundary condition given by Eq. (112) (which is Eq. (113) for the hardcore potential). (4) Compute also the derivatives $f'(m_i, h, l)$ recursively for $i = k, k-1, \dots, 2, 1$ using Eq. (122) with the boundary condition given by Eq. (123) (which is Eq. (124) for the hardcore potential). (5) Compute functions $P(m_i, h, l)$ recursively for $i = 1, \dots, k$ using Eq. (119) with the boundary condition given by Eq. (120). (6) Compute $\kappa_i(l)$ for $i = 0, 1, \dots, k$ using Eq. (117). (7) Compute $G_i(l)$ for $i = 0, 1, \dots, k$ using Eq. (126). (8) Compute $Q_i(l)$ for $i = 0, 1, \dots, k$ using Eq. (91).
3. Do the following (1)-(6) for $l = 1, 2, \dots, L-1$. (1) Compute $\epsilon_i(l)$ for $i = 0, 1, 2, \dots, k$ using Eq. (116). (2) Compute $\Lambda_i^{\text{Ising}}(l)$ for $i = 0, 1, 2, \dots, k$ using Eq. (94). (3) Compute functions $f_{\text{Ising}}(m_i, h, l)$ recursively for $i = k, k-1, \dots, 0$ using Eq. (95) with the boundary condition given by Eq. (96). (4) Compute also the derivatives $f'_{\text{Ising}}(m_i, h, l)$

recursively for $i = k, k-1, \dots, 2, 1$ using Eq. (106) with the boundary condition given by Eq. (107). (5) Compute functions $P_{\text{Ising}}(m_i, h, l)$ recursively for $i = 1, \dots, k$ using Eq. (104) with the boundary condition given by Eq. (105). (6) Compute $q_i(l)$ for $i = 0, 1, \dots, k$ using Eq. (101).

4. Return to 2.

The above procedure 1.-4. must be repeated until the solution converges. The values of m_i s ($0 < m_1 < m_2 \dots < m_k < 1$ (see Fig. 20 c))) are chosen such that $\log m_i$ s are equally spaced between $\log m_1$ and $\log m_{k+1} = 0$. We chose $m_1 = 0.0001$ in the numerical analysis shown in this paper. Numerical integrations are done by the simple rectangle rule with an integration step 0.01.

C RSB solution for the teacher-student setting

Here we derive the RSB solution using the Parisi's ansatz explained in sec. A.5.2.

C.1 Entropic part of the free-energy

C.1.1 Entropic part of the free-energy due to 'bonds'

Within the ansatz for the teacher-student setting, the entropic part of the free-energy Eq. (67) due to the 'bonds' can be evaluated as follows. First we find,

$$\det \hat{Q}^{1+s} = \det(\hat{Q}^s - R^2). \quad (127)$$

Thus we find

$$\begin{aligned} \partial_s S_{\text{ent, bond}}[\hat{Q}^{1+s}] \Big|_{s=0} &= \frac{1}{2} \partial_s \ln \det(\hat{Q}^s - R^2) \Big|_{s=0} \\ &= \frac{1}{2} \frac{Q_0 - R^2}{G_0} + \frac{1}{2} \frac{1}{m_1} \ln G_0 \\ &\quad + \frac{1}{2} \sum_{i=1}^k \left(\frac{1}{m_{i+1}} - \frac{1}{m_i} \right) \ln G_i \end{aligned} \quad (128)$$

with

$$G_i = 1 + \sum_{j=i}^k (m_j - m_{j+1}) Q_j - m_i Q_i \quad i = 0, 1, \dots, k \quad (129)$$

which implies

$$Q_i = 1 - G_k + \sum_{j=i+1}^k \frac{1}{m_j} (G_j - G_{j-1}) \quad i = 0, 1, \dots, k \quad (130)$$

Note that above equations slightly modify Eq. (90) and Eq. (91).

C.1.2 Entropic part of the free-energy due to 'spins'

Within the same ansatz, the entropic part of the free-energy Eq. (68) due to the 'spins' can be evaluated as follows,

$$\begin{aligned}
S_{\text{ent,spin}}[\hat{\epsilon}^{1+s}, \hat{q}^{1+s}] &= s\epsilon_r r + \frac{1}{2}\epsilon_r + \frac{s}{2} \sum_{i=0}^k \epsilon_i q_i (m_i - m_{i+1}) + \frac{s}{2}\epsilon_k \\
&+ \ln \exp \left[\frac{\Lambda_{\text{com}}^{\text{Ising}}}{2} \sum_{a,b=0}^s \frac{\partial^2}{\partial h_a \partial h_b} \right] \prod_{i=0}^k \exp \left[\frac{\Lambda_i^{\text{Ising}}}{2} \sum_{a,b=1}^s I_{ab}^{m_i} \frac{\partial^2}{\partial h_a \partial h_b} \right] \prod_{a=0}^s (2 \cosh(h_a)) \Big|_{\{h_a=0\}} \\
&= s\epsilon_r r + \frac{1}{2}\epsilon_r + \frac{s}{2} \sum_{i=0}^k \epsilon_i q_i (m_i - m_{i+1}) + \frac{s}{2}\epsilon_k \\
&+ \ln \gamma_{\Lambda_{\text{com}}} \otimes (2 \cosh(h) \gamma_{\Lambda_0^{\text{Ising}}} \otimes e^{-s f^{\text{Ising}}(m_1, h)}) \Big|_{h=0}
\end{aligned} \tag{131}$$

where ϵ_r and ϵ_i 's must be fixed through saddle point equations with respect to variations of them (see below).

In Eq. (131) $I_{ab}^{m_i}$ is defined similarly as those used in Eq. (80)-Eq. (82) (see Fig. 20) but with size $s \times s$ instead of $n \times n$. We have also introduced,

$$\begin{aligned}
\Lambda_{\text{com}}^{\text{Ising}} &= -\epsilon_r \\
\Lambda_i^{\text{Ising}} &= \begin{cases} -\epsilon_0 + \epsilon_r & (i=0) \\ -\epsilon_i + \epsilon_{i-1} & (i=1, 2, \dots, k) \end{cases}
\end{aligned} \tag{132}$$

and used the family of functions defined recursively for $i = 0, 1, 2, \dots, k$ using Eq. (95) and the initial condition Eq. (96). One must keep in mind that Λ_0^{Ising} in Eq. (132) is shifted with respect to that in Eq. (94) due to ϵ_r .

The saddle point equations with respect to variations of $\hat{\epsilon}^{1+s}$ Eq. (69) yield q_i 's and r . Variation with respect to ϵ_i yields the equation for the q_i 's, which is formally the same as Eq. (101),

$$q_i = \int dh P_{\text{Ising}}(m_i, h) (-f'_{\text{Ising}}(m_i, h))^2 \tag{133}$$

for $i = 0, 1, 2, \dots, k$. Here $P_{\text{Ising}}(m_i, h)$ can be obtained from the equation Eq. (104). However the initial condition is modified from Eq. (105) to

$$P_{\text{Ising}}(m_0, h) = \frac{\int Dz_{\text{com}} 2 \cosh(\sqrt{\Lambda_{\text{com}}^{\text{Ising}}} z_{\text{com}}) \frac{1}{\sqrt{2\pi\Lambda_0^{\text{Ising}}}} e^{-\frac{(h - \sqrt{\Lambda_{\text{com}}^{\text{Ising}}} z_{\text{com}})^2}{2\Lambda_0^{\text{Ising}}}}}{\int Dz_{\text{com}} 2 \cosh(\sqrt{\Lambda_{\text{com}}^{\text{Ising}}} z_{\text{com}})} \tag{134}$$

Variation with respect to ϵ_r yields the equation for the r as the following. Using

$$\begin{aligned}
0 &= \frac{\partial}{\partial \epsilon_r} S_{\text{ent,spin}}[\hat{\epsilon}, \hat{q}^{1+s}] = sr + \frac{1}{2} - \frac{1}{2} \\
&- s \frac{\int Dz_{\text{com}} 2 \sinh(\sqrt{\Lambda_{\text{com}}^{\text{Ising}}} z_{\text{com}}) \int Dz_0 (-f'_{\text{Ising}}(m_1, \sqrt{\Lambda_{\text{com}}^{\text{Ising}}} z_{\text{com}} + \sqrt{\Lambda_0^{\text{Ising}}} z_0))}{\int Dz_{\text{com}} 2 \cosh(\sqrt{\Lambda_{\text{com}}^{\text{Ising}}} z_{\text{com}})} + O(s^2)
\end{aligned} \tag{135}$$

Thus we find

$$r = \frac{\int Dz_{\text{com}} 2 \sinh(\sqrt{\Lambda_{\text{com}}} z_{\text{com}}) \int Dz_0 (-f'_{\text{Ising}}(m_1, \sqrt{\Lambda_{\text{com}}} z_{\text{com}} + \sqrt{\Lambda_0^{\text{Ising}}} z_0))}{\int Dz_{\text{com}} 2 \cosh(\sqrt{\Lambda_{\text{com}}} z_{\text{com}})} \quad (136)$$

C.2 Interaction part of the free-energy

Within the same ansatz, the interaction part of the free-energy Eq. (77) becomes,

$$\begin{aligned} \partial_s \mathcal{F}_{\text{int}}[\hat{q}^{1+s}(l-1), \hat{Q}^{1+s}(l), \hat{q}^{1+s}(l)] \Big|_{s=0} &= \partial_s \ln \exp \left[\frac{\Lambda_{\text{com}}(l)}{2} \sum_{a,b=0}^s \frac{\partial^2}{\partial h_a \partial h_b} \right] \exp \left[\frac{\Lambda_{\text{teacher}}(l)}{2} \frac{\partial^2}{\partial h_0^2} \right] \\ &\prod_{i=0}^{k+1} \exp \left[\frac{\Lambda_i(l)}{2} \sum_{a,b=1}^s I_{ab}^{m_i} \frac{\partial^2}{\partial h_a \partial h_b} \right] \prod_{a=0}^s e^{-\beta V(r(h_a))} \Big|_{\{h_a=0\}_{s=0}} \\ &= \partial_s \ln \int Dz_{\text{com}} \int Dz_{\text{teacher}} e^{-\beta V(\sqrt{\Lambda_{\text{com}}(l)} z_{\text{com}} + \sqrt{\Lambda_{\text{teacher}}(l)} z_{\text{teacher}})} \\ &\quad \int Dz_0 f(m_1, \sqrt{\Lambda_{\text{com}}(l)} z_{\text{com}} + \sqrt{\Lambda_0(l)} z_0) \Big|_{s=0} \end{aligned} \quad (137)$$

with, for $l = 1, 2, \dots, L$. Here we introduced,

$$\begin{aligned} \Lambda_{\text{com}}(l) &= r(l-1)R(l)r(l) \\ \Lambda_{\text{teacher}}(l) &= 1 - r(l-1)R(l)r(l) \\ \Lambda_i(l) &= \begin{cases} \lambda_0(l) - \Lambda_{\text{com}}(l) & (i=0) \\ \lambda_i(l) - \lambda_{i-1}(l) & (i=1, 2, \dots, k+1) \end{cases} \end{aligned} \quad (138)$$

with $\lambda_i(l)$'s defined in Eq. (110) which reads as,

$$\lambda_i(l) = q_i(l-1)Q_i(l)q_i(l) \quad (139)$$

We also used the family of functions $f(m_i, h)$ defined recursively for $i = 0, 1, 2, \dots, k$ and $l = 1, 2, \dots, L$ by Eq. (111) with the initial condition Eq. (112). Note that Λ_0 is shifted with respect to that in Eq. (109) due to R and r .

C.3 Saddle point equations

C.3.1 Variation of $q_i(l)$'s

For the saddle point equations Eq. (79), we find formally the same result as Eq. (116) which reads as,

$$\epsilon_i(l) = -q_i(l-1)Q_i(l)\kappa_i(l) - Q_i(l+1)q_i(l+1)\kappa_i(l+1) \quad (140)$$

with κ_i defined as Eq. (117) which reads as,

$$\kappa_i(l) \equiv \int dh P(m_i, h, l) (-f'(m_{i+1}, h, l))^2. \quad (141)$$

The function $P(m_i, h, l)$ can be also be obtained by the same equations as before Eq. (119) but with the initial condition Eq. (120) modified as,

$$P(m_0, h, l) = \frac{\int Dz_{\text{com}} \int Dz_{\text{teacher}} e^{-\beta V(\sqrt{\Lambda_{\text{com}}(l)} z_{\text{com}} + \sqrt{\Lambda_{\text{teacher}}(l)} z_{\text{teacher}})} \frac{1}{\sqrt{2\pi\Lambda_0(l)}} e^{-\frac{(h - \sqrt{\Lambda_{\text{com}}(l)} z_{\text{com}})^2}{2\Lambda_0(l)}}}{\int Dz_{\text{com}} \int Dz_{\text{teacher}} e^{-\beta V(\sqrt{\Lambda_{\text{com}}(l)} z_{\text{com}} + \sqrt{\Lambda_{\text{teacher}}(l)} z_{\text{teacher}})}} \quad (142)$$

Note also that Λ_0 is shifted as in Eq. (138). For the hardcore potential Eq. (7) we find,

$$P(m_0, h, l) = \frac{1}{\int Dz \Theta\left(\frac{\sqrt{\Lambda_{\text{com}}(l)} z}{\sqrt{2(\Lambda_{\text{teacher}}(l))}}\right)} \int Dz \Theta\left(\frac{\sqrt{\Lambda_{\text{com}}(l)} z}{\sqrt{2\Lambda_{\text{teacher}}(l)}}\right) \frac{1}{\sqrt{2\pi\Lambda_0(l)}} e^{-\frac{(h - \sqrt{\Lambda_{\text{com}}(l)} z)^2}{2\Lambda_0(l)}} \quad (143)$$

with $\Theta(h)$ defined in Eq. (114).

C.3.2 Variation of $G_i(l)$'s

For the saddle point equations Eq. (78), we just need to modify slightly Eq. (126), with G_i 's defined in Eq. (129),

$$\begin{aligned} \frac{Q_0(l) - R^2(l)}{G_0^2(l)} &= \alpha q_0(l) q_0(l-1) \kappa_0(l) \\ \frac{1}{G_i(l)} - \frac{1}{G_0(l)} &= \alpha \left(\sum_{j=0}^{i-1} (m_j - m_{j+1}) q_j(l) q_j(l-1) \kappa_j(l) + m_i q_i(l) q_i(l-1) \kappa_i(l) \right) \end{aligned} \quad (144)$$

for $l = 1, 2, \dots, L$.

C.3.3 Variation of r

Here we consider variation of the free-energy Eq. (17) (see also Eq. (76)) with respect to $r(l)$, for $l = 1, 2, \dots, L-1$,

$$\begin{aligned} 0 &= \frac{\partial}{\partial r(l)} \partial_s S_{1+s}[\{\hat{Q}(l), \hat{q}(l)\}] \Big|_{s=0} \\ &= \frac{\partial}{\partial r(l)} \partial_s S_{\text{ent,spin}}[\hat{q}^{1+s}(l)] \Big|_{s=0} - \frac{\partial}{\partial r(l)} \sum_{l'=1}^L \partial_s \mathcal{F}_{\text{int}}[\hat{q}^{1+s}(l'-1), \hat{Q}^{1+s}(l'), \hat{q}^{1+s}(l')] \Big|_{s=0} \end{aligned} \quad (145)$$

Variation of the entropic part (spin) of the free-energy Eq. (131) yields,

$$\frac{\partial}{\partial r} \partial_s S_{\text{ent,spin}}[\hat{q}^{1+s}] \Big|_{s=0} = \epsilon_r \quad (146)$$

On the other hand, variation of the interaction part of the free-energy Eq. (137) yields, for

$$l = 1, 2, \dots, L-1,$$

$$\begin{aligned} & -\frac{\partial}{\partial r(l)} \sum_{l'=1}^L \partial_s \mathcal{F}_{\text{int}}[\hat{q}^{1+s}(l-1), \hat{Q}^{1+s}(l), \hat{q}^{1+s}(l)] \Big|_{s=0} \\ & = -\sum_{l'=1}^L \left(\frac{\partial \Lambda_{\text{com}}(l')}{\partial r(l)} \frac{\partial}{\partial \Lambda_{\text{com}}(l')} + \frac{\partial \Lambda_{\text{teacher}}(l')}{\partial r(l)} \frac{\partial}{\partial \Lambda_{\text{teacher}}(l')} + \frac{\partial \Lambda_0(l')}{\partial r(l)} \frac{\partial}{\partial \Lambda_0(l')} \right) \\ & \quad \partial_s \mathcal{F}_{\text{int}}[\hat{q}^{1+s}(l-1), \hat{Q}^{1+s}(l), \hat{q}^{1+s}(l)] \Big|_{s=0} \\ & = r(l-1)R(l)\kappa_{\text{inter}}(l) + R(l+1)r(l+1)\kappa_{\text{inter}}(l+1) \end{aligned} \quad (147)$$

where we introduced

$$\kappa_{\text{inter}}(l) \equiv \frac{\int Dz_{\text{com}} g'_{\text{teacher}}(\sqrt{\Lambda_{\text{com}}(l)} z_{\text{com}}) \int Dz_0 (-f'(m_1, \sqrt{\Lambda_{\text{com}}(l)} z_{\text{com}} + \sqrt{\Lambda_0(l)} z_0))}{\int Dz_{\text{com}} g_{\text{teacher}}(\sqrt{\Lambda_{\text{com}}(l)} z_{\text{com}})} \quad (148)$$

with

$$g_{\text{teacher}}(h) \equiv \int Dz_{\text{teacher}} e^{-\beta V(h - \sqrt{\Lambda_{\text{teacher}}} z_{\text{teacher}})} \quad (149)$$

For the hardcore potential Eq. (7), $g_{\text{teacher}}(h) = \Theta(h/\sqrt{2\Lambda_{\text{teacher}}})$ with $\Theta(h)$ defined in Eq. (114) and $g'_{\text{teacher}}(h) = e^{-h^2/2\Lambda_{\text{teacher}}} / \sqrt{2\pi\Lambda_{\text{teacher}}}$.

Using the above results we find, for $l = 1, 2, \dots, L-1$,

$$\epsilon_r(l) = -r(l-1)R(l)\kappa_{\text{inter}}(l) - R(l+1)r(l+1)\kappa_{\text{inter}}(l+1) \quad (150)$$

C.3.4 Variation of R

Finally we consider variation of the free-energy Eq. (17) (see also Eq. (76)) with respect to $R(l)$, for $l = 1, 2, \dots, L$,

$$\begin{aligned} 0 &= \frac{\partial}{\partial R(l)} \partial_s S_{1+s}[\{\hat{Q}(l), \hat{q}(l)\}] \Big|_{s=0} \\ &= \frac{\partial}{\partial R(l)} \frac{1}{\alpha} \partial_s S_{\text{ent,bond}}[\hat{Q}^{1+s}(l)] \Big|_{s=0} - \frac{\partial}{\partial R(l)} \mathcal{F}_{\text{int}}[\{\hat{Q}^{1+s}(l), \hat{q}^{1+s}(l)\}] \Big|_{s=0} \end{aligned} \quad (151)$$

Variation of the entropic part (bond) of the free-energy Eq. (128) yields,

$$\frac{\partial}{\partial R} \partial_s S_{\text{ent,bond}}[\hat{Q}^{1+s}] \Big|_{s=0} = -\frac{R}{G_0} \quad (152)$$

On the other hand, variation of the interaction part of the free-energy Eq. (137) yields,

$$\begin{aligned} & -\frac{\partial}{\partial R(l)} \partial_s \mathcal{F}_{\text{int}}[\hat{q}^{1+s}(l-1), \hat{Q}^{1+s}(l), \hat{q}^{1+s}(l)] \Big|_{s=0} \\ & = -\left(\frac{\partial \Lambda_{\text{com}}(l)}{\partial R(l)} \frac{\partial}{\partial \Lambda_{\text{com}}(l)} + \frac{\partial \Lambda_{\text{teacher}}(l)}{\partial R(l)} \frac{\partial}{\partial \Lambda_{\text{teacher}}(l)} + \frac{\partial \Lambda_0(l)}{\partial R(l)} \frac{\partial}{\partial \Lambda_0(l)} \right) \\ & \quad \partial_s \mathcal{F}_{\text{int}}[\hat{q}^{1+s}(l-1), \hat{Q}^{1+s}(l), \hat{q}^{1+s}(l)] \Big|_{s=0} \\ & = r(l-1)r(l)\kappa_{\text{inter}}(l) \end{aligned} \quad (153)$$

with $\kappa_{\text{inter}}(l)$ defined in Eq. (148). Using these results in Eq. (151) we find,

$$R(l) = \alpha G_0 r(l-1)r(l)\kappa_{\text{inter}}(l) \quad (154)$$